NATIONAL TECHNICAL UNIVERSITY OF ATHENS
SCHOOL OF MECHANICAL ENGINEERING
SECTION M.D. & A.C.
Laboratory of Automatic Control

Diploma Thesis

Model Predictive Control for Space Manipulator Systems with Parametric Uncertainty & Subject to Disturbances

Evangelos Psomiadis

Supervisor: E. G. Papadopoulos

ATHENS 2021

Περίληψη

Το διάστημα αποτελεί μία εξελισσόμενη και πολλά υποσχόμενη βιομηχανία με χώρες και ιδιώτες να επενδύουν τεράστια χρηματικά ποσά κάθε χρόνο. Το 2021 σημειώθηκε ότι πάνω από 6000 δορυφόροι βρίσκονταν σε τροχιά γύρω από τη Γη. Η μεγάλη αύξηση του αριθμού των δορυφόρων απαιτεί τη διοργάνωση διαστημικών αποστολών οι οποίες θα παρέχουν ένα μεγάλο εύρος υπηρεσιών σε τροχιά. Οι πιθανοί κίνδυνοι του διαστήματος καθιστούν τα διαστημικά ρομποτικά συστήματα ως τη καταλληλότερη επιλογή για να φέρουν εις πέρας αυτές τις εργασίες.

Σε αυτή τη διπλωματική εργασία, χρησιμοποιείται ένας Προβλεπτικός Έλεγχος (MPC) για τον έλεγχο του βραχίονα ενός διαστημικού ρομποτικού συστήματος σε πολλά διαφορετικά σενάρια. Ο νόμος ελέγχου συγκρίνεται με έναν συνηθισμένο PID έλεγχο με σκοπό να προσδιοριστούν τα πλεονεκτήματα και τα μειονεκτήματά του. Αρχικά, παρατίθεται η θεωρία της κινηματικής και της δυναμικής ενός Ελεύθερα Αιωρούμενου Διαστημικού Ρομποτικού Συστήματος (ΕΑΔΡΣ) όπως και η θεωρία του σχεδιασμού του MPC -με και χωρίς περιορισμούς-. Όταν το σύστημα είναι Ελεύθερα Αιωρούμενο, το σύστημα ελέγχου της βάσης είναι απενεργοποιημένο και λειτουργεί μόνο το σύστημα ελέγχου του βραχίονα. Διάφορες προσομοιώσεις πραγματοποιούνται χρησιμοποιώντας ένα επίπεδο ΕΑΔΡΣ με έναν βραχίονα 3 Βαθμών Ελευθερίας (ΒΕ). Οι προσομοιώσεις γίνονται χρησιμοποιώντας το Matlab/Simulink καθώς και το λογισμικό MSC Adams.

Τα μελετούμενα σενάρια περιέχουν διαφορετικές αποστολές με διάφορους σχεδιασμούς τροχιάς και εμπόδια (όπως διαταραχές, παραμετρική αβεβαιότητα και θόρυβο) που ίσως αντιμετωπίσει ο νόμος ελέγχου του ΕΑΔΡΣ κατά τις αποστολές του. Το πρώτο σενάριο περιέχει τη μελέτη της λειτουργίας ενός MPC όταν εφαρμόζονται σταθερές διαταραχές στους επενεργητές του βραχίονα ενός ΕΑΔΡΣ. Αυτές οι διαταραχές μπορεί να προέρχονται από πιθανές τριβές που εμφανίζονται λόγω της εκτεταμένης χρήσης του βραχίονα. Ο MPC συγκρίνεται με έναν απλό PID έλεγχο με βάση διάφορα κριτήρια όπως το σφάλμα της θέσης και του προσανατολισμού του τελικού σημείου δράσης, τις προκύπτουσες ροπές, τη σύγκλιση του σφάλματος στη μόνιμη κατάσταση και τον υπολογιστικό χρόνο προσομοίωσης. Η κίνηση του ΕΑΔΡΣ, του οποίου ο σκοπός είναι να πιάσει ένα σταθερό σώμα-στόχο, σχεδιάζεται στον Καρτεσιανό χώρο.

Παρόμοιες μελέτες πραγματοποιήθηκαν και για τα υπόλοιπα σενάρια. Το δεύτερο σενάριο περιέχει τη σύγκριση των νόμων ελέγχου όταν οι παράμετροι της διάταξης δεν είναι γνωστές με ακρίβεια. Πραγματοποιείται μία προσομοίωση Monte-Carlo για 200 διαφορετικούς συνδυασμούς παραμέτρων και οι έλεγχοι συγκρίνονται με βάση τα σφάλματα και τις ροπές. Η κίνηση σχεδιάζεται στον Καρτεσιανό Χώρο για σταθερό στόχο. Στο τρίτο σενάριο, παρουσιάζεται η σύγκριση των νόμων ελέγχου, όταν το ΕΑΔΡΣ έχει ήδη πιάσει και σταθεροποιήσει έναν στόχο απροσδιόριστης μάζας με σκοπό να τον κινήσει. Η κίνηση του ΕΑΔΡΣ για αυτό το σενάριο σχεδιάζεται στο χώρο των αρθρώσεων.

Τέλος, στο τέταρτο σενάριο, δύο διαφορετικά είδη θορύβου εισέρχονται στις μετρούμενες μεταβλητές και η λειτουργία κάθε νόμου ελέγχου ελέγχεται με βάση την ικανότητά του να αντισταθμίζει τον θόρυβο. Η κίνηση του ΕΑΔΡΣ σχεδιάζεται στον Καρτεσιανό χώρο. Ωστόσο, ο στόχος δεν θεωρείται σταθερός αλλά κινείται με σταθερή σχετική ταχύτητα. Επομένως, τα σφάλματα των τελικών ταχυτήτων του τελικού σημείου δράσης λαμβάνονται επίσης υπόψη για τη μελέτη.

Abstract

Space constitutes a nascent and promising industry with countries and individuals investing a tremendous amount of money every year. By 2021, more than 6000 satellites were orbiting Earth. The immense increase in the number of satellites mandates the organization of missions which would provide a wide range of on-orbit servicing operations. The potential dangers of space render space robotic systems the most appropriate choice for these tasks.

In this thesis, a Model Predictive Controller (MPC) is used for the control of the manipulator of a space robotic system for a variety of different scenarios. The controller is compared to a regular PID Controller to manifest its benefits and shortcomings. Firstly, the kinematics and dynamics of a Free-Floating Space Robotic System (FFSMS) as well as the theory for the design of the MPC -with and without constraints- are presented. When the system operates in Free-Floating mode, the controller of the base is turned off and only the manipulator's controller is active. A plethora of simulations is performed using a planar FFSMS with a single manipulator of 3 Degrees of Freedom (DoF). The simulations are conducted using Matlab/Simulink as well as the Multibody Dynamics software MSC Adams.

The studied scenarios involve different missions with various path planning techniques and impediments (like disturbances, parametric uncertainties and noise) which the controller of an FFSMS might face throughout its various missions. The first scenario contains the study of the performance of the MPC when constant disturbances are applied to the joints' actuators of an FFSMS. These disturbances can model the friction that might appear due to the extensive usage of the manipulator. The MPC is compared to a regular PID using various criteria like the error of the end-effector's position and orientation, the resulted torques, the convergence of the errors at the steady-state and the simulation time. The motion of the FFSMS, whose purpose is to capture a stationary object-target, is planned in the Cartesian space.

Similar studies were performed for the rest of the scenarios. The second scenario includes the comparison of the aforementioned controllers when the plant's parameters are not accurately known but estimated. A Monte-Carlo simulation is performed for 200 different combinations of parameters and the controllers' performance is compared based on the resulting errors and torques. The motion is planned in the Cartesian space for a stationary target. In the third scenario, the comparison of the controllers, when the FFSMS has already captured and stabilized a target of undefined mass with the intention to move it, is presented. The motion of the FFSMS for this scenario was planned in the joint space.

Finally, in the fourth scenario, two different types of noise are inserted in the process variables and the performance of each controller is examined based on their ability to compensate for the noise. The motion of the FFSMS is planned in the Cartesian space. However, the target is not considered stationary but it moves with a constant velocity. Therefore, the errors of the final velocities of the end-effector have to be considered too.

Acknowledgments

First, I would like to express my gratitude to my supervisor, Professor Evangelos G. Papadopoulos. I was honored to be given the opportunity to be a member of the Controls System Laboratory of NTUA and work on a highly interesting topic and in the fascinating field of space robotics. I am thankful for his constant guidance and help throughout the conduction of this study as well as the commitment that he showed in our slightly prolonged meetings to find solutions to the problems that I was facing. His problem-solving experience and his advice altered my engineering insight and cultivated my zeal to work in the field of space control systems. Secondly, I would also like to thank Dr. Konstantinos Nanos for his support and prompt advice, whenever I needed his help.

Finally, I would like to thank my family for always being there for me, believing in me and supporting me, even though they did not realize why and what exactly I was doing. I am also thankful to my friends for accompanying me along the journey and always being eager to listen to my concerns.

Contents

List of Figures

List of Tables

Nomenclature

English

SMS	Space Manipulator System
AOCS	Attitude and Orbit Control Systems
MPC	Model Predictive Control
FFSMS	Free-Floating Space Manipulator Systems
DS	Dynamic Singularities
DoF	Degrees of Freedom
CM	Center of Mass
PDW	Path Dependent Workspace
PIW	Path Independent Workspace
SISO	Single-Input Single-Output
PID	Proportional, Integral, Derivative
PD	Proportional, Derivative

Greek

ΕΑΔΡΣ	Ελεύθερα Αιωρούμενο Διαστημικό Ρομποτικό Σύστημα
ΒΕ	Βαθμοί Ελευθερίας

1 Introduction

1.1 Objective

The alarmingly emerging problem of the immense increase of space debris as well as the wide variety of space operations like catching, refueling, repairing and re-orbiting of satellites and objects with unknown parameters in general, mandate the development of space systems, capable to cope with these tasks. Considering the fact that space is an inhospitable environment to humans, a Space Manipulator System (SMS) is the most appropriate choice.

An SMS consists of the satellite-base and the manipulators. The base transfers and orients in space using its Attitude and Orbit Control Systems (AOCS) which controls the momentum control devices such as the reaction wheels and the thrusters. Every manipulator has its own control system and joint motors to reach the desired position and orientation of its end-effector. However, the motion of the end-effector affects the motion of the base and vice versa due to the dynamic coupling. If it is considered necessary, the AOCS is used to counterbalance this effect. Some notable examples of SMS are the ETS-7 [24] and the Orbital-Express [25] . Figure 1-1 presents a photorealistic image of an SMS with three manipulators.

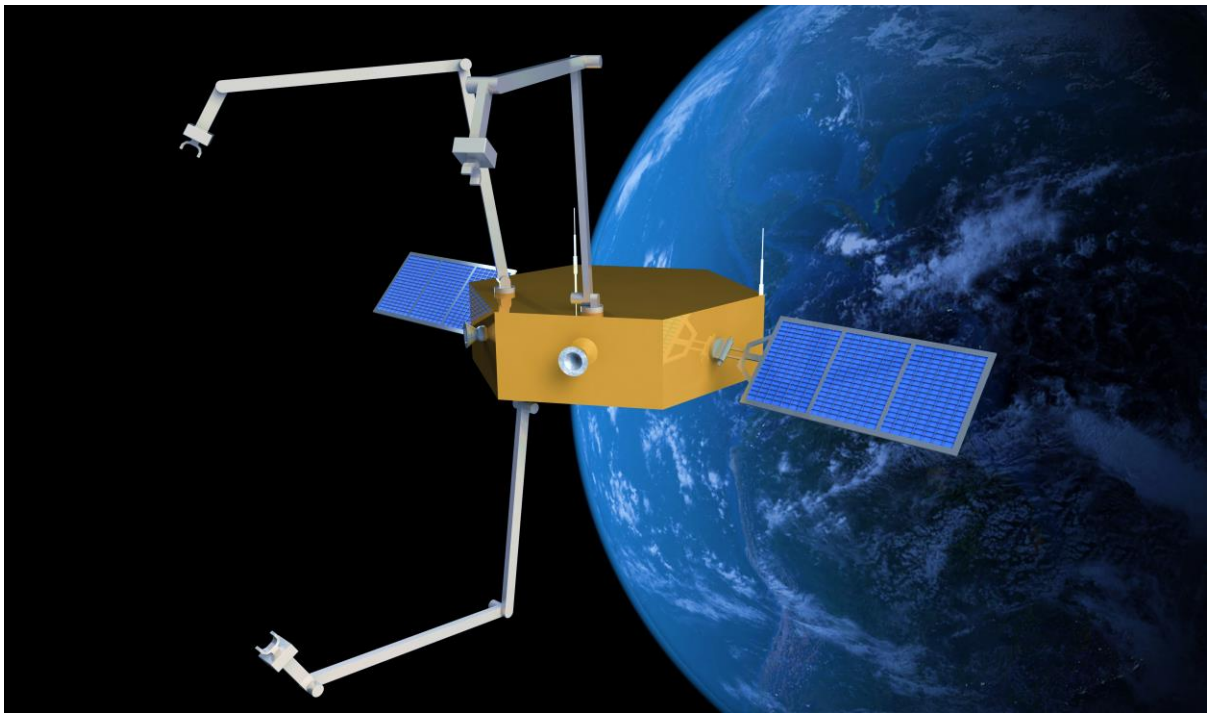

Figure 1-1. Photorealistic Picture of a Typical SMS (the image was rendered using Solidworks).

As Rekleitis et al. [31] present, there are seven main operations that are conducted in a typical on-orbit servicing mission. These operations are:

1. Long-Range Rendezvous
2. Short-Range Rendezvous
3. Station Keeping

4. Capture
5. Securing the Target Satellite
6. Service Operations
7. Release

In this thesis, the fourth of the aforementioned phases is studied thoroughly. In this phase, the SMS operates in a Free-Floating mode, during which the AOCS is turned-off to avoid any disturbances from the thrusters of the base and minimize fuel consumption. Besides that, an additional post-capture scenario of the fifth phase is also presented. According to this, the SMS has already captured the target and stabilized it and it desires to change its position and orientation.

A Model Predictive Control (MPC) algorithm for the actuators of the manipulator is suggested to compensate for the effect of external disturbances, noise as well as parametric uncertainties that occur during most of these phases. The Controller would be applied in a planar SMS with a single manipulator of three joints for both motions in the joint and Cartesian space. The results would be compared with a PID Controller to show its advantages and disadvantages.

The main reason behind the parametric uncertainties of an SMS is the variance of the mass of the base due to fuel consumption, since the fuel tanks are embedded in the base. Some other uncertainties that should be noted are discrepancies in the lengths of the manipulator's components due to the temperature variation as well as small variance of the masses of the manipulator's parts because of inaccuracies between real and simulation model. As far as the external disturbances are concerned, these might be the result of collisions of the satellite with unidentified small bodies that float into space.

The preservation of the stability and performance, despite the preceding disturbances, requires a robust controller, which ensures an acceptable performance under bounded parametric uncertainties. Although proofs about robustness and stability of Model Predictive Control are hard to acquire due to the usage of constraints and the finite horizon -a characteristic that would be described in Chapter 3, a plethora of applications illustrates its robustness. Another alternative for this task would be an Adaptive Controller, which "learns" the system parameters on its own and adapts accordingly. However, due to the limited number of sensors and consequently the data that today's SMS obtain, it is a rather unrealistic option for the present.

1.2 Bibliographic Review

1.2.1 Dynamics & Kinematics of SMS

The aforementioned dynamic coupling between the base and the manipulators of an SMS renders the study of this system significantly different from the one used for a fixed-base manipulator. During the past decades, many researchers have studied the dynamics and kinematics of an SMS and ample noteworthy papers have been published in this domain.

Papadopoulos and Dubowsky [27] & [29] described the kinematics and dynamics of Free-Floating Space Manipulator Systems (FFSMS) using the Barycentric vector approach and proved that any fixed-base control algorithm can be applied to FFSMS under some conditions. The same authors introduced the idea of Dynamic Singularities (DS) that occur in an FFSMS due to the dependence of the velocity of the end-effector to the motion of the manipulator as well as the motion of the base [28] .

Umetani and Yoshida [39] presented the Generalized Jacobian Matrix for an FFSMS and a control method based on it. Caccavale and Siciliano [2] solved the inverse kinematics of an FFSMS using the Generalized Jacobian Matrix. Nanos and Papadopoulos extended the study of the dynamics and control of FFSMS with the additional condition of non-zero angular momentum [23] as well as flexible joint space manipulators [22] . In this thesis, although the results can be generalized by considering the accumulation of the angular momentum, a flexible manipulator and three-dimensional space, a rigid planar manipulator with three joints and zero angular momentum is studied for the sake of simplicity.

1.2.2 Model Predictive Control

While some underlying ideas of MPC were presented in the sixties, a complete idea of MPC was introduced in the late seventies with the papers of Richalet et al. [32] & [33] where a dynamic model was used to predict the future control input by minimizing the error variance and by repeating the optimization after each sampling period, as well as the paper of Cutler and Ramaker [5] where a Dynamic Matrix Control was implemented. This engendered the alacrity to study and apply this kind of algorithms in a wide variety of domains, mostly in slow systems, like the ones appearing in chemical process industries [7] .

A few decades later, the evolution of computational hardware as well as the simplicity and effectiveness of the MPC in handling multi-variable and multi-constrained control problems permitted its application to faster systems like robots. Gomez-Ortega and Camacho [8] implemented a Model-Based Predictive Controller for path tracking of a mobile robot with the use of a neural network. Ullah et al. [38] compared an MPC algorithm with an H_∞ controller for a robot manipulator. Maasoumy et al. [18] applied a robust MPC to handle the parametric uncertainties of a building and maximize its energy efficiency. Dai et al. [6] presented a robust model predictive control with joint state constraints and input torque limits to deal with the disturbances as well as parametric uncertainties problem and implemented the results in a Baxter robot. For further study of MPCs handling parametric uncertainties, Camacho and Bordons in their book [3] applied a min-max MPC algorithm to handle the parametric uncertainties and improve the robustness of the controller.

With the start of the new century, MPC algorithms were applied in space systems too. Richards and How [34] presented a robust MPC formulation to minimize fuel consumption in the performance of spacecraft rendezvous given an unknown but bounded disturbance. Kayastha et al. [12] presented a nonlinear MPC for a free-flying planar space manipulator with 3 links and compared the results with a Sliding Mode Control. Rybus et al. [36] & [37] proposed a Non-Linear Model Predictive Controller for FFSMS and presented simulation examples with realistic parameters.

As it can be concluded from the preceding bibliography, although some MPC algorithms have been applied to FFSMS in the past, complete results about its competence to deal with disturbances and parametric uncertainties that occur in FFSMS have not been presented. In this thesis, an MPC would be implemented in an FFSMS for various scenarios and its performance would be compared with a PID Controller.

1.3 Thesis Outline

This thesis consists of six chapters. The first chapter contains the introduction, the bibliographic review and the thesis outline. The purpose of the thesis is presented and the most important publications about the dynamics and control of FFSMS and the applications of MPC are briefly mentioned.

The second chapter presents the kinematics, inverse kinematics, differential kinematics and dynamics of an FFSMS. The equations that relate the angles of the joints to the end-effector's position and orientation are presented as well as the equations that relate their respective velocities. This leads to the formation of the Jacobian and the finding of the positions that dynamic singularities might occur. Furthermore, the equations of motion of the FFSMS are derived. These equations are fundamental for the implementation of the controller.

The third chapter contains the theory and methodology of the MPC that is implemented. The Laguerre functions that are used for the representation of the control signal are presented and the different steps that the MPC follows (prediction, minimization, implementation) are described extensively. Moreover, input and output constraints are integrated in the design using Hildreth's quadratic programming procedure. At the end of this chapter, a simple example is presented according to which an MPC desires to control the motion of a mass-spring-damper model. Constraints are also inserted in the design.

The fourth chapter contains the implementation of different control laws in an FFSMS. The control signal's equations for a Model Based PD Controller, Model Based PID Controller and Model Based PD Controller with an auxiliary MPC input are presented for motion in the joint and Cartesian space. The plant that is used in the simulation is also defined using MSC Adams. At the end of this chapter, an example of implementing a Model Based PID Controller and a Model Based PD Controller with an auxiliary MPC input in an FFSMS for motion in the joint space is presented to validate the design of the controllers.

The fifth chapter contains the simulations and various scenarios that are performed to compare the Model Based PID Controller to the Model Based PD Controller with an auxiliary MPC input. For the first scenario, the path planning is determined in the Cartesian space and the target is considered relatively stationary. Constant disturbances are applied to the actuators of the joints. The criteria of the comparison are the errors of the position and orientation of the end-effector, the maximum torques that each controller produces as well as the duration of the simulation. For the second scenario, the same path planning and parameters of controllers are used. However, the parameters of the FFSMS are not accurately known but estimated. Therefore, parametric uncertainties occur. A Monte-Carlo simulation is performed for 200 different combinations of parameters. A more scrutinous study is performed containing the parameters that result in the maximum error of the x-coordinate of the end-effector.

For the third scenario, the path planning is determined in the joint space. However, the target is considered captured by the FFSMS and it is desired to change its position and orientation. The parameters of the target are not accurately known but estimated. Therefore, parametric uncertainties occur. For the fourth and final scenario, the path planning is determined in the Cartesian space but the target is considered to move with a relatively constant velocity. Two different types of noise are also inserted in the study to illustrate the performance of the controllers in the presence of noise.

The sixth chapter presents the conclusions and proposals for future work.

2 Kinematics & Dynamics of Planar Free-Floating Space Manipulator System (FFSMS)

2.1 Introduction

There are two main modes that a Space Manipulator System (SMS) -which is regarded as the “chaser”- will use to capture a target. The Free-Flying mode and the Free-Floating mode. The former mode is being applied when the SMS is considerably distant from the target. According to this mode, the Attitude and Orbit Control Systems (AOCS) and its actuators are used to reach the target. The control system of the manipulator of the SMS -which is usually independent of the AOCS- might also be used, if it is regarded as necessary. However, the dynamic coupling between the satellite and the manipulator affects the motion of the end effector and the motion of the base. In the case that the base must follow a predetermined path, the AOCS is applied to compensate for this effect.

Nevertheless, when the SMS is significantly close to the target, the AOCS should not be used since the base thrusters might disturb the target or the position and/or orientation of the manipulator’s end-effector. This is called the Free-Floating mode. The position and orientation of the end-effector are determined by the manipulator’s controller as well as the path that the end-effector will follow.

In this chapter, the kinematics and dynamics of a planar Free-Floating Space Manipulator System (FFSMS) with a single manipulator consisting of three joints are presented. The manipulator is non-redundant to simplify the modelling procedure and to minimize the mass of the system. It should be noted that there are three extra Degrees of Freedom (DOF) due to the position and the orientation of the base. The manipulator is also characterized as open-chain and its three joints are revolute, for the maximization of the workspace.

The study is performed under the assumptions that the forces and torques which are produced by the Earth’s gravitational and magnetic field as well as the air’s resistance are small enough and therefore negligible. Besides that, the links of the manipulator are considered inflexible and the angular momentum of the system equals zero.

First, the forward and inverse kinematics of the general problem of a spatial FFSMS are presented. Then, the results are simplified for the specific case of a planar FFSMS with a 3-DoF manipulator. Secondly, the differential forward and inverse kinematics are studied to elicit the equations of the velocities. From the derived equations, the positions on the Cartesian plain where a singularity might occur are presented. Finally, the dynamics of the general spatial FFSMS problem as well as the simplified planar problem are presented. These equations are of integral importance for the control of an FFSMS which is studied in Chapter 4.

2.2 Kinematics

The main goal of the study of the kinematics of an FFSMS is to obtain the equations for the position of the end-effector. In contrast to the kinematics of the clasical manipulators with a stable base, the aforementioned dynamic coupling between the manipulator and the base of an FFSMS results in the dependence of the position of each joint on the position and the mass properties of all the joints and the base. For this reason, the Barycentric Vector Approach, presented in [26] is applied.

The notation that will be used from now on defines bold lowercase symbols to represent column vectors and bold uppercase symbols to represent matrices.

Considering a planar FFSMS, the rotation of the base is described by the rotation matrix:

$$\mathbf{R_0}(\theta_0) = \begin{bmatrix} \cos(\theta_0) & -\sin(\theta_0) \\ \sin(\theta_0) & \cos(\theta_0) \end{bmatrix} \tag{2-1}$$

Assuming a point o on the k-th joint, the position vector with respect to a given inertial frame of reference (x, y, z) (Figure 2-1) is described by:

$$\mathbf{r}_{k,o} = \mathbf{r}_{cm} + \boldsymbol{\rho}_k + \bar{\mathbf{r}}_{k,o} \tag{2-2}$$

where $\mathbf{r}_{cm}$ is the position vector of the Center of Mass (CM) of the whole model with respect to the inertial frame, $\boldsymbol{\rho}_k$ is the position vector of the CM of the k-th joint with respect to the CM of the whole model and $\bar{\mathbf{r}}_{k,o}$ is the position vector of the point o with respect to the CM of the k-th joint.

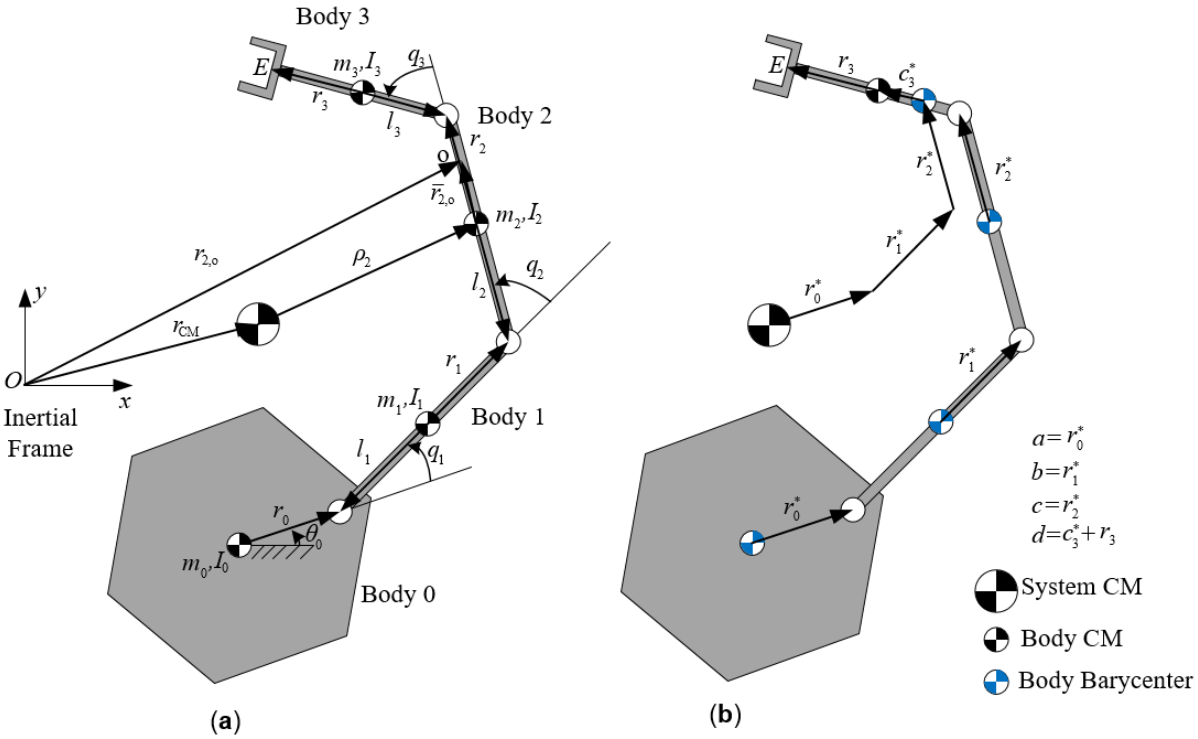

Figure 2-1. Planar FFSMS with a manipulator of 3 DoF (a) Geometrical & Dynamic parameters (b) Parameters of the Barycenters.

As shown in [26] , the position vector $\boldsymbol{\rho}_k$ can be calculated by finding the barycenter of each of the joints and the base. The barycenter of the i-th body is the CM of the augmented body which is formed by adding a point mass equal to $M\mu_i$ to the i-th joint and a point mass $M(1\text{-}\mu_{i+1})$ to the joint i+1 where:

$$M=\sum_{i=0}^{N} m_i \quad and \quad \mu_i=\begin{cases} 0, & i=0 \\ \sum_{j=0}^{i-1}\frac{m_i}{M}, & i=1,\ldots,N \\ 1, & i=N+1 \end{cases} \tag{2-3}$$

Then, if the position vectors $\mathbf{l}_i$ and $\mathbf{r}_i$ of the i-th joint and joint i+1 (respectively) with respect to the i-th body CM are known, the position vectors with respect to each barycenter can be calculated by (see Figure 2-2):

$$\begin{aligned} \mathbf{c}_i &= \mathbf{l}_i\mu_i+\mathbf{r}_i(1-\mu_i),\ i=0,\ldots,N \\ \mathbf{c}_i^* &= -\mathbf{c}_i \\ \mathbf{r}_i^* &= \mathbf{r}_i-\mathbf{c}_i \\ \mathbf{l}_i^* &= \mathbf{l}_i-\mathbf{c}_i \end{aligned} \tag{2-4}$$

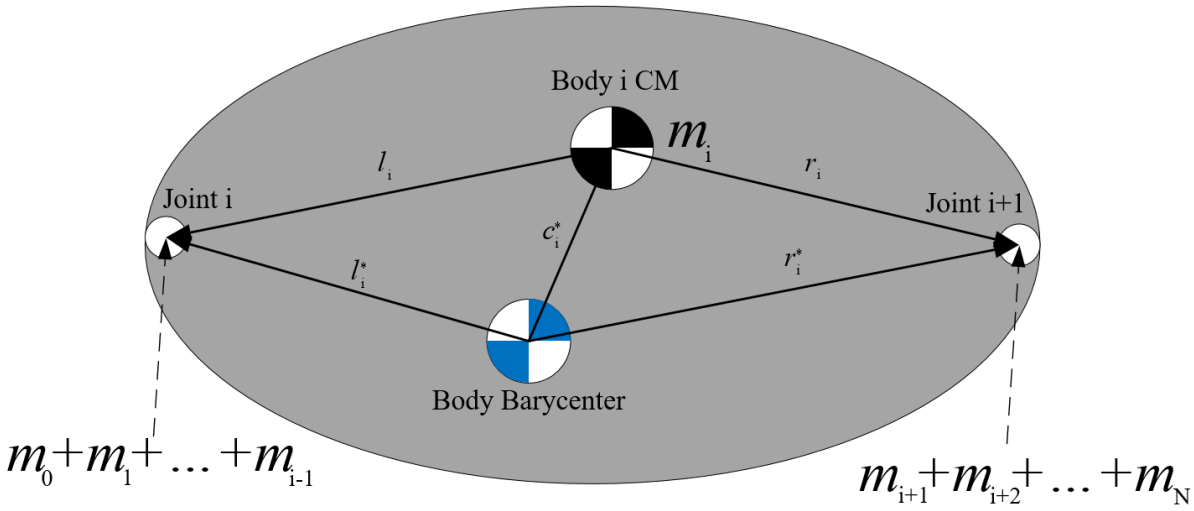

Figure 2-2. Definition of Barycenter and its parameters.

Finally, the position vector $\boldsymbol{\rho}_k$ is given by:

$$\boldsymbol{\rho}_k=\sum_{i=0}^{N}\mathbf{v}_{i,k} \quad with \quad \mathbf{v}_{i,k}=\begin{cases} \mathbf{r}_i^* & i<k \\ \mathbf{c}_i^* & i=k \\ \mathbf{l}_i^* & i>k \end{cases} \tag{2-5}$$

Substituting Eq. (2-5) into (2-2) it can be derived:

$$\mathbf{r}_{k,o}=\mathbf{r}_{cm}+\sum_{i=0}^{N}\mathbf{v}_{i,k,o} \quad with \quad \mathbf{v}_{i,k,o}=\mathbf{v}_{i,k}+\delta_{i,k}\bar{\mathbf{r}}_{k,o} \tag{2-6}$$

where $\delta_{i,k}$ is the Kronecker delta.

Before the preceding methodology is applied to an FFSMS with a 3-DOF manipulator, it is of immense importance to point out that if all the external forces are considered negligible, therefore equal to zero, it can be derived from the derivative of the linear momentum $\mathbf{p}$ that:

$$\frac{d\mathbf{p}}{dt} = \frac{d(M\dot{\mathbf{r}}_{CM})}{dt} = \sum \mathbf{F}_{external} = 0 \Rightarrow \dot{\mathbf{r}}_{CM} = const \tag{2-7}$$

Assuming that the initial linear momentum is zero, then:

$$\dot{\mathbf{r}}_{CM} = 0 \Rightarrow \mathbf{r}_{CM} = const \tag{2-8}$$

Therefore, from now it will be considered that the origin of the inertial frame is at the system's CM.

Considering these assumptions, the position and the rotation of the end-effector of an FFSMS with a 3-DOF manipulator is given by [21] (see Figure 2-1):

$$\begin{aligned} x_E &= a\,\mathrm{c}_{\theta_o} + b\,\mathrm{c}_{\theta_o+q_1} + c\,\mathrm{c}_{\theta_o+q_1+q_2} + d\,\mathrm{c}_{\theta_o+q_1+q_2+q_3} \\ y_E &= a\,\mathrm{s}_{\theta_o} + b\,\mathrm{s}_{\theta_o+q_1} + c\,\mathrm{s}_{\theta_o+q_1+q_2} + d\,\mathrm{s}_{\theta_o+q_1+q_2+q_3} \\ \theta_E &= \theta_o + q_1 + q_2 + q_3 \end{aligned} \tag{2-9}$$

where:

$$\begin{aligned} a &= \frac{m_0 r_0}{M} \\ b &= \frac{m_0 l_1 + (m_0 + m_1) r_1}{M} \\ c &= \frac{(m_0 + m_1) l_2 + (m_0 + m_1 + m_2) r_2}{M} \\ d &= \frac{(m_0 + m_1 + m_2) l_3}{M} + r_3 \\ M &= m_0 + m_1 + m_2 + m_3 \end{aligned} \tag{2-10}$$

For the inverse kinematics problem, it is considered that the base's orientation θ_0, the end-effector's coordinates x_E and y_E as well as the end-effector's rotation θ_E are known. By raising Eq. (2-9) to the second power and subtract them, it is derived:

$$\begin{aligned} \cos(q_2) &= \frac{(x_E - a\,\mathrm{c}_{\theta_o} - d\,\mathrm{c}_{\theta_o+q_1+q_2+q_3})^2 + (y_E - a\,\mathrm{s}_{\theta_o} - d\,\mathrm{s}_{\theta_o+q_1+q_2+q_3})^2 - b^2 - c^2}{2bc} \\ \sin(q_2) &= \pm\sqrt{1 - \mathrm{c}_{q_2}^2} \\ \sin(\theta_o + q_1) &= -\frac{A_{kin}(x_E - a\,\mathrm{c}_{\theta_o} - d\,\mathrm{c}_{\theta_o+q_1+q_2+q_3}) - B_{kin}(y_E - a\,\mathrm{s}_{\theta_o} - d\,\mathrm{s}_{\theta_o+q_1+q_2+q_3})}{b^2 + c^2 + 2bc\,\mathrm{c}_{q_2}} \\ \cos(\theta_o + q_1) &= \frac{A_{kin}(y_E - a\,\mathrm{s}_{\theta_o} - d\,\mathrm{s}_{\theta_o+q_1+q_2+q_3}) + B_{kin}(x_E - a\,\mathrm{c}_{\theta_o} - d\,\mathrm{c}_{\theta_o+q_1+q_2+q_3})}{b^2 + c^2 + 2bc\,\mathrm{c}_{q_2}} \end{aligned} \tag{2-11}$$

where:

$$\begin{aligned} A_{kin} &= c\,\mathrm{s}_{q_2} \\ B_{kin} &= b + c\,\mathrm{c}_{q_2} \end{aligned} \tag{2-12}$$

Finally, the joint's angles are given by:

$$\begin{aligned} q_2 &= \operatorname{atan2}(\sin(q_2), \cos(q_2)) \\ q_1 &= \operatorname{atan2}(\sin(\theta_o + q_1), \cos(\theta_o + q_1)) - \theta_o \\ q_3 &= \theta_E - \theta_o - q_1 - q_2 \end{aligned} \tag{2-13}$$

where $\operatorname{atan2}(y,x)$ is defined as the four-quadrant $(-\pi,\pi)$ inverse tangent of the numbers (x,y).

2.3 Differential Kinematics

The equations of differential kinematics describe the relation between linear and angular velocity of the end-effector to the joints' angular velocity as well as the angular velocity of the base and vice versa. The derivation of these equations requires the equation of the angular velocity of the k-th body with respect to the inertial frame of reference. For the general problem of spatial FFSMS is given by [26] :

$$\begin{aligned} \boldsymbol{\omega}_k &= \boldsymbol{\omega}_0 + \mathbf{R}_0 \sum_{i=1}^{k} {}^0\mathbf{R}_i(\mathbf{q})\, {}^i\mathbf{z}_i \dot{q}_i = \mathbf{R}_0 \left({}^0\boldsymbol{\omega}_0 + {}^0\mathbf{F}_k \dot{\mathbf{q}} \right) \\ {}^0\mathbf{F}_k &= \begin{bmatrix} {}^0\mathbf{R}_1\, {}^1\mathbf{z}_1 & \dots & {}^0\mathbf{R}_k\, {}^k\mathbf{z}_k & \mathbf{0}_{3(N-k)} \end{bmatrix} \end{aligned} \tag{2-14}$$

where left superscripts are interpreted as "expressed in frame". Missing left superscript means that it is expressed in the inertial frame. The $\boldsymbol{\omega}_0$ is the angular velocity of the base, ${}^0\mathbf{R}_i$ is the rotation matrix of the frame of reference $\{i\}$ expressed in the frame of reference $\{0\}$. ${}^i\mathbf{z}_i$ is the unit vector parallel to the axis of the i-th joint (for the planar case, they are all perpendicular to the model) and $\mathbf{0}_{3(N-k)}$ is a $3(\mathrm{N\text{-}k})$ zero vector.

By differentiating Eq. (2-6), the linear velocity of point o on the k-th joint is:

$$\dot{\mathbf{r}}_{k,o} = \dot{\mathbf{r}}_{cm} + \sum_{i=0}^{N} \boldsymbol{\omega}_i \times \mathbf{v}_{i,k,o} = \dot{\mathbf{r}}_{cm} - \sum_{i=0}^{N} \mathbf{v}^{\times}_{i,k,o} \boldsymbol{\omega}_i \tag{2-15}$$

where the cross-product operator is given by:

$$(\cdot)^{\times} = \begin{bmatrix} 0 & -(\cdot)_z & (\cdot)_y \\ (\cdot)_z & 0 & -(\cdot)_x \\ -(\cdot)_y & (\cdot)_x & 0 \end{bmatrix} \tag{2-16}$$

According to a property of the cross-product, the following holds:

$$\mathbf{v}^{\times}_{i,k,o} = \left(\mathbf{R}_0\, {}^0\mathbf{v}_{i,k,o} \right)^{\times} = \mathbf{R}_0\, {}^0\mathbf{v}^{\times}_{i,k,o} \mathbf{R}_0^T = \mathbf{R}_0\, {}^0\mathbf{v}^{\times}_{i,k,o} \mathbf{R}_0^{-1} \tag{2-17}$$

Substituting Eq. (2-14) and Eq. (2-17) into Eq. (2-15):

$$\dot{\mathbf{r}}_{k,o} = \dot{\mathbf{r}}_{cm} + \mathbf{R}_0 \left[-\sum_{i=0}^{N} \left({}^0\mathbf{R}_i\, {}^i\mathbf{v}_{i,k,o} \right)^{\times} {}^0\boldsymbol{\omega}_0 - \sum_{i=1}^{N} \left({}^0\mathbf{R}_i\, {}^i\mathbf{v}_{i,k,o} \right)^{\times} {}^0\mathbf{F}_i \dot{\mathbf{q}} \right] \tag{2-18}$$

To conclude, the angular velocity of the k-th joint and the linear velocity of a point o on one of the joints is given by:

$$\begin{aligned} \dot{\mathbf{r}}_{k,o} &= \dot{\mathbf{r}}_{cm} + \mathbf{R}_0 \left({}^0\mathbf{J}_{11,k}\, {}^0\boldsymbol{\omega}_0 + {}^0\mathbf{J}_{12,k} \dot{\mathbf{q}} \right) \\ \boldsymbol{\omega}_k &= \mathbf{R}_0 \left({}^0\boldsymbol{\omega}_0 + {}^0\mathbf{J}_{22,k} \dot{\mathbf{q}} \right) \end{aligned} \tag{2-19}$$

with ${}^0\mathbf{J}_{11,k} = -\sum_{i=0}^{N} \left({}^0\mathbf{R}_i\, {}^i\mathbf{v}_{i,k,o} \right)^{\times}$, ${}^0\mathbf{J}_{12,k} = -\sum_{i=1}^{N} \left({}^0\mathbf{R}_i\, {}^i\mathbf{v}_{i,k,o} \right)^{\times} {}^0\mathbf{F}_i$ *and* ${}^0\mathbf{J}_{22,k} = {}^0\mathbf{F}_k$

Considering the assumption of zero linear momentum (and the initial linear momentum too), Eq. (2-8) gives that $\dot{\mathbf{r}}_{CM} = 0$. Consequently, the linear velocity of the end-effector of an FFSMS with a 3-DOF manipulator is given by [21] (see Figure 2-1):

$$\begin{aligned}
\dot{\mathbf{r}}_E &= \mathbf{R}_0 \left({}^0\mathbf{j}_{11}\dot{\theta}_0 + {}^0\mathbf{J}_{12}\dot{\mathbf{q}} \right) \\
\mathbf{R_0}(\theta_0) &= \begin{bmatrix} \mathrm{c}_{\theta_o} & -\mathrm{s}_{\theta_o} \\ \mathrm{s}_{\theta_o} & \mathrm{c}_{\theta_o} \end{bmatrix} \\
{}^0\mathbf{j}_{11}(\mathbf{q}) &= \begin{bmatrix} -\left(b\,\mathrm{s}_{q_1} + c\,\mathrm{s}_{q_1+q_2} + d\,\mathrm{s}_{q_1+q_2+q_3} \right) \\ a + b\,\mathrm{c}_{q_1} + c\,\mathrm{c}_{q_1+q_2} + d\,\mathrm{c}_{q_1+q_2+q_3} \end{bmatrix} \\
{}^0\mathbf{J}_{12}(\mathbf{q}) &= \begin{bmatrix} -\left(b\,\mathrm{s}_{q_1} + c\,\mathrm{s}_{q_1+q_2} + d\,\mathrm{s}_{q_1+q_2+q_3} \right) & -\left(c\,\mathrm{s}_{q_1+q_2} + d\,\mathrm{s}_{q_1+q_2+q_3} \right) & -d\,\mathrm{s}_{q_1+q_2+q_3} \\ b\,\mathrm{c}_{q_1} + c\,\mathrm{c}_{q_1+q_2} + d\,\mathrm{c}_{q_1+q_2+q_3} & c\,\mathrm{c}_{q_1+q_2} + d\,\mathrm{c}_{q_1+q_2+q_3} & d\,\mathrm{c}_{q_1+q_2+q_3} \end{bmatrix}
\end{aligned} \tag{2-20}$$

where θ_0 is the orientation of the base and $\mathbf{q} = [q_1\ q_2\ q_3]^{\mathrm{T}}$.

The angular velocity of the end-effector is given by:

$$\begin{aligned}
\dot{\theta}_{\mathrm{E}} &= \dot{\theta}_0 + {}^0\mathbf{j}_{22}\dot{\mathbf{q}} \\
{}^0\mathbf{j}_{22}(\mathbf{q}) &= \begin{bmatrix} 1 & 1 & 1 \end{bmatrix}
\end{aligned} \tag{2-21}$$

2.3.1 Conservation of Angular Momentum

The angular momentum with respect to the system's CM of the general spatial problem is given by:

$$\mathbf{h}_{CM} = \sum_{k=0}^{N} \left(\mathbf{I}_k \boldsymbol{\omega}_k + m_k \boldsymbol{\rho}_\kappa \times \dot{\boldsymbol{\rho}}_\kappa \right) \tag{2-22}$$

where $\mathbf{I}_k$ is the inertia matrix of the k-th body, $\boldsymbol{\omega}_k$ is the angular velocity of the k-th body and $\boldsymbol{\rho}_k$ is the position vector of the system's CM to the k-th body's CM. The derivative of $\boldsymbol{\rho}_k$ is given by the differentiation of Eq. (2-5):

$$\dot{\boldsymbol{\rho}}_k = \sum_{i=0}^{N} \boldsymbol{\omega}_i \times \mathbf{v}_{i,k} \tag{2-23}$$

Substituting Eq. (2-5) and Eq. (2-23) into Eq. (2-22):

$$\mathbf{h}_{CM} = \sum_{j=0}^{N} \sum_{i=0}^{N} \delta_{ij} \mathbf{I}_i \boldsymbol{\omega}_j + \sum_{j=0}^{N} \sum_{i=0}^{N} \sum_{k=0}^{N} m_k \left(\mathbf{v}_{i,k} \times \boldsymbol{\omega}_j \times \mathbf{v}_{j,k} \right) \tag{2-24}$$

Finally, by using the following property of the cross-product:

$$\mathbf{a} \times \mathbf{b} \times \mathbf{c} = \mathbf{b}(\mathbf{a} \cdot \mathbf{c}) - \mathbf{c}(\mathbf{a} \cdot \mathbf{b}) = \left[(\mathbf{c} \cdot \mathbf{a})\mathbf{1} - \mathbf{ca} \right] \cdot \mathbf{b} \tag{2-25}$$

where $\mathbf{1}$ is the unit dyadic and substituting the angular velocity from Eq. (2-14), Eq. (2-24) can be written as:

$$\mathbf{h}_{CM} = \mathbf{R}_0 \left({}^0\mathbf{D}\,{}^0\boldsymbol{\omega}_0 + {}^0\mathbf{D}_q \dot{\mathbf{q}} \right) \tag{2-26}$$

with:

$$
\begin{aligned}
{}^{0}\mathbf{D} &= \sum_{j=0}^{N} {}^{0}\mathbf{D}_{j} \\
{}^{0}\mathbf{D}_{j} &= \sum_{i=0}^{N} {}^{0}\mathbf{D}_{ij} \\
{}^{0}\mathbf{D}_{ij} &= \mathbf{R}_{0}^{T}\mathbf{D}_{ij}\mathbf{R}_{0} \\
\mathbf{D}_{ij} &= \delta_{ij}\mathbf{I}_{i} + \sum_{k=0}^{N} m_{k}\left[\left(\mathbf{v}_{j,k}\cdot\mathbf{v}_{i,k}\right)\mathbf{1} - \left(\mathbf{v}_{j,k}\mathbf{v}_{i,k}\right)\right] \\
{}^{0}\mathbf{D}_{q} &= \sum_{j=1}^{N} {}^{0}\mathbf{D}_{j}\,{}^{0}\mathbf{F}_{j}
\end{aligned}
\tag{2-27}
$$

Applying the preceding equations into a planar FFSMS with a 3-DOF manipulator, the angular momentum is given by [21] :

$$
h_{CM} = {}^{0}D\dot{\theta}_{0} + {}^{0}\mathbf{D}_{q}\dot{\mathbf{q}} \tag{2-28}
$$

with:

$$
\begin{aligned}
{}^{0}D &= {}^{0}D_{0} + {}^{0}D_{1} + {}^{0}D_{2} + {}^{0}D_{3} \\
{}^{0}\mathbf{D}_{q} &= \begin{bmatrix} {}^{0}D_{1} + {}^{0}D_{2} + {}^{0}D_{3} & {}^{0}D_{2} + {}^{0}D_{3} & {}^{0}D_{3} \end{bmatrix} \\
{}^{0}D_{0} &= a_{00} + a_{01}\,\mathrm{c}_{q_1} + a_{02}\,\mathrm{c}_{q_1+q_2} + am_3l_3\,\mathrm{c}_{q_1+q_2+q_3} \\
{}^{0}D_{1} &= a_{01}\,\mathrm{c}_{q_1} + a_{11} + a_{12}\,\mathrm{c}_{q_2} + bm_3l_3\,\mathrm{c}_{q_2+q_3} \\
{}^{0}D_{2} &= a_{02}\,\mathrm{c}_{q_1+q_2} + a_{12}\,\mathrm{c}_{q_2} + a_{22} + cm_3l_3\,\mathrm{c}_{q_3} \\
{}^{0}D_{3} &= a_{33} + cm_3l_3\,\mathrm{c}_{q_3} + bm_3l_3\,\mathrm{c}_{q_2+q_3} + am_3l_3\,\mathrm{c}_{q_1+q_2+q_3}
\end{aligned}
\tag{2-29}
$$

where a, b and c are given by Eq. (2-10) and:

$$
\begin{aligned}
a_{00} &= I_{0} + \frac{m_{0}\left(m_{1}+m_{2}+m_{3}\right)r_{0}^{2}}{M} \\
a_{01} &= \frac{m_{0}r_{0}\left[l_{1}\left(m_{1}+m_{2}+m_{3}\right) + r_{1}\left(m_{2}+m_{3}\right)\right]}{M} \\
a_{02} &= \frac{m_{0}r_{0}\left[l_{2}\left(m_{2}+m_{3}\right) + r_{2}m_{3}\right]}{M} \\
a_{11} &= I_{1} + \frac{m_{0}m_{1}l_{1}^{2} + m_{1}\left(m_{2}+m_{3}\right)r_{1}^{2} + m_{0}\left(m_{2}+m_{3}\right)\left(l_{1}+r_{1}\right)^{2}}{M} \\
a_{12} &= \frac{\left[l_{1}m_{0} + \left(m_{0}+m_{1}\right)r_{1}\right]\left[l_{2}\left(m_{2}+m_{3}\right) + m_{3}r_{2}\right]}{M} \\
a_{22} &= I_{2} + \frac{m_{2}m_{3}r_{2}^{2} + m_{2}\left(m_{0}+m_{1}\right)l_{2}^{2} + m_{3}\left(m_{0}+m_{1}\right)\left(l_{2}+r_{2}\right)^{2}}{M} \\
a_{33} &= I_{3} + \frac{m_{3}\left(m_{0}+m_{1}+m_{2}\right)l_{3}^{2}}{M}
\end{aligned}
\tag{2-30}
$$

2.3.2 Jacobian & Dynamic Singularities

Eq. (2-20), Eq. (2-21) and Eq. (2-28) form a system of four equations with four unknown variables (for the forward or inverse kinematic problem). They can be written in a more compact form:

$$\begin{bmatrix} h_{CM} \\ \dot{\mathbf{r}}_E \\ \dot{\theta}_{\mathrm{E}} \end{bmatrix} = \begin{bmatrix} 1 & \mathbf{0}_{1\times 2} & 0 \\ \mathbf{0}_{2\times 1} & \mathbf{R}_0 & \mathbf{0}_{2\times 1} \\ 0 & \mathbf{0}_{1\times 2} & 1 \end{bmatrix} \begin{bmatrix} {}^0D & {}^0\mathbf{D}_q \\ {}^0\mathbf{j}_{11} & {}^0\mathbf{J}_{12} \\ 1 & {}^0\mathbf{j}_{22} \end{bmatrix} \begin{bmatrix} \dot{\theta}_0 \\ \dot{\mathbf{q}} \end{bmatrix} \tag{2-31}$$

where $\mathbf{0_{2x1}}$ is a 2x1 column zero vector and $\mathbf{0_{1x2}}$ is a 1x2 row zero vector. Knowing that the first matrix on the right side of the equation which contains the rotation matrix is always invertible, the second matrix can be characterized as the Jacobian of the problem:

$${}^0\mathbf{J} = \begin{bmatrix} {}^0D & {}^0\mathbf{D}_q \\ {}^0\mathbf{j}_{11} & {}^0\mathbf{J}_{12} \\ 1 & {}^0\mathbf{j}_{22} \end{bmatrix} \tag{2-32}$$

It is evident that the Jacobian contains not only kinematic terms like link lengths and joint angles, but also dynamic terms like masses and inertias. This characteristic results in the existence of dynamic singularities along with kinematic ones. Due to the dynamic coupling between the manipulator and the base, a Cartesian point might develop a dynamic singularity depending on the attitude of the base. In other words, the manipulator might lose a Degree of Freedom, depending on the orientation of the base. This is also one of the fundamental discrepancies between FFSMS and manipulators with stable base. The finding of the positions that singularities occur requires the study of the Jacobian.

Since the manipulator of the FFSMS is non-redundant, the solution of the inverse kinematic problem requires the Jacobian to be invertible. Therefore, it is required:

$$\det(\mathbf{J}) \neq 0 \tag{2-33}$$

By using the following property of matrix determinant:

$$\det\begin{bmatrix} \mathbf{A} & \mathbf{B} \\ \mathbf{C} & \mathbf{D} \end{bmatrix} = \det(\mathbf{A})\det(\mathbf{D} - \mathbf{C}\mathbf{A}^{-1}\mathbf{B}) \;\; (\mathbf{A}: \textit{invertible}) \tag{2-34}$$

the determinant of $\mathbf{J}$ can be written as:

$$\det(\mathbf{J}) = \det\left({}^0D\right)\det\left(\begin{bmatrix} {}^0\mathbf{J}_{12} \\ {}^0\mathbf{j}_{22} \end{bmatrix} - \begin{bmatrix} {}^0\mathbf{j}_{11} \\ 1 \end{bmatrix}\left({}^0D\right)^{-1}{}^0\mathbf{D}_q\right) \tag{2-35}$$

where ${}^0\mathbf{D}_q$ has dimensions 1x3, ${}^0\mathbf{J}_{12}$ has dimensions 2x3, ${}^0\mathbf{j}_{22}$ has dimensions 1x3 and ${}^0\mathbf{j}_{11}$ has dimensions 2x1.

Since ${}^0D$ is depended on the inertia of the FFSMS in reference to its CM, it is always non-zero. Consequently, substituting Eq. (2-35) into Eq. (2-33) it can be concluded that a prerequisite of the solution of the inverse kinematic problem is:

$$\det\left(\begin{bmatrix} {}^0\mathbf{J}_{12} \\ {}^0\mathbf{j}_{22} \end{bmatrix} - \begin{bmatrix} {}^0\mathbf{j}_{11} \\ 1 \end{bmatrix}\left({}^0D\right)^{-1}{}^0\mathbf{D}_q\right) \neq 0 \tag{2-36}$$

The matrix:

$$\mathbf{J}^{*}=\begin{bmatrix}{}^{0}\mathbf{J}_{12}\\ {}^{0}\mathbf{j}_{22}\end{bmatrix}-\begin{bmatrix}{}^{0}\mathbf{j}_{11}\\ 1\end{bmatrix}\left({}^{0}D\right)^{-1}{}^{0}\mathbf{D}_{q} \tag{2-37}$$

is called the Generalized Jacobian Matrix [39] . The same matrix can also be derived if h_{CM} is zero and $\dot{\theta}_0(\dot{\mathbf{q}})$ from Eq. (2-28) is substituted to Eq. (2-20) and Eq. (2-21).

After substituting ${}^{0}\mathbf{J}_{12}$, ${}^{0}\mathbf{j}_{22}$, ${}^{0}\mathbf{j}_{11}$, ${}^{0}\mathrm{D}$ and ${}^{0}\mathbf{D}_{q}$ from Eq. (2-20), Eq. (2-21) and Eq. (2-29) into the determinant of the Generalized Jacobian Matrix, it can be written as [21] :

$$\det\left(\mathbf{J}^{*}\right)=\frac{ab\,{}^{0}D_{2}\,\mathrm{s}_{q_1}+bc\,{}^{0}D_{0}\,\mathrm{s}_{q_2}-ac\,{}^{0}D_{1}\,\mathrm{s}_{q_1+q_2}}{{}^{0}D} \tag{2-38}$$

Therefore, the determinant equals zero if and only if the following quantity equals zero:

$$j^{*}=ab\,{}^{0}D_{2}\,\mathrm{s}_{q_1}+bc\,{}^{0}D_{0}\,\mathrm{s}_{q_2}-ac\,{}^{0}D_{1}\,\mathrm{s}_{q_1+q_2} \tag{2-39}$$

After substitution, j^{*} can be written as:

$$j^{*}=k_0(q_1)+k_1(q_1)\sin(q_2)+k_2(q_1)\cos(q_2) \tag{2-40}$$

where:

$$\begin{aligned}k_0&=b(aa_{22}-ca_{02})\sin(q_1)\\ k_1&=-\frac{aba_{02}+aca_{01}-2bca_{00}}{2}+c(-aa_{11}+ba_{01})\cos(q_1)+\frac{a(ba_{02}-ca_{01})\cos(2q_1)}{2}\\ k_2&=a(ba_{12}-ca_{11})\sin(q_1)+\frac{a(ba_{02}-ca_{01})\sin(2q_1)}{2}\end{aligned} \tag{2-41}$$

Eq. (2-40) can give joint angle q_2 with respect to joint angle q_1 and j^{*}:

$$\begin{aligned}q_2(q_1)&=\arcsin\left[\frac{\left(j^{*}-k_0\right)\cos\varphi}{k_1}\right]-\varphi\\ q_2(q_1)&=\pi-\arcsin\left[\frac{\left(j^{*}-k_0\right)\cos\varphi}{k_1}\right]-\varphi\end{aligned} \tag{2-42}$$

where:

$$\varphi=\arctan\left(\frac{k_2}{k_1}\right) \tag{2-43}$$

It is obvious that Eq. (2-42) and Eq. (2-43) that will be used for the finding of the dynamic singularities do not depend on the joint angle q_3. Therefore, the dynamic singularities' positions will be defined with respect to the barycenter of the 3rd link.

The distance of the 3rd link's barycenter and the system CM is defined by the equation:

$$R=\left\|R_0(\theta_0)\,{}^{0}r_3(q_1,q_2)\right\|=\left\|R_0(\theta_0)\right\|\left\|{}^{0}r_3(q_1,q_2)\right\|=\left\|{}^{0}r_3(q_1,q_2)\right\| \tag{2-44}$$

which is independent of the rotation of the base θ_0. Therefore, it can be assumed that $\theta_0 = 0$.

Thus:

$$R = \sqrt{x_3^2 + y_3^2} \Rightarrow$$
$$\Rightarrow R = \sqrt{a^2 + b^2 + c^2 + 2ab\cos(q_1) + 2ac\cos(q_1 + q_2) + 2bc\cos(q_2)} \quad (2\text{-}45)$$

where x_3 and y_3 are the x and y distance of the 3rd link's barycenter from the system CM respectively.

Eq. (2-42) and Eq. (2-43) should be substituted into Eq. (2-45) to find the positions in the Cartesian space that dynamic singularities might occur. This can be done by considering j^* = 0 and vary the joint angle q_1 in the interval [0,2π). From each of the Eq. (2-42) a pair of a minimum and a maximum distance R is derived. These pairs will demarcate two different surfaces in the workspace. These are the surfaces that if the barycenter of the 3rd link enters, a dynamic singularity might occur. It is noteworthy to point out again that the same position might develop or not a singularity depending on the rotation of the base. The subspace of these two surfaces that a dynamic singularity might occur is named Path Dependent Workspace (PDW). The rest space is named Path Independent Workspace (PIW). Figure 2-3 presents the curves q_2 (q_1) that singularities occur for a planar FFSMS with a 3 DoF manipulator as well as its Workspace.

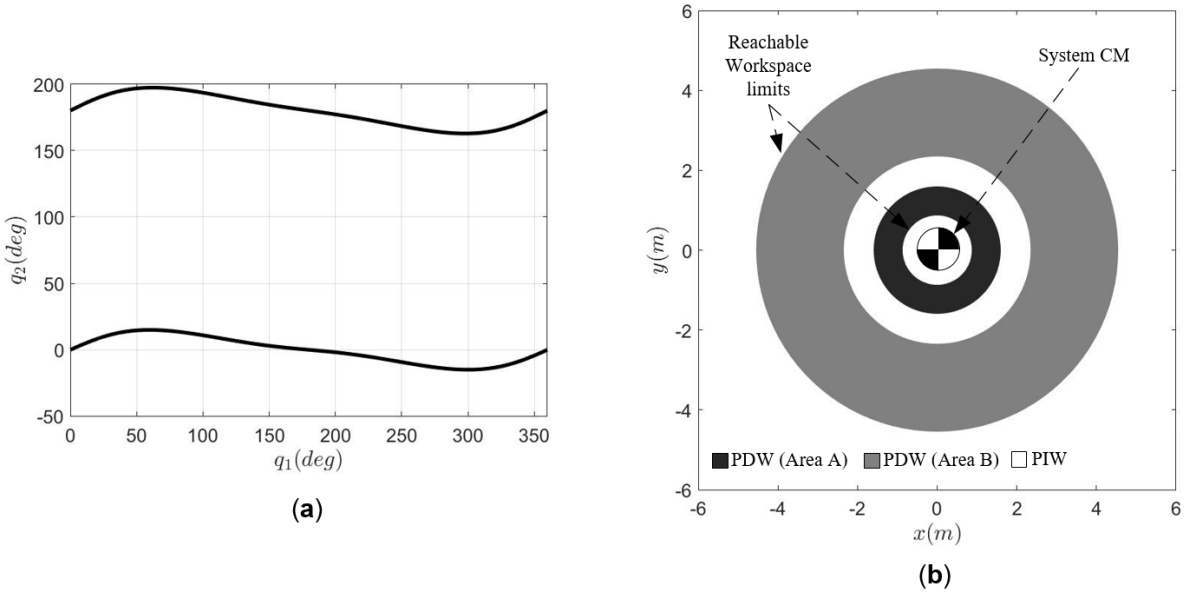

Figure 2-3. (a) Curves of Angles q_1 and q_2 of a Planar FFSMS with a 3-DoF Manipulator that Singularities occur according to Eq. (2-42) (b) Workspace of a Planar FFSMS with a 3-DoF Manipulator.

2.4 Dynamics

The formulation of the equations that describe the dynamics of an FFSMS requires the potential and the kinetic energy of the system. Since the system is considered inflexible, the potential energy is equal to zero. Hence, only the kinetic energy is required and for the general spatial problem it is given by:

$$T = \frac{1}{2}\sum_{k=0}^{N} m_k \dot{\boldsymbol{\rho}}_k \cdot \dot{\boldsymbol{\rho}}_k + \frac{1}{2}\sum_{k=0}^{N} \boldsymbol{\omega}_k \cdot \mathbf{I}_k \cdot \boldsymbol{\omega}_k \tag{2-46}$$

where m_k is the mass of the k-th body, $\mathbf{I}_k$ is the inertia matrix of the k-th body, $\boldsymbol{\omega}_k$ is the angular velocity of the k-th body and $\boldsymbol{\rho}_k$ is the position vector of the system's CM to the k-th body's CM.

After calculations and substitution of the variables [21] , the kinetic energy can be written as:

$$T = \frac{1}{2}\begin{bmatrix} {}^0\boldsymbol{\omega}_0^T & \dot{\mathbf{q}}^T \end{bmatrix} \mathbf{H}^*(\mathbf{q}) \begin{bmatrix} {}^0\boldsymbol{\omega}_0 \\ \dot{\mathbf{q}} \end{bmatrix} \tag{2-47}$$

where:

$$\begin{gathered} \mathbf{H}^*(\mathbf{q}) = \begin{bmatrix} {}^0\mathbf{D} & {}^0\mathbf{D}_q \\ {}^0\mathbf{D}_q^T & {}^0\mathbf{D}_{qq} \end{bmatrix} \\ {}^0\mathbf{D}_{qq} = \sum_{j=1}^{N}\sum_{i=1}^{N} {}^0\mathbf{F}_i^T \, {}^0\mathbf{D}_{ij} \, {}^0\mathbf{F}_j \end{gathered} \tag{2-48}$$

${}^0\mathbf{D}$, ${}^0\mathbf{D}_q$ are given by Eq. (2-27) and ${}^0\mathbf{F}$ is given by Eq. (2-14).

The next step to the derivation of the equations of motion is the application of the Lagrange method [20] . First, the Lagrangian is found:

$$L = T - U = \frac{1}{2} {}^0\boldsymbol{\omega}_0^T \, {}^0\mathbf{D} \, {}^0\boldsymbol{\omega}_0 + {}^0\boldsymbol{\omega}_0^T \, {}^0\mathbf{D}_q \dot{\mathbf{q}} + \frac{1}{2}\dot{\mathbf{q}}^T \, {}^0\mathbf{D}_{qq} \dot{\mathbf{q}} \tag{2-49}$$

where U is the total potential energy of the system.

The Lagrangian will be used in the Lagrange equations:

$$\begin{gathered} \frac{d}{dt}\left(\frac{\partial L({}^0\boldsymbol{\omega}_0, \mathbf{q}, \dot{\mathbf{q}})}{\partial {}^0\boldsymbol{\omega}_0} \right) + {}^0\boldsymbol{\omega}_0^{\times} \frac{\partial L({}^0\boldsymbol{\omega}_0, \mathbf{q}, \dot{\mathbf{q}})}{\partial {}^0\boldsymbol{\omega}_0} = \mathbf{R}_0^T \mathbf{g}_{CM} \\ \frac{d}{dt}\left(\frac{\partial L({}^0\boldsymbol{\omega}_0, \mathbf{q}, \dot{\mathbf{q}})}{\partial \dot{\mathbf{q}}} \right) - \frac{\partial L({}^0\boldsymbol{\omega}_0, \mathbf{q}, \dot{\mathbf{q}})}{\partial \mathbf{q}} = \boldsymbol{\tau} \end{gathered} \tag{2-50}$$

where $\mathbf{g}_{CM}$ is the vector of the external torques that act on the base produced by the thrusters and the reaction wheels which for an FFSMS equals zero, $(\cdot)^{\mathrm{x}}$ is the cross-product operator given by Eq. (2-16) and $\boldsymbol{\tau}$ is the vector containing the torques of the manipulator's actuators. It should be noted that for $\mathbf{g}_{CM}$ = 0, the first part of Eq. (2-50) is the differentiated angular momentum Eq. (2-26).

Finding the derivatives of Eq. (2-50), considering $\mathbf{g}_{CM}$ = 0 and substituting the velocity ${}^{0}\boldsymbol{\omega}_{0}$ from Eq. (2-26), the equations of motion for a spatial FFSMS are given by [21] :

$$\mathbf{H}\ddot{\mathbf{q}} + \mathbf{C}^{*}\dot{\mathbf{q}} + \mathbf{g}_{h} = \boldsymbol{\tau} \tag{2-51}$$

where:

$$\begin{gathered}
\mathbf{H} = {}^{0}\mathbf{D}_{qq} - {}^{0}\mathbf{D}_{q}^{T}\,{}^{0}\mathbf{D}^{-1}\,{}^{0}\mathbf{D}_{q} \\
{}^{0}\mathbf{D}_{qq} = \sum_{j=1}^{N}\sum_{i=1}^{N} {}^{0}\mathbf{F}_{i}^{T}\,{}^{0}\mathbf{D}_{ij}\,{}^{0}\mathbf{F}_{j} \\
\mathbf{C}^{*} = \mathbf{C} + \mathbf{C}_{h} \\
\mathbf{C} = \frac{1}{2}\frac{\partial\left(\dot{\mathbf{q}}^{T}\,{}^{0}\mathbf{D}_{q}^{T}\,{}^{0}\mathbf{D}^{-1}\,{}^{0}\mathbf{D}_{q}\right)}{\partial\mathbf{q}} + \frac{\partial\left({}^{0}\mathbf{D}_{qq}\dot{\mathbf{q}}\right)}{\partial\mathbf{q}} - \frac{1}{2}\frac{\partial\left(\dot{\mathbf{q}}^{T}\,{}^{0}\mathbf{D}_{qq}\right)}{\partial\mathbf{q}} - \frac{\partial\left({}^{0}\mathbf{D}_{q}^{T}\,{}^{0}\mathbf{D}^{-1}\,{}^{0}\mathbf{D}_{q}\dot{\mathbf{q}}\right)}{\partial\mathbf{q}} \\
\mathbf{C}_{h} = \frac{\partial\left({}^{0}\mathbf{D}_{q}^{T}\,{}^{0}\mathbf{D}^{-1}\mathbf{R}_{0}^{T}\mathbf{h}_{CM}\right)}{\partial\mathbf{q}} - \frac{\partial\left(\mathbf{h}_{CM}^{T}\mathbf{R}_{0}\,{}^{0}\mathbf{D}^{-1}\,{}^{0}\mathbf{D}_{q}\right)}{\partial\mathbf{q}} \\
\mathbf{g}_{h} = \frac{1}{2}\frac{\partial\left(\mathbf{h}_{CM}^{T}\mathbf{R}_{0}\,{}^{0}\mathbf{D}^{-1}\mathbf{R}_{0}^{T}\right)}{\partial\mathbf{q}}\mathbf{h}_{CM} - {}^{0}\mathbf{D}_{q}^{T}\,{}^{0}\mathbf{D}^{-1}\left[{}^{0}\mathbf{D}^{-1}\left(\mathbf{R}_{0}^{T}\mathbf{h}_{CM} - {}^{0}\mathbf{D}_{q}\dot{\mathbf{q}}\right)\right]^{\times}\mathbf{R}_{0}^{T}\mathbf{h}_{CM}
\end{gathered} \tag{2-52}$$

It is obvious that when the angular momentum is equal to zero, the terms $\mathbf{g}_h$ and $\mathbf{C}_h$ are also zero.

The aforementioned methodology and equations can be simplified significantly for the problem of a planar FFSMS with a 3-DOF manipulator. For this case, the Lagrangian is given by:

$$L(\dot{\theta}_{0}, \mathbf{q}, \dot{\mathbf{q}}) = \frac{1}{2}\,{}^{0}\mathbf{D}\,\dot{\theta}_{0} + \dot{\theta}_{0}\,{}^{0}\mathbf{D}_{q}\dot{\mathbf{q}} + \frac{1}{2}\dot{\mathbf{q}}^{T}\,{}^{0}\mathbf{D}_{qq}\dot{\mathbf{q}} \tag{2-53}$$

Because the terms of the Lagrangian are independent of the base's rotation, θ_0 is a cyclic coordinate [20] . Therefore, instead of the Lagrangian, the Routhian can be used:

$$R(\mathbf{q}, \dot{\mathbf{q}}) = L(\dot{\theta}_{0}, \mathbf{q}, \dot{\mathbf{q}}) - \frac{\partial L}{\partial \dot{\theta}_{0}}\dot{\theta}_{0} = L(\dot{\theta}_{0}, \mathbf{q}, \dot{\mathbf{q}}) - h_{CM}\dot{\theta}_{0} \tag{2-54}$$

Substituting Eq. (2-28) into the Eq. (2-54), the Routhian can be written as:

$$\begin{gathered}
R(\mathbf{q}, \dot{\mathbf{q}}) = \frac{1}{2}\dot{\mathbf{q}}^{T}\mathbf{H}(\mathbf{q})\dot{\mathbf{q}} + h_{CM}\,{}^{0}D^{-1}\,{}^{0}\mathbf{D}_{q}\dot{\mathbf{q}} - \frac{1}{2}h_{CM}^{2}\,{}^{0}D^{-1} \\
\mathbf{H}(\mathbf{q}) = {}^{0}\mathbf{D}_{qq} - {}^{0}\mathbf{D}_{q}^{T}\,{}^{0}D^{-1}\,{}^{0}\mathbf{D}_{q}
\end{gathered} \tag{2-55}$$

Finally, by using the Lagrange equation on the Routhian, the equations of motion for a planar FFSMS with a 3-DOF manipulator can be written as:

$$\mathbf{H}(\mathbf{q})\ddot{\mathbf{q}} + \mathbf{C}^{*}(\mathbf{q}, \dot{\mathbf{q}}, h_{CM})\dot{\mathbf{q}} + \mathbf{g}_{h}(\mathbf{q}, h_{CM}) = \boldsymbol{\tau} \tag{2-56}$$

where:

$$\mathbf{H}(\mathbf{q}) = {}^{0}\mathbf{D}_{qq} - {}^{0}\mathbf{D}_{q}^{T}\,{}^{0}D^{-1}\,{}^{0}\mathbf{D}_{q}$$

$${}^{0}\mathbf{D}_{qq} = \sum_{j=1}^{N}\sum_{i=1}^{N} {}^{0}\mathbf{F}_{i}^{T}\,{}^{0}\mathbf{D}_{ij}\,{}^{0}\mathbf{F}_{j}$$

$$\mathbf{C}^{*}(\mathbf{q},\dot{\mathbf{q}},h_{CM}) = \mathbf{C} + \mathbf{C}_{h}$$

$$\mathbf{C}(\mathbf{q},\dot{\mathbf{q}}) = \frac{1}{2}\frac{\partial\left(\dot{\mathbf{q}}^{T}\,{}^{0}\,{}^{0}D^{-1}\,{}^{0}\mathbf{D}_{q}\right)}{\partial\mathbf{q}} + \frac{\partial\left({}^{0}\mathbf{D}_{qq}\dot{\mathbf{q}}\right)}{\partial\mathbf{q}} - \frac{1}{2}\frac{\partial\left(\dot{\mathbf{q}}^{T}\,{}^{0}\mathbf{D}_{qq}\right)}{\partial\mathbf{q}} - \frac{\partial\left({}^{0}\mathbf{D}_{q}^{T}\,{}^{0}D^{-1}\,{}^{0}\mathbf{D}_{q}\dot{\mathbf{q}}\right)}{\partial\mathbf{q}} \qquad (2\text{-}57)$$

$$\mathbf{C}_{h}(\mathbf{q},h_{CM}) = h_{CM}\left[\frac{\partial\left({}^{0}D^{-1}\,{}^{0}\mathbf{D}_{q}^{T}\right)}{\partial\mathbf{q}} - \frac{\partial\left({}^{0}D^{-1}\,{}^{0}\mathbf{D}_{q}\right)}{\partial\mathbf{q}}\right]$$

$$\mathbf{g}_{h} = \frac{1}{2}h_{CM}^{2}\frac{\partial\left({}^{0}D^{-1}\right)}{\partial\mathbf{q}}$$

and ${}^{0}D$, ${}^{0}\mathbf{D}_{q}$ are given by Eq. (2-29) and ${}^{0}\mathbf{F}$ is given by Eq. (2-14).

3 Model Predictive Control (MPC)

3.1 Introduction

The term Model Predictive Control (MPC) designates a plethora of advanced control methods which use a model to predict the output at future time instants while minimizing an objective function to obtain the control sequence. Some other notable characteristics of these controllers is the “receding strategy” or “receding horizon” according to which the final future time instant is consistently displaced towards the future as well as the fact that only the first control signal of the sequence is applied to the plant.

The vast dissemination of MPC among the industry and the research community can be attributed to its simple implementation and its ability to discover the optimum solution based on an objective function while it compensates for measurable disturbances and dead times, and handles input and output constraints. Another important benefit is the ability to deal with multivariable problems easily. Nonetheless, MPC presents also some shortcomings. The need for an accurate model of the process and the surge of computational power when constraints are considered, are the most important drawbacks. Albeit most MPC algorithms are quite robust, the number and significance of discrepancies between the dynamic model that MPC uses and the real model is inversely proportional to the successful performance of the controller.

There are ample different categorizations of MPC algorithms. As Camacho and Bordons [3] point out, the main criteria to classify the algorithms are the model used to represent the process (and the noise) and the cost function which is minimized. The basic types of the first category include the Truncated Impulse Response Model, the Step Response Model, the Transfer Function Model and the State Space Model. The distilled idea of the first two is the measurement of the output when an impulse or step input is used to excite the process. Both of these methods are quite simple which is also the reason for the immense usage in industrial applications. The third type uses the Transfer Function of the Model to implement the MPC algorithm while the fourth uses the State Space representation of the model. As far as the second category is concerned, the main representatives are the MPC algorithms that use a quadratic cost function which consists of the past inputs and outputs as well as the future reference trajectory. However, when constraints are considered, which is one of the main advantages of MPC, different numerical algorithms are created.

Besides the aforementioned categories, some other classes of MPC which are worth mentioning too is the Robust MPC which considers the bounded disturbances of the model and the constraints. Its most common types are the Min-max MPC [4] , [13] , [1] , the Constraint Tightening MPC [9] , [35] , MPC using tubes [15] and Multi-stage MPC [17] . Apart from that, Marruedo et al. [19] proved that under certain assumptions, MPC is always stable and feasible despite the existence of uncertainties.

Although there are boundless different MPC algorithms, all of them follow a basic strategy which will be briefly presented below. As it was previously stated, MPC requires an accurate model of the process to predict the future outputs of the system. In particular, the controller predicts the outputs y on a finite horizon of N samples or time T after the present output, which is also reffered as the prediction horizon of the MPC:

$$y(t+\tau \mid t) \quad for \quad \tau \in (0, \mathrm{T}] \tag{3-1}$$

The preceding notation designates the prediction at time instant $t+\tau$ computed at time instant t. It is evident that the prediction of the outputs depends on the inputs and outputs (until the time instant t) as well as the future control sequence:

$$u(t+\tau \mid t) \quad for \quad \tau \in [0, \mathrm{T}] \tag{3-2}$$

In some MPC algorithms, the predicted horizon T which is used for the outputs is larger than the one for the control values, which is called the control horizon, to abate the required computational power. The control signal after the control horizon is considered constant.

The control signals result from the optimization of a criterion which includes information about the error between the output and the desired trajectory (or just the output) and/or the control effort. Most MPC algorithms use quadratic functions for this task which might take the form of:

$$J = \int_0^T (\mathbf{y}(t+\tau \mid t)^T \mathbf{Q}\mathbf{y}(t+\tau \mid t) + \mathbf{u}(\tau)^T \mathbf{R}\mathbf{u}(\tau)) d\tau \tag{3-3}$$

The matrices $\mathbf{Q}$ and $\mathbf{R}$ are weighting factors and can be used to tune the performance index fittingly. In the case the criterion is quadratic, the model is linear, and there is no usage of constraints, then an explicit solution can be acquired and, in some cases, it can be obtained off-line to save computational power. In all other cases, an iterative optimization method is required.

From the time-set of control signals, only the first one is sent to the process while the others are rejected. The above methodology is repeated for its time instant while the receding horizon “moves” with every step.

In Figure 3-1 a qualitative example of the application of an MPC at a time instant is presented, while in Figure 3-2 the block diagram of a basic MPC is depicted.

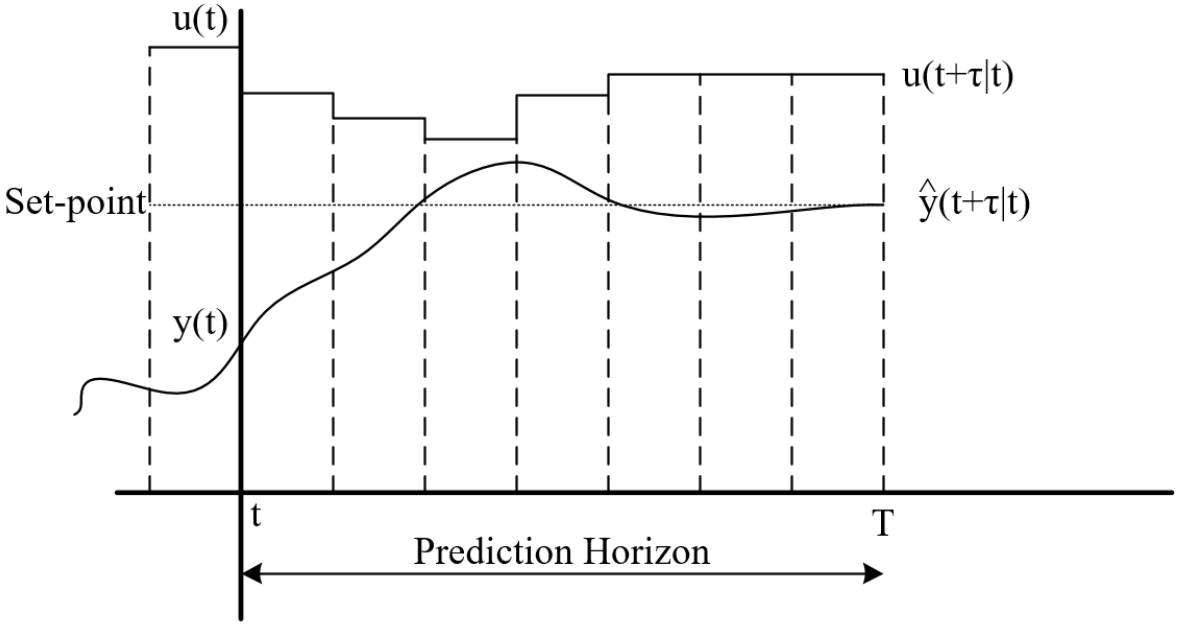

Figure 3-1. Example of Model Predictive Control’s strategy.

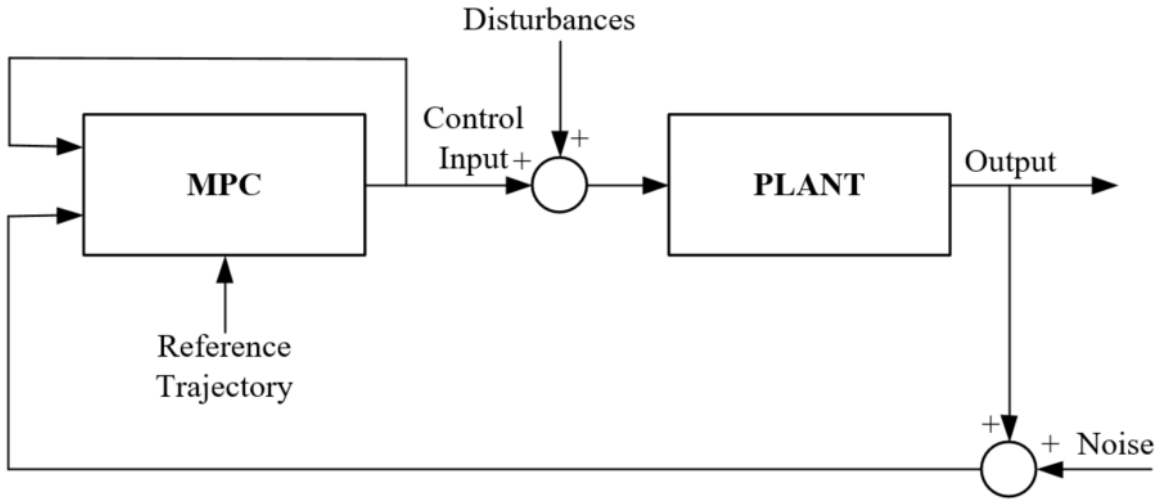

(a)

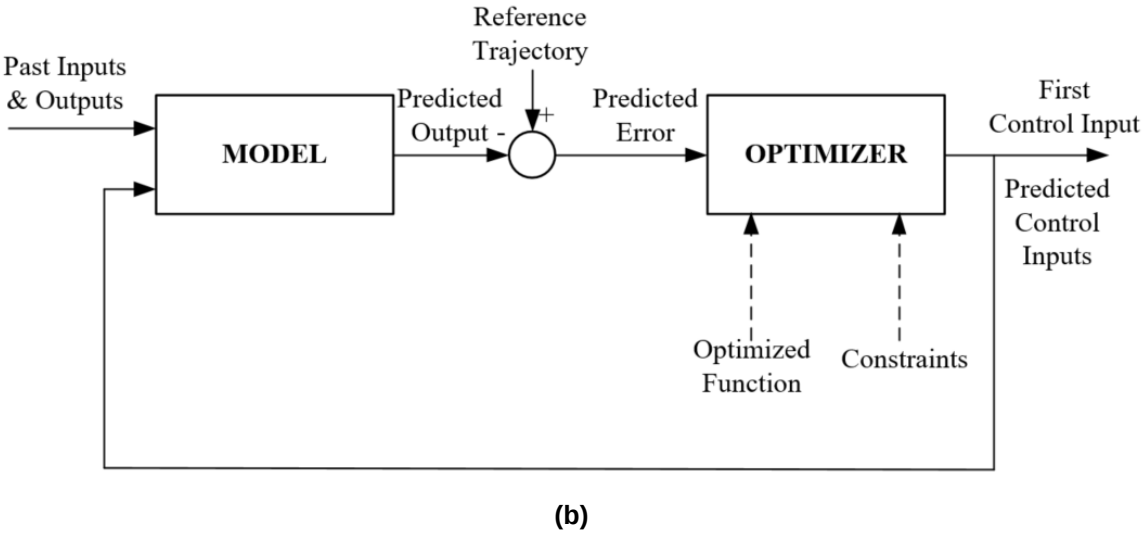

(b)

Figure 3-2. (a) Block Diagram (b) General Model Predictive Controller strategy.

The MPC algorithm that is implemented in this thesis is a linear MPC with a State Space Model due to its simplicity and its ability to deal with bounded disturbances. The technique is based on the methodology provided in the book of Wang [40] . An application of non-linear MPC was avoided because of its implementation complexity and the increase of computational power. The linearization of the model is accomplished through Feedback Linearization which is presented thoroughly in Chapter 4.

3.2 Design of Model Predictive Controller

In this section, the design of the model Predictive Controller which is used for the control of a Free-Floating Space Manipulator System (FFSMS) is presented. Although the implementation is performed in a digital environment, the controller is studied in continuous-time to connect it directly with the requirements that the study of the control of an FFSMS sets. First, the studied model is formed. After that, the so-called Laguerre functions which MPC requires to approximate the control signal are presented. Finally, the prediction and the optimization procedure are showed and the control signal of the plant is acquired.

3.2.1 Model

The model that is used for the process is an augmented model with an embedded integrator (but with the same output as the initial model) since the derivative of the control signal is required. The reason for that is the fact that the orthonormal function which is used for the representation of the control signal and will be presented in the Section 3.2.2 mandates its variable's integral squared value to be bounded (Eq. (3-12)). Consequently, the convergence to a set-point input or the counterbalance of constant disturbances require the use of the derivative.

Consider the plant is described by the following state-space model:

$$\begin{aligned} \dot{\mathbf{x}}_\mathbf{m}(t) &= \mathbf{A}_\mathbf{m}\mathbf{x}_\mathbf{m}(t) + \mathbf{B}_\mathbf{m}\mathbf{u}(t) \\ \mathbf{y}(t) &= \mathbf{C}_\mathbf{m}\mathbf{x}_\mathbf{m}(t) \end{aligned} \tag{3-4}$$

where $\mathbf{x_m}$ is the state vector of dimension n_1, $\mathbf{u}$ is the input with dimension m and $\mathbf{y}$ is the output with dimension q ($q \leq m$) and the matrices $\mathbf{A_m}$, $\mathbf{B_m}$, $\mathbf{C_m}$ contain constant values.

The differentiation of the preceding equation results in the augmented model:

$$\begin{aligned} \dot{\mathbf{x}}(t) &= \begin{bmatrix} \ddot{\mathbf{x}}_\mathbf{m}(t) \\ \dot{\mathbf{y}}(t) \end{bmatrix} = \begin{bmatrix} \mathbf{A}_\mathbf{m} & \mathbf{0}_\mathbf{m}^\mathbf{T} \\ \mathbf{C}_\mathbf{m} & \mathbf{0}_{\mathbf{q}\times\mathbf{q}} \end{bmatrix} \begin{bmatrix} \dot{\mathbf{x}}_\mathbf{m}(t) \\ \mathbf{y}(t) \end{bmatrix} + \begin{bmatrix} \mathbf{B}_\mathbf{m} \\ \mathbf{0}_{\mathbf{q}\times\mathbf{m}} \end{bmatrix} \dot{\mathbf{u}}(t) = \mathbf{A}\mathbf{x}(t) + \mathbf{B}\dot{\mathbf{u}}(t) \\ \mathbf{y}(t) &= \begin{bmatrix} \mathbf{0}_\mathbf{m} & \mathbf{I}_{\mathbf{q}\times\mathbf{q}} \end{bmatrix} \begin{bmatrix} \dot{\mathbf{x}}_\mathbf{m}(t) \\ \mathbf{y}(t) \end{bmatrix} = \mathbf{C}\mathbf{x}(t) \end{aligned} \tag{3-5}$$

where $\mathbf{x}$ is the state vector of the augmented model with dimensions $n = n_1 + q$, $\mathbf{I_{qxq}}$ is the identity matrix with dimensions $q \times q$, $\mathbf{0_{qxq}}$ is a $q \times q$ zero matrix, $\mathbf{0_{qxm}}$ is a $q \times m$ zero matrix and $\mathbf{0_m}$ is a $q \times n_1$ zero matrix.

The preceding augmented model is both controllable and observable in the assumption that the plant model described in Eq. (3-4) has a minimal realization and no zero at $s=0$.

In the case of unmeasured disturbances $\boldsymbol{\omega}(t)$, the plant model presented in Eq. (3-4) becomes:

$$\begin{aligned} \dot{\mathbf{x}}_\mathbf{m}(t) &= \mathbf{A}_\mathbf{m}\mathbf{x}_\mathbf{m}(t) + \mathbf{B}_\mathbf{m}\mathbf{u}(t) + \mathbf{B}_\mathbf{d}\boldsymbol{\omega}(t) \\ \mathbf{y}(t) &= \mathbf{C}_\mathbf{m}\mathbf{x}_\mathbf{m}(t) \end{aligned} \tag{3-6}$$

When the disturbance is a deterministic constant disturbance or a stochastic integrated white noise with the form presented in Eq. (3-7), then the augmented model compensates for these disturbances:

$$\begin{aligned} &\omega_i(t) = \int_0^t \varepsilon(\tau)d\tau \quad i = 1, 2, \ldots d \\ &with \ \mathrm{E}\left\{\frac{d\omega_i(t)}{dt}\right\} = \mathrm{E}\{\varepsilon(\tau)\} = 0, \ \mathrm{E}\{\varepsilon(t)\varepsilon(\tau)\} = W_\omega\delta(t-\tau) \end{aligned} \tag{3-7}$$

where $\varepsilon()$ is a band-limited, zero-mean, white noise, $\mathrm{E}\{\}$ is the expectation and $\delta()$ is the Dirac function.

3.2.2 Laguerre Functions & Control Signal

The MPC design that will be presented in this study, requires a set of orthonormal function to approximate the trajectory of the desired control signal. For this task, Laguerre functions [16] were selected for their efficiency in handling this issue as well as their simplicity.

To be designated as orthonormal over the interval $[0,\infty)$, a set of real functions $l_i(t)$, $i = 1,2,\ldots$ should satisfy the properties [40] :

$$\int_0^\infty l_i^2(t)dt = 1 \quad and \quad \int_0^\infty l_i(t)l_j(t)dt = 0 \;\; (i \neq j) \tag{3-8}$$

A set of orthonormal functions $l_i(t)$ is characterized as complete if the relation:

$$\int_0^\infty f(t)l_i(t)dt = 0 \tag{3-9}$$

is true for all values of i, only if $f(t)$ satisfies the relation:

$$\int_0^\infty f^2(t)dt = 0 \tag{3-10}$$

Taking into account the preceding theorem, it can be shown [16] that an arbitrary function $f(t)$ has a formal expansion with respect to a set of orthonormal and complete functions $l_i(t)$, $i = 1,2,\ldots$ over the interval $[0,\infty)$, which can be described by:

$$f(t) = \sum_{i=1}^{\infty} c_i l_i(t) \quad with \quad c_i = \int_0^\infty l_i f(t)dt \;\; (i = 1,2,...) \tag{3-11}$$

The number of the expansion's coefficients can become finite due to the completeness of the functions since it can be derived [16] that for any piece-wise continuous function $f(t)$ with:

$$\int_0^\infty f^2(t)dt < \infty \tag{3-12}$$

and any $\varepsilon>0$, there exists an integer N such that:

$$\int_0^\infty (f(t)dt - \sum_{i=1}^{N} c_i l_i(t))^2 dt < \varepsilon \tag{3-13}$$

A set of Laguerre functions $\mathbf{L}(t) = [l_1(t)\ l_2(t)\ \ldots\ l_N(t)]^T$ satisfies the properties of orthonormality and completeness described in Eq. (3-8) to Eq. (3-11) and is designated as:

$$\mathbf{L}(t) = e^{\mathbf{A}_p t}\mathbf{L}(0)$$

$$with \quad \mathbf{A_p} = \begin{bmatrix} -p & 0 & \ldots & 0 \\ -2p & -p & \ldots & 0 \\ \vdots & \ddots & \ddots & \vdots \\ -2p & \ldots & -2p & -p \end{bmatrix} \quad and \quad \mathbf{L}(0) = \sqrt{2p}\begin{bmatrix} 1 \\ 1 \\ \vdots \\ 1 \end{bmatrix} \tag{3-14}$$

where the parameter p is called the time scaling factor. It is a design requirement (as well as the number of Laguerre functions N) and determines the exponential decay rate of the set of functions.

According to Wang [40] , to apply the aforementioned theory about Laguerre functions in modelling the control signal, suppose that the augmented model is described by Eq. (3-5), t_i is the present time instant, T_p the control/prediction horizon, τ the variable within the

prediction time window $[t_i,\ t_i + T_p]$ which takes values in $[0,T_p]$ and $\mathbf{K}$ the gain matrix of the feedback control. By knowing the initial value of the state vector $\mathbf{x}(t_i)$, the control of the augmented model (derivative of the control signal) takes the form:

$$\dot{\mathbf{u}}(\tau) = -\mathbf{K}\mathbf{x}(\tau) \quad with \quad 0 \le \tau \le T_p \tag{3-15}$$

Substituting it into Eq. (3-5), the closed-loop system is described by:

$$\begin{aligned} \mathbf{x}(\tau) &= e^{(\mathbf{A}-\mathbf{BK})\tau}\mathbf{x}(t_i) \quad with \quad 0 \le \tau \le T_p \\ \dot{\mathbf{u}}(\tau) &= -\mathbf{K}e^{(\mathbf{A}-\mathbf{BK})\tau}\mathbf{x}(t_i) \end{aligned} \tag{3-16}$$

Taking into account the requirement that the eigenvalues of the closed-loop system should be strictly within the left-half complex plane, the control value decays exponentially to zero. A direct result from this fact is that the control signal of the augmented model is bounded and satisfies the requirement of Eq. (3-12):

$$\lim_{T_p \to \infty} \int_0^{T_p} \dot{\mathbf{u}}^2(\tau) d\tau < \infty \tag{3-17}$$

Hence, a set of Laguerre functions can be used to describe each of the i ($1 \le i \le m$) inputs of the control signal of the augmented model (derivative of the control signal of the plant model):

$$\dot{u}_i(\tau) = \sum_{j=1}^{\mathrm{N}} c_j l_j(t) = \mathbf{L}_i(\tau)^{\mathrm{T}} \boldsymbol{\eta}_i \qquad i = 1, 2, \ldots m \tag{3-18}$$

Where $\boldsymbol{\eta}_\mathbf{i} = [c_1 \ \ c_2 \ \ \ldots \ c_N]^{\mathrm{T}}$ is the vector of coefficients and $\mathbf{L_i}$ is the set of Laguerre function given by Eq. (3-14) for a given scaling factor p_i>0 and number of functions $\mathrm{N_i}$.

3.2.3 Prediction

One of the main characteristics of the MPC is the prediction of the plant response which is used in the optimization. Consider that the initial state variable $\mathbf{x}(t_i)$ is known, the solution of the differential Eq. (3-5) yields the predicted state space variable:

$$\mathbf{x}(t_i + \tau \mid t_i) = e^{\mathbf{A}\tau}\mathbf{x}(t_i) + \int_0^{\tau} e^{\mathbf{A}(\tau-\gamma)}\mathbf{B}\dot{\mathbf{u}}(\gamma) d\gamma \tag{3-19}$$

where $\mathbf{x}$ has dimensions n and $\dot{\mathbf{u}}$ has dimensions m.

For each one of the m inputs, there is a set of Laguerre functions $\mathbf{L}$ and coefficients $\boldsymbol{\eta}$ to describe their trajectory (see Eq. (3-18)). Therefore, there are m pairs of scaling factors p and parameters N, one for each input. These pairs are described as $\mathbf{p}$ and $\mathbf{N}$ (an exception to the classic notation since it is a vector and not a matrix) correspondingly. By substituting Eq. (3-18) into Eq. (3-19):

$$\begin{aligned} &\mathbf{x}(t_i + \tau \mid t_i) = e^{\mathbf{A}\tau}\mathbf{x}(t_i) + \boldsymbol{\Phi}(\tau)^{\mathrm{T}}\boldsymbol{\eta} \\ &with \quad \boldsymbol{\Phi}(\tau)^{\mathrm{T}} = \int_0^{\tau} e^{\mathbf{A}(\tau-\gamma)} \left[\mathbf{B_1}\mathbf{L_1}(\gamma)^{\mathrm{T}} \quad \mathbf{B_2}\mathbf{L_2}(\gamma)^{\mathrm{T}} \quad \ldots \quad \mathbf{B_m}\mathbf{L_m}(\gamma)^{\mathrm{T}} \right] d\gamma \\ &and \quad \boldsymbol{\eta} = \left[\boldsymbol{\eta}_\mathbf{1} \quad \boldsymbol{\eta}_\mathbf{2} \quad \ldots \quad \boldsymbol{\eta}_\mathbf{m} \right]^T \end{aligned} \tag{3-20}$$

where $\mathbf{B_i}$ is the i-th column of the $\mathbf{B}$ matrix.

Taking into account Eq. (3-5) and Eq. (3-20), it is evident that the predicted output is:

$$\mathbf{y}(t_i+\tau\,|\,t_i)=\mathbf{C}e^{\mathbf{A}\tau}\mathbf{x}(t_i)+\mathbf{C}\boldsymbol{\Phi}(\tau)^{\mathrm{T}}\boldsymbol{\eta} \tag{3-21}$$

By taking a closer look into Eq. (3-20), it can be concluded that the convolution integral $\boldsymbol{\Phi}(\tau)$ is uniquely determined considering that $\mathbf{A}$, $\mathbf{B}$ and $\mathbf{L}$ are known. Consequently, the coefficients $\boldsymbol{\eta}$ are the ones to capture the prediction of the state variable.

It is obvious that the numerical calculation of the integral $\boldsymbol{\Phi}(\tau)$ will consume an immense amount of computational power. For this reason, Wang [40] proved that for a given time τ, the i-th sub-matrix (dimensions n x $\mathrm{N_i}$) of the matrix $\boldsymbol{\Phi}(\tau)$ satisfies the relation:

$$\mathbf{A}\boldsymbol{\varphi}_i(\tau)^T-\boldsymbol{\Phi}_i(\tau)^T\mathbf{A}_{\mathbf{p}_i}^T=-\mathbf{B}_i\mathbf{L}_i(\tau)^T+e^{\mathbf{A}\tau}\mathbf{B}_i\mathbf{L}_i(0)^T \qquad i=1,2,\ldots m \tag{3-22}$$

where $\mathbf{L_i}(\tau)^{\mathrm{T}}$, $\mathbf{L_i}(0)^{\mathrm{T}}$ and $\mathbf{A_{p}}_i$ are given by Eq. (3-14)

The right side of Eq. (3-22) is determined. Hence, a profound abatement of the computation power can be achieved by finding the matrix $\boldsymbol{\Phi}(\tau)$ numerically through the solution of this linear algebraic equation.

3.2.4 Optimization

As was stated at the beginning of this chapter, the most usual criterion used for optimization in MPC algorithms is a quadratic function like the one presented in Eq. (3-3). This is the one that will be used for this study too. However, prior to proceeding with the function, it is crucial to point out that if the desired trajectory is a constant set-point within the prediction window given by $y_d(t_i)$, then the augmented model of Eq. (3-5) can be converted to:

$$\begin{aligned}\dot{\mathbf{x}}(t_i+\tau\,|\,t_i)&=\begin{bmatrix}\ddot{\mathbf{x}}_{\mathbf{m}}(t_i+\tau\,|\,t_i)\\ \dot{\mathbf{e}}(t_i+\tau\,|\,t_i)\end{bmatrix}=\begin{bmatrix}\mathbf{A_m} & \mathbf{0_m^T}\\ \mathbf{C_m} & \mathbf{0_{q\times q}}\end{bmatrix}\begin{bmatrix}\dot{\mathbf{x}}_{\mathbf{m}}(t_i+\tau\,|\,t_i)\\ \mathbf{e}(t_i+\tau\,|\,t_i)\end{bmatrix}+\begin{bmatrix}\mathbf{B_m}\\ \mathbf{0_{q\times m}}\end{bmatrix}\dot{\mathbf{u}}(\tau) \quad 0\le\tau\le T_p\\ \mathbf{e}(t_i+\tau\,|\,t_i)&=\begin{bmatrix}\mathbf{0_m} & \mathbf{I_{q\times q}}\end{bmatrix}\begin{bmatrix}\dot{\mathbf{x}}_{\mathbf{m}}(t_i+\tau\,|\,t_i)\\ \mathbf{e}(t_i+\tau\,|\,t_i)\end{bmatrix}=\mathbf{C}\mathbf{x}(t_i+\tau\,|\,t_i)\end{aligned} \tag{3-23}$$

since $\mathbf{e}(t_i+\tau\,|\,t_i)=\mathbf{y}(t_i+\tau\,|\,t_i)-\mathbf{y}_d(t_i)$ and $\dot{\mathbf{e}}(t_i+\tau\,|\,t_i)=\dot{\mathbf{y}}(t_i+\tau\,|\,t_i)$.

By using the new variable $\dot{\mathbf{x}}$ of the above equation, the cost function of Eq. (3-3) becomes:

$$J=\int_0^{T_p}(\mathbf{x}(t_i+\tau\,|\,t_i)^T\mathbf{Q}\mathbf{x}(t_i+\tau\,|\,t_i)+\dot{\mathbf{u}}(\tau)^T\mathbf{R}\dot{\mathbf{u}}(\tau))d\tau \quad 0\le\tau\le T_p \tag{3-24}$$

where without loss of generality it was considered $\mathbf{Q}=\mathbf{C}^T\mathbf{Q}_{old}\mathbf{C}$. The matrices $\mathbf{Q}\ge\mathbf{0}$ and $\mathbf{R}\ge\mathbf{0}$ are weighting factors and can be used to tune the performance index fittingly.

Considering $\mathbf{R}$ to be diagonal with elements r_1, r_2,… r_m as well as a sufficiently large prediction horizon T_p to assume $\dot{\mathbf{u}}\simeq 0$ for $\tau\ge T_p$, then the second term of the cost function can be written as:

$$\begin{aligned}J&=\int_0^{T_p}\dot{\mathbf{u}}(\tau)^T\mathbf{R}\dot{\mathbf{u}}(\tau)d\tau=\sum_{k=1}^{m}r_k\int_0^{T_p}\dot{u}_k(\tau)^T\dot{u}_k(\tau)d\tau\approx\sum_{k=1}^{m}r_k\int_0^{\infty}\boldsymbol{\eta}_{\mathbf{k}}^T\mathbf{L}_{\mathbf{k}}(\tau)\mathbf{L}_{\mathbf{k}}(\tau)^T\boldsymbol{\eta}_{\mathbf{k}}d\tau=\\ &=\sum_{k=1}^{m}r_{\mathbf{k}}\boldsymbol{\eta}_{\mathbf{k}}^T\boldsymbol{\eta}_{\mathbf{k}}=\boldsymbol{\eta}^T\mathbf{R}_{\mathbf{L}}\boldsymbol{\eta}\quad with\quad \mathbf{R}_{\mathbf{L}}=diag\{r_k\mathbf{I}_{\mathbf{N_k}\times\mathbf{N_k}}\}\end{aligned} \tag{3-25}$$

due to the use of the orthonormality property (Eq. (3-8)). The matrix $\mathbf{R_L}$ is a block diagonal matrix and $\mathbf{I_{NkxNk}}$ is the identity matrix with dimensions $\mathrm{N_k}$ x $\mathrm{N_k}$ (number of Laguerre functions).

By substituting Eq. (3-25) and Eq. (3-20) into Eq. (3-24), the cost function takes the form:

$$J = \int_0^{T_p} (e^{\mathbf{A}\tau}\mathbf{x}(t_i) + \mathbf{\Phi}(\tau)^{\mathrm{T}}\boldsymbol{\eta})^T \mathbf{Q}(e^{\mathbf{A}\tau}\mathbf{x}(t_i) + \mathbf{\Phi}(\tau)^{\mathrm{T}}\boldsymbol{\eta})d\tau + \boldsymbol{\eta}^T\mathbf{R}_{\mathbf{L}}\boldsymbol{\eta} \qquad 0 \le \tau \le T_p \tag{3-26}$$

After calculations, the cost function can be also written in a more convenient form:

$$\begin{aligned} &J = [\boldsymbol{\eta} + \mathbf{\Omega}^{-1}\mathbf{\Psi}\mathbf{x}(t_i)]^T \mathbf{\Omega}[\boldsymbol{\eta} + \mathbf{\Omega}^{-1}\mathbf{\Psi}\mathbf{x}(t_i)] + \mathbf{x}(t_i)^T \int_0^{T_p} e^{\mathbf{A}^T\tau}\mathbf{Q}e^{\mathbf{A}\tau}d\tau\mathbf{x}(t_i) - \mathbf{x}(t_i)^T\mathbf{\Psi}^T\mathbf{\Omega}^{-1}\mathbf{\Psi}\mathbf{x}(t_i) \\ &with \quad \mathbf{\Omega} = \int_0^{T_p} \mathbf{\Phi}(\tau)\mathbf{Q}\mathbf{\Phi}(\tau)^{\mathrm{T}}d\tau + \mathbf{R}_{\mathbf{L}} \quad \& \quad \mathbf{\Psi} = \int_0^{T_p} \mathbf{\Phi}(\tau)\mathbf{Q}e^{\mathbf{A}\tau}d\tau \qquad 0 \le \tau \le T_p \end{aligned} \tag{3-27}$$

The matrices $\mathbf{\Omega}$ and $\mathbf{\Psi}$ are constant and can be computed off-line.

Therefore, it is obvious from the preceding equation that the minimization of the cost function occurs when:

$$\boldsymbol{\eta} = -\mathbf{\Omega}^{-1}\mathbf{\Psi}\mathbf{x}(t_i) \tag{3-28}$$

and the optimized cost function is:

$$J_{\min} = \mathbf{x}(t_i)^T \left[\int_0^{T_p} e^{\mathbf{A}^T\tau}\mathbf{Q}e^{\mathbf{A}\tau}d\tau - \mathbf{\Psi}^T\mathbf{\Omega}^{-1}\mathbf{\Psi} \right] \mathbf{x}(t_i) \qquad 0 \le \tau \le T_p \tag{3-29}$$

3.2.5 Controller & Implementation

The substitution of the optimum $\boldsymbol{\eta}$ from Eq. (3-28) into Eq. (3-18) gives the optimum control signal of the augmented model over the prediction horizon considering t_i constant. In this point, it is crucial to clarify that this control signal is for each prediction horizon only since the prediction is based on the variable $\mathbf{x}(t_i + \tau \mid t_i)$ (see Eq. (3-19)). This is the reason why the optimum $\boldsymbol{\eta}$ depends on $\mathbf{x}(t_i)$ too.

The control signal of the augmented model for each time step is derived from Eq. (3-18) but considering only the first value of the Laguerre function multiplied by the optimum coefficients $\boldsymbol{\eta}$ from Eq. (3-28) and with a varying t_i. This satisfies the principle of the receding horizon control that only the control signal at $\tau=0$ is considered and the prediction horizon "moves" as the variable t_i increases. To describe it mathematically, for an arbitrary time t ($t = t_i$), the control for the augmented model is:

$$\begin{aligned} \dot{\mathbf{u}}(t) &= \begin{bmatrix} \mathbf{L_1}(0)^T & \mathbf{0_2} & \dots & \mathbf{0_m} \\ \mathbf{0_1} & \mathbf{L_2}(0)^T & \dots & \mathbf{0_m} \\ \vdots & \vdots & \ddots & \vdots \\ \mathbf{0_1} & \mathbf{0_2} & \dots & \mathbf{L_m}(0)^T \end{bmatrix} \begin{bmatrix} \boldsymbol{\eta}_1 \\ \boldsymbol{\eta}_2 \\ \vdots \\ \boldsymbol{\eta}_m \end{bmatrix} = \\ &= -\begin{bmatrix} \mathbf{L_1}(0)^T & \mathbf{0_2} & \dots & \mathbf{0_m} \\ \mathbf{0_1} & \mathbf{L_2}(0)^T & \dots & \mathbf{0_m} \\ \vdots & \vdots & \ddots & \vdots \\ \mathbf{0_1} & \mathbf{0_2} & \dots & \mathbf{L_m}(0)^T \end{bmatrix} \mathbf{\Omega}^{-1}\mathbf{\Psi} \begin{bmatrix} \dot{\mathbf{x}}_{\mathbf{m}}(t) \\ \mathbf{y}(t) - \mathbf{y}_d(t) \end{bmatrix} \end{aligned} \tag{3-30}$$

It is obvious that the presented MPC is by nature a state feedback control, since it depends on the current state variable $\mathbf{x}(t)$. Hence, the feedback gain matrix of the controller is:

$$K_{MPC} = \begin{bmatrix} \mathbf{L_1}(0)^T & \mathbf{0_2} & \dots & \mathbf{0_m} \\ \mathbf{0_1} & \mathbf{L_2}(0)^T & \dots & \mathbf{0_m} \\ \vdots & \vdots & \ddots & \vdots \\ \mathbf{0_1} & \mathbf{0_2} & \dots & \mathbf{L_m}(0)^T \end{bmatrix} \mathbf{\Omega}^{-1}\mathbf{\Psi} \tag{3-31}$$

The ultimate goal is to obtain the control signal for the plant model. This can be done through the integration of the control signal of the augmented plant given by Eq. (3-30):

$$\mathbf{u}(t) = \int_0^t \dot{\mathbf{u}}(\gamma) d\gamma \tag{3-32}$$

3.3 Constraints

The effective handling and easy integration of input and/or output constraints is one of the main advantages of MPC. The most frequent used types of constraints are three:

- Constraints on the derivative of the manipulated variable $\dot{\mathbf{u}}$
- Constraints on the amplitude of the manipulated variable $\mathbf{u}$
- Constraints on the output $\mathbf{y}$ or state variable $\mathbf{x}$

In this thesis, the last two types of constraints are presented considering the requirements that the following study of FFSMS sets. The constraints have to become a part of the MPC strategy and be embedded in the procedure. Therefore, after taking the form of linear inequalities, the constraints use the same orthonormal basis function as the ones presented in *Section 3.1* and affects the parameter vector $\boldsymbol{\eta}$. This task requires the usage of a method called Hildreth's quadratic programming procedure that is presented in *Section 3.2.1*. A notable characteristic of MPC with constraints is that the nature of receding horizon implies that the constraints may vary with the progression of the horizon.

3.3.1 Integration of Constraints & Hildreth's Quadratic Programming Procedure

In this section, the integration of the constraints into the optimization procedure is studied, a prerequisite for the handling of the constraints by an MPC. Some basic quadratic programming information is presented to comprehend the distilled idea of Hildreth's quadratic programming procedure.

After calculations in Eq. (3-27), the cost function can also take the form:

$$\begin{aligned} &J = \boldsymbol{\eta}^T \mathbf{\Omega} \boldsymbol{\eta} + 2\boldsymbol{\eta}^T \mathbf{\Psi} \mathbf{x}(t_i) + \mathbf{x}(t_i)^T \int_0^{T_p} e^{\mathbf{A}^T \tau} \mathbf{Q} e^{\mathbf{A}\tau} d\tau \mathbf{x}(t_i) \qquad 0 \le \tau \le T_p \\ &with \quad \mathbf{\Omega} = \int_0^{T_p} \mathbf{\Phi}(\tau) \mathbf{Q} \mathbf{\Phi}(\tau)^{\mathrm{T}} d\tau + \mathbf{R_L}, \quad \mathbf{\Psi} = \int_0^{T_p} \mathbf{\Phi}(\tau) \mathbf{Q} e^{\mathbf{A}\tau} d\tau \\ &\& \quad \mathbf{\Phi}(\tau)^{\mathrm{T}} = \int_0^{\tau} e^{\mathbf{A}(\tau-\gamma)} \mathbf{B} \mathbf{L}(\gamma)^{\mathrm{T}} d\gamma \end{aligned} \tag{3-33}$$

Let's also consider that the constraints are in the form of linear inequalities:

$$\mathbf{A}_{constr} \boldsymbol{\eta} \le \mathbf{b} \tag{3-34}$$

Since the last term in Eq. (3-33) is constant and not affected by $\boldsymbol{\eta}$, the cost function can be written in a more convenient way:

$$J' = \frac{J - \mathbf{x}(t_i)^T \int_0^{T_p} e^{\mathbf{A}^T\tau}\mathbf{Q}e^{\mathbf{A}\tau}d\tau\mathbf{x}(t_i)}{2} = \frac{1}{2}\boldsymbol{\eta}^T\mathbf{E}\boldsymbol{\eta} + \boldsymbol{\eta}^T\mathbf{f} \qquad (3\text{-}35)$$
$$with \;\; \mathbf{E} = \boldsymbol{\Omega}, \quad \mathbf{f} = 2\boldsymbol{\Psi}\mathbf{x}(t_i)$$

If the constraints were equalities only, they could be easily integrated into the cost function using some parameters called Lagrange multipliers:

$$J' = \frac{1}{2}\boldsymbol{\eta}^T\mathbf{E}\boldsymbol{\eta} + \boldsymbol{\eta}^T\mathbf{f} + \boldsymbol{\lambda}^T(\mathbf{A}_{constr}\boldsymbol{\eta} - \mathbf{b}) \;\; \& \;\; \mathbf{A}_{constr}\boldsymbol{\eta} = \mathbf{b} \qquad (3\text{-}36)$$
$$with \;\; \mathbf{E} = \boldsymbol{\Omega}, \quad \mathbf{f} = 2\boldsymbol{\Psi}\mathbf{x}(t_i)$$

Using this method, from now on the variable of the objective function is not only $\boldsymbol{\eta}$ but also $\boldsymbol{\lambda}$. By setting the first derivatives of the cost function of Eq. (3-36) with respect to $\boldsymbol{\eta}$ and $\boldsymbol{\lambda}$ equal to zero (condition for extremum):

$$\frac{\partial J'}{\partial \boldsymbol{\eta}} = \mathbf{E}\boldsymbol{\eta} + \mathbf{f} + \mathbf{A}_{constr}^T\boldsymbol{\lambda} = 0$$
$$\frac{\partial J'}{\partial \boldsymbol{\lambda}} = \mathbf{A}_{constr}\boldsymbol{\eta} - \mathbf{b} = 0 \qquad (3\text{-}37)$$

The solution of the linear system yields the optimal $\boldsymbol{\eta}$ and $\boldsymbol{\lambda}$ (where the first term of $\boldsymbol{\eta}$ is the global optimal solution of the cost function without constraints):

$$\boldsymbol{\lambda} = -(\mathbf{A}_{constr}\mathbf{E}^{-1}\mathbf{A}_{constr}^T)^{-1}(\mathbf{b} + \mathbf{A}_{constr}\mathbf{E}^{-1}\mathbf{f})$$
$$\boldsymbol{\eta} = -\mathbf{E}^{-1}\mathbf{A}_{constr}^T\boldsymbol{\lambda} - \mathbf{E}^{-1}\mathbf{f} \qquad (3\text{-}38)$$

The preceding method which was used for equality constraints can be extended to satisfy inequality constraints too, using the Kuhn-Tucker Conditions [14] . In particular, by designating an inequality $\mathbf{A}_{constr,i}\boldsymbol{\eta}_i \le b_i$ as active condition if $\mathbf{A}_{constr,i}\boldsymbol{\eta}_i = b_i$ and as inactive if $\mathbf{A}_{constr,i}\boldsymbol{\eta}_i < b_i$, Eq. (3-37) can be used for inequality constraints too if $\boldsymbol{\lambda}$=0 for inactive conditions($\mathbf{A}_{constr,i}$ is the *i*th row of the matrix). The Kuhn-Tucker conditions can be expressed in the form:

$$\mathbf{E}\boldsymbol{\eta} + \mathbf{f} + \mathbf{A}_{constr}^T\boldsymbol{\lambda} = 0$$
$$\mathbf{A}_{constr}\boldsymbol{\eta} - \mathbf{b} \le 0$$
$$\boldsymbol{\lambda}^T(\mathbf{A}_{constr}\boldsymbol{\eta} - \mathbf{b}) = 0$$
$$\boldsymbol{\lambda} \ge 0 \qquad (3\text{-}39)$$

It is worth to mention that the active constraints need to be linearly independent and the number of active constraints needs to be less or equal to that of the decision variables.

To minimize the computational load, the solution of the aforementioned problem (Eq. (3-39)) is not based on the decision variables $\boldsymbol{\eta}$ (primal variables) but on the Lagrange multipliers $\boldsymbol{\lambda}$ (dual variables)). Consider that there exists a feasible point $\boldsymbol{\eta}$, the solution of the Eq. (3-36) can be expressed as:

$$\max_{\boldsymbol{\lambda}\ge 0}\min_{\boldsymbol{\eta}}\left[\frac{1}{2}\boldsymbol{\eta}^T\mathbf{E}\boldsymbol{\eta} + \boldsymbol{\eta}^T\mathbf{f} + \boldsymbol{\lambda}^T(\mathbf{A}_{constr}\boldsymbol{\eta} - \mathbf{b})\right] \qquad (3\text{-}40)$$

Substituting the optimal $\boldsymbol{\eta}$ of Eq. (3-38) into the preceding equation:

$$\max_{\boldsymbol{\lambda}\geq 0}\left[-\frac{1}{2}\boldsymbol{\lambda}^T\mathbf{H}\boldsymbol{\lambda}-\boldsymbol{\lambda}^T\mathbf{k}-\frac{1}{2}\mathbf{f}^T\mathbf{E}^{-1}\mathbf{f}\right] \quad \text{with} \quad \mathbf{H}=\mathbf{A}_{constr}\mathbf{E}^{-1}\mathbf{A}_{constr}{}^T \;\;\&\;\; \mathbf{k}=\mathbf{b}+\mathbf{A}_{constr}\mathbf{E}^{-1}\mathbf{f} \tag{3-41}$$

The third term of Eq. (3-41) is independent of $\boldsymbol{\lambda}$. Therefore, an equivalent cost function which minimization results in the same values of $\boldsymbol{\lambda}$ is:

$$\min_{\boldsymbol{\lambda}\geq 0}\left[\frac{1}{2}\boldsymbol{\lambda}^T\mathbf{H}\boldsymbol{\lambda}+\boldsymbol{\lambda}^T\mathbf{k}\right] \quad \text{with} \quad \mathbf{H}=\mathbf{A}_{constr}\mathbf{E}^{-1}\mathbf{A}_{constr}{}^T \;\;\&\;\; \mathbf{k}=\mathbf{b}+\mathbf{A}_{constr}\mathbf{E}^{-1}\mathbf{f} \tag{3-42}$$

which is also the form of the required dual problem.

Hildreth's quadratic programming procedure was proposed in [10] to solve the aforementioned dual problem. It is a simple iterative algorithm that runs until the convergence of the Lagrange multipliers $\boldsymbol{\lambda}$ is achieved. According to this method, the variables $\boldsymbol{\lambda}$ are given by:

$$\begin{aligned}\lambda_i^{p+1} &= \max(0, w_i^{p+1})\\ w_i^{p+1} &= -\frac{1}{h_{ii}}\left(k_i+\sum_{j=1}^{i-1}h_{ij}\lambda_j^{p+1}+\sum_{j=i+1}^{m}h_{ij}\lambda_j^{p}\right)\end{aligned} \tag{3-43}$$

where on the up-right corner of the variables λ and w, the iteration cycle is denoted and on the down-right corner of the variables λ, w, k, and h, the number of the element. The h_{ij} is the ij-th element of the matrix $\mathbf{H}$, and k_i is the i-th element of the vector $\mathbf{k}$. The iteration cycle begins by setting $\boldsymbol{\lambda}^0 = [0, 0, \ldots 0]$. After the convergence is accomplished, the optimal $\boldsymbol{\lambda}_{\text{opt}}$ is substituting in the second part of Eq. (3-38) to find the optimal decision variables $\boldsymbol{\eta}$. It is noteworthy to point out that in most cases even if the constraints are ill-defined (linearly dependent and/or active constraints are more than decision variables), the algorithm will give a near-optimal solution.

3.3.2 Constraints on the Amplitude of the Manipulated Variable

As it was stated in the previous section and can be clearly concluded from Eq. (3-34), the constraints should take the form of linear inequalities. By setting an upper and lower limit for the amplitude of the control signal, the following inequalities are derived:

$$\mathbf{u}_{\min}\leq\mathbf{u}(t_i)\leq\mathbf{u}_{\max} \tag{3-44}$$

Assuming adequately small sampling interval Δt and using Eq. (3-30), the constraints for the control signal at the first sample time are:

$$\begin{aligned}&\frac{\mathbf{u}_{\min}-\mathbf{u}(t_i-\Delta t)}{\Delta t}\leq\frac{\mathbf{u}(t_i)-\mathbf{u}(t_i-\Delta t)}{\Delta t}\leq\frac{\mathbf{u}_{\max}-\mathbf{u}(t_i-\Delta t)}{\Delta t}\Rightarrow\\ &\mathbf{u}_{\min}-\mathbf{u}(t_i-\Delta t)\leq\Delta t\mathbf{L}(0)^T\boldsymbol{\eta}\leq\mathbf{u}_{\max}-\mathbf{u}(t_i-\Delta t)\end{aligned} \tag{3-45}$$

The previous equation can be written in a more convenient form:

$$\begin{bmatrix}\Delta t\mathbf{L}(0)^T\\ -\Delta t\mathbf{L}(0)^T\end{bmatrix}\boldsymbol{\eta}\leq\begin{bmatrix}\mathbf{u}_{\max}-\mathbf{u}(t_i-\Delta t)\\ -(\mathbf{u}_{\min}-\mathbf{u}(t_i-\Delta t))\end{bmatrix} \tag{3-46}$$

which is a suitable form for the method presented in *Section 3.2.1*.

3.3.3 Constraints on the Output or State Variable

To set constraints on the initial state-space problem (Eq. (3-4), an equation that related all the derivatives and the values of the constraints has to be found. Introducing an upper and lower limit on the *j*-th element of the state variable $\mathbf{x_m}$:

$$x_{m(j),\min} \le x_{m(j)}(t_i) \le x_{m(j),\max} \tag{3-47}$$

Assuming adequately small sampling interval Δt, Eq. (3-47) can set constraints on the first derivative of the variable:

$$\frac{x_{m(j),\min} - x_{m(j)}(t_i - \Delta t)}{\Delta t} \le \dot{x}_{m(j)}(t_i) \le \frac{x_{m(j),\max} - x_{m(j)}(t_i - \Delta t)}{\Delta t} \Rightarrow \\ \dot{x}_{m(j),\min} \le \dot{x}_{m(j)}(t_i) \le \dot{x}_{m(j),\max} \tag{3-48}$$

Following the same procedure, the second derivative can be written as:

$$\frac{\dot{x}_{m(j),\min} - \dot{x}_{m(j)}(t_i - \Delta t)}{\Delta t} \le \ddot{x}_{m(j)}(t_i) \le \frac{\dot{x}_{m(j),\max} - \dot{x}_{m(j)}(t_i - \Delta t)}{\Delta t} \Rightarrow \\ \ddot{x}_{m(j),\min} \le \ddot{x}_{m(j)}(t_i) \le \ddot{x}_{m(j),\max} \tag{3-49}$$

The same method is used for higher derivatives, if it is required.

Considering a SISO system, by substituting Eq. (3-47)-(3-49) into the augmented model (Eq. (3-5) (the output may contain the error if it is a set-point trajectory), the following is obtained:

$$\dot{\mathbf{x}}_{\min} - \mathbf{A}\mathbf{x}_{\min} \le \mathbf{b}\dot{\mathbf{u}}(t_i) \le \dot{\mathbf{x}}_{\max} - \mathbf{A}\mathbf{x}_{\max} \tag{3-50}$$

where $\mathbf{b}$ is the corresponding SISO vector of the matrix $\mathbf{B}$ from Eq. (3-5). The $\mathbf{x}_{\min}$ and $\mathbf{x}_{\max}$ contain either the derivatives of the constrained state variable $x_{m(j)}$ taking by Eq. (3-47)-(3-49) or the past values of the independent state variables. The same applies for $\dot{\mathbf{x}}_{\min}$ and $\dot{\mathbf{x}}_{\max}$.

By considering Eq. (3-30), Eq. (3-50) can be written as:

$$\dot{\mathbf{x}}_{\min} - \mathbf{A}\mathbf{x}_{\min} \le \mathbf{b}\mathbf{L}(0)^T \boldsymbol{\eta}(t_i) \le \dot{\mathbf{x}}_{\max} - \mathbf{A}\mathbf{x}_{\max} \tag{3-51}$$

In most cases, the control signal is applied only in one equation of the state space model. Therefore, the above methodology is simplified profoundly.

It is notable to point out that the output constraints may result in severe nonlinearities which may lead to close-loop oscillation or instability. Therefore, they should be regarded as soft constraints, which means that they have to be “relaxed” in case the performance of the model is not the desired one. This problem can also be tackled by setting input constraints as a priority.

3.4 Example: Design of MPC Controller for a Simple Mass-Damper-Spring Model

Consider a body with mass m = 10kg attached to a vertical wall with a spring of spring constant k = 5N/m and a damper with damping coefficient b = 5Ns/m. The body can move at the horizontal x direction. A force u is applied to the body calculated by an MPC. Assuming the body is stable at $x = 0$, it has to reach the set-point of $x_d = 1\text{m}$. The whole dynamic model is depicted in Figure 3-3.

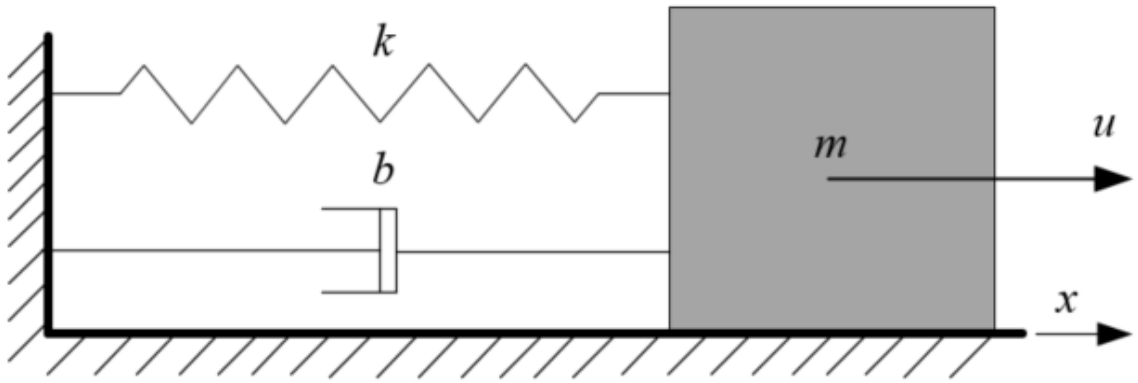

Figure 3-3. Dynamic model containing mass, damper and spring.

The first step is to find the dynamic equation of the model, using Lagrangian mechanics:

$$m\ddot{x}(t)+b\dot{x}(t)+kx(t)=u(t) \tag{3-52}$$

Then, the state-space model can be formed:

$$\begin{aligned}\dot{\mathbf{x}}_\mathbf{m}(t)&=\mathbf{A}_\mathbf{m}\mathbf{x}_\mathbf{m}(t)+\mathbf{B}_\mathbf{m}u(t)\\ y(t)&=\mathbf{C}_\mathbf{m}\mathbf{x}_\mathbf{m}(t)\end{aligned} \tag{3-53}$$

$$with\ \ \mathbf{x}_\mathbf{m}=\begin{bmatrix}x_{m,1}\\ x_{m,2}\end{bmatrix}=\begin{bmatrix}x\\ \dot{x}\end{bmatrix},\ \mathbf{A}_\mathbf{m}=\begin{bmatrix}0 & 1\\ -\frac{k}{m} & -\frac{b}{m}\end{bmatrix},\ \mathbf{B}_\mathbf{m}=\begin{bmatrix}0\\ \frac{1}{m}\end{bmatrix},\ \mathbf{C}_\mathbf{m}=\begin{bmatrix}1 & 0\end{bmatrix}$$

To implement the MPC algorithm, the augmented model of Eq. (3-5) is formed:

$$\begin{aligned}\dot{\mathbf{x}}(t)&=\mathbf{A}\mathbf{x}(t)+\mathbf{B}\dot{u}(t)\\ y(t)&=\mathbf{C}\mathbf{x}(t)\end{aligned} \tag{3-54}$$

$$with\ \ \mathbf{x}=\begin{bmatrix}\dot{x}_{m,1}\\ \dot{x}_{m,2}\\ y\end{bmatrix},\ \mathbf{A}=\begin{bmatrix}0 & 1 & 0\\ -\frac{k}{m} & -\frac{b}{m} & 0\\ 1 & 0 & 0\end{bmatrix},\ \mathbf{B}=\begin{bmatrix}0\\ \frac{1}{m}\\ 0\end{bmatrix},\ \mathbf{C}=\begin{bmatrix}0 & 0 & 1\end{bmatrix}$$

The next step is to determine the scaling factor p, the number of Laguerre functions N as well as the prediction horizon T_p. The last two parameters should be considered as large as possible to achieve adequate representation of the control signal using Laguerre functions. However, the larger they are, the more computationally demanding the algorithm is. After ample tests, they have been chosen as: T_p = 10s and N = 10.

The scaling factor p is chosen equal to the absolute value of the dominant pole of the Linear Quadratic Regulator problem [40] . By using the Matlab function lqr(), the poles are determined. Therefore, the scaling factor is chosen as p = 2.3075.

Finally, the parameters $\mathbf{Q}$ and $\mathbf{R}$ are selected to achieve the best performance, without any force limit. For this reason, they are chosen as:

$$\mathbf{Q} = \mathbf{C}'\mathbf{C} = \begin{bmatrix} 0 & 0 & 0 \\ 0 & 0 & 0 \\ 0 & 0 & 1 \end{bmatrix} \quad \& \quad \mathbf{R} = r = 10^{-5} \tag{3-55}$$

Having determined the aforementioned parameters, the methodology which was presented in Section 3.2 is followed to apply the unconstrained MPC and the methodology presented in Section 3.3 for the constrained MPC. After the implementation, the MPC gains and the poles of the augmented controlled system are:

- K_{mpc} = [410.07 86.00 960.12]
- Poles: -2.24 ± 3.97i, -4.61

Figure 3-4 presents the position and the error of the unconstrained and the constrained problem, considering output limit $x_{max} = 1.081\text{m}$. It is calculated that the maximum position of the unconstrained problem is $x_{max} = 1.082\text{m}$, while in the constrained problem the position does not exceed the regarded limit. The output limit could have been set even lower, but it would have resulted in an immense surge of the control force at some time points, as it is shown by Figure 3-5.

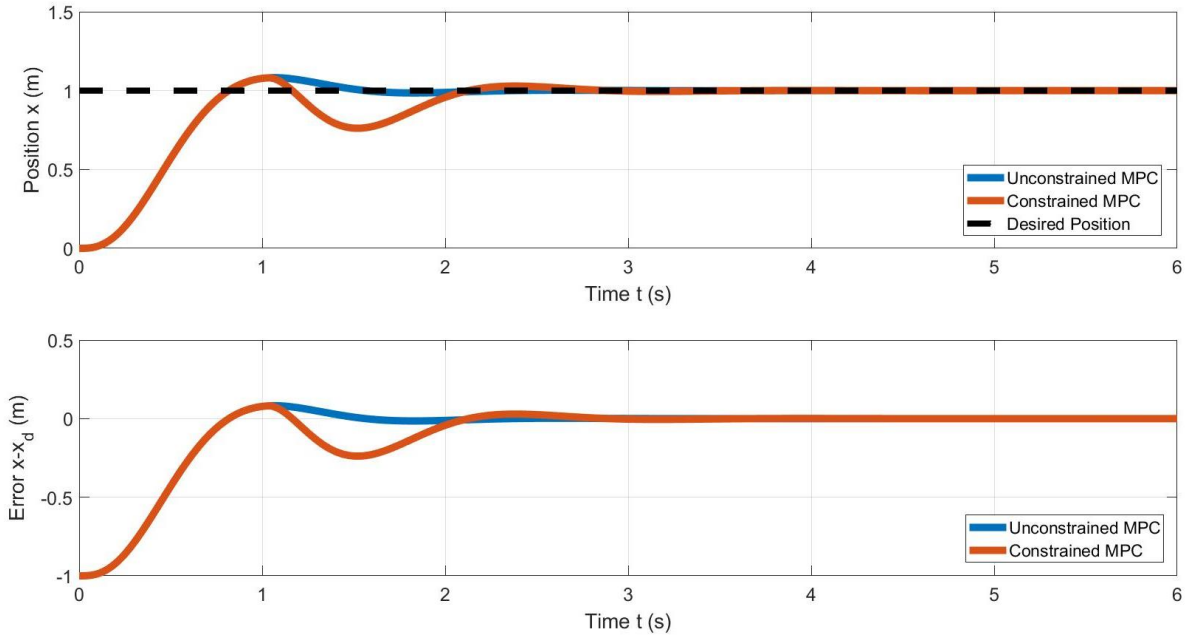

Figure 3-4. Position and error of the Constrained and the Unconstrained MPC for the mass-damper-spring example.

Figure 3-5 shows the control force of the unconstrained and the constrained problem. It can be clearly realized that at time instant $t = 1.033\text{s}$, when the position tends to exceed the output limit, the control force plummets to compensate for it. If the output limit had been set lower, the absolute value of the control force would have been even larger and after a point it would have resulted in close-loop oscillation or instability.

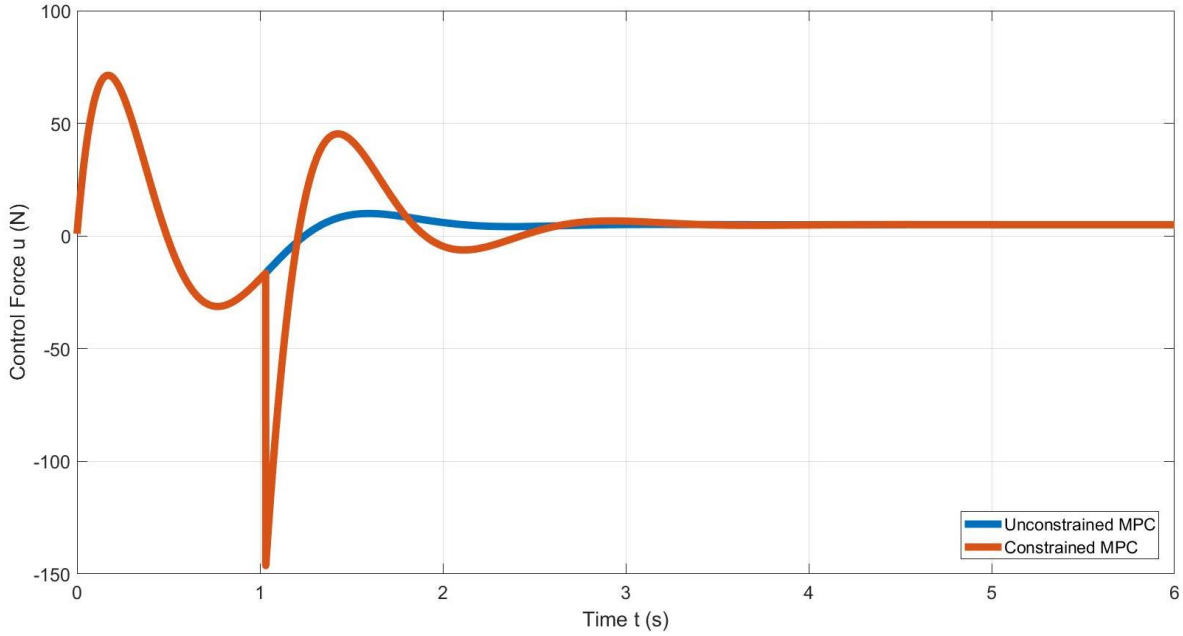

Figure 3-5. Control force of the Constrained and the Unconstrained MPC for the mass-damper-spring example.

In this thesis, two methods are used to tackle the problem of instability of the output constraints. According to the first, safety constraints on the controller's input can be considered as a higher priority to the output constraints. Therefore, if the control force exceeds the input limit, the input constraints become active and they will be the ones that produce the next control signal. According to the other method, the output constraints can become active only for a limited time period. Both of these methods are discussed in Chapter 4 more thoroughly. Apart from them, the problem of disturbances, model parameter uncertainties, as well as noise is presented in Chapter 5 and the performance of the MPC is compared to the performance of a PID controller.

4 Implementation of Model Predictive Controller (MPC) to Free-Floating Space Manipulator Systems (FFSMS)

4.1 Introduction

In this chapter, the MPC presented in Chapter 3 is applied to an FFSMS for both motions in the joint and Cartesian space. Evidently, prerequisites for the implementation are the equations which describe the MPC and can be found in Chapter 3 as well as the equations of the kinematics and dynamics of an FFSMS which can be found in Chapter 2.

As it was stated in Chapter 2, the dynamics of an FFSMS manifest intense non-linearities. The implementation of the preceding MPC requires a linear system. Consequently, the FFSMS should be linearized. The methodology that was chosen to tackle this problem is the Feedback Linearization or, in other words, a Model-Based Controller. According to this method, the model of the system is used to compensate for the non-linear terms and form a linear system. It is obvious that the method -as well as the MPC- requires an accurate model of the system. Any parametric uncertainties would be regarded as non-constant disturbances. Another profound characteristic of this technique is the de-coupling of the manipulator, since the equation that describes the errors of each joint is not affected by the other joints.

First, the Design of a Model Based PD and PID Controller is presented for motion in the joint space. Since the scenarios of Chapter 5 contain a planar FFSMS with a 3-DoF manipulator, the design is based on these data. After that, the design of a Model Based PD Controller with an auxiliary MPC input is presented. Next step is the derivation of the aforementioned controllers for motion in the Cartesian space too. The evaluation of the controllers requires simulations which are accomplished with the help of Matlab/Simulink and MSC Adams for the formation of the plant. The procedure that is followed for the design of the plant is also presented. Finally, an example implementing both Model Based PID Controller and Model Based PD Controller with MPC input is presented.

4.2 Design of a Controller in the Joint Space

There are ample occasions that require the determination of the manipulator's motion in the joint space. Primary examples are the regulation of the manipulator to achieve a desired form and the trajectory tracking in the joint space for deployment. As it was mentioned Section 4.1, the implementation of an MPC requires the design of Model Based PD Controller.

4.2.1 Model Based PD & PID Controller

The main requirement for the application of a controller is the equation that describes the dynamics of the system. For a planar FFSMS with a 3-DoF manipulator, it is given by Eq. (2-56) and it is repeated here for facilitation:

$$\mathbf{H}(\mathbf{q})\ddot{\mathbf{q}} + \mathbf{C}^{*}(\mathbf{q}, \dot{\mathbf{q}}, h_{CM})\dot{\mathbf{q}} + \mathbf{g}_{h}(\mathbf{q}, h_{CM}) = \boldsymbol{\tau} \tag{4-1}$$

where $\mathbf{H(q)}$, $\mathbf{C}^*(\mathbf{q},\dot{\mathbf{q}},h_{CM})$ and $\mathbf{g}_h(\mathbf{q},h_{CM})$ are given by Eq. (2-57), h_{CM} is the initial angular momentum which is considered as zero, $\mathbf{q}$ is the vector containing the manipulators angles and $\boldsymbol{\tau}$ is the vector containing the torques of the joints of the manipulator:

$$\begin{aligned}\mathbf{q} &= \begin{bmatrix} q_1 & q_2 & q_3 \end{bmatrix}^T \\ \boldsymbol{\tau} &= \begin{bmatrix} \tau_1 & \tau_2 & \tau_3 \end{bmatrix}^T\end{aligned} \tag{4-2}$$

The primary purpose of a Model Based Controller is to convert a non-linear system to a linear one. This can be accomplished by using the model to compensate for the non-linear terms. Considering that the matrices and vector $\mathbf{H(q)}$, $\mathbf{C}^*(\mathbf{q},\dot{\mathbf{q}},h_{CM})$ and $\mathbf{g}_h(\mathbf{q},h_{CM})$ can be accurately calculated using the model, the desired trajectories of the angles $\mathbf{q}_d(t)$, the angular velocities $\dot{\mathbf{q}}_d(t)$ and the angular accelarations $\ddot{\mathbf{q}}_d(t)$ of the joints are defined and sensors are used for the measurement of the manipulator's joints angles $\mathbf{q}$ and angular velocities $\dot{\mathbf{q}}$, the Model Based PD Controller takes the form:

$$\boldsymbol{\tau} = \hat{\mathbf{H}}\left[\ddot{\mathbf{q}}_d + \mathbf{K}_D\left(\dot{\mathbf{q}}_d - \dot{\mathbf{q}}\right) + \mathbf{K}_P\left(\mathbf{q}_d - \mathbf{q}\right)\right] + \hat{\mathbf{C}}^*\dot{\mathbf{q}} + \hat{\mathbf{g}}_h \tag{4-3}$$

where $\mathbf{K_D}$ and $\mathbf{K_P}$ are 3x3 diagonal matrices containing the gains of the PD part of the controller which determines the desired dynamic response of the system and the hat (^) above $\mathbf{H}$, $\mathbf{C}^*$ and $\mathbf{g}_h$ indicates that they are conjectured and not perfectly known.

Substituting Eq. (4-3) into Eq. (4-1) the equations of dynamics of the angles' errors are given by:

$$\begin{aligned}\ddot{\mathbf{e}} + \mathbf{K}_D\dot{\mathbf{e}} + \mathbf{K}_P\mathbf{e} &= \hat{\mathbf{H}}^{-1}\left(\left(\mathbf{H} - \hat{\mathbf{H}}\right)\ddot{\mathbf{q}} + \left(\mathbf{C}^* - \hat{\mathbf{C}}^*\right)\dot{\mathbf{q}} + \mathbf{g}_h - \hat{\mathbf{g}}_h\right) \\ \mathbf{e} &= \mathbf{q}_d - \mathbf{q}\end{aligned} \tag{4-4}$$

If the estimations of the matrices are accurate enough, the right part of the preceding equation equals zero and the errors' dynamics are described by:

$$\begin{aligned}\ddot{\mathbf{e}} + \mathbf{K}_D\dot{\mathbf{e}} + \mathbf{K}_P\mathbf{e} &= 0 \\ \mathbf{e} &= \mathbf{q}_d - \mathbf{q}\end{aligned} \tag{4-5}$$

These equations describe a decoupled system of linear equations. If the gains are chosen appropriately, the error tends to zero for the steady-state.

Figure 4-1 presents the block diagram of the Model Based PD Controller.

The same methodology can be used for the Model Based PID Controller. The torques are given by:

$$\boldsymbol{\tau} = \hat{\mathbf{H}}\left[\ddot{\mathbf{q}}_d + \mathbf{K}_D\left(\dot{\mathbf{q}}_d - \dot{\mathbf{q}}\right) + \mathbf{K}_P\left(\mathbf{q}_d - \mathbf{q}\right) + \mathbf{K}_I\int_0^t\left(\mathbf{q}_d(x) - \mathbf{q}(x)\right)dx\right] + \hat{\mathbf{C}}^*\dot{\mathbf{q}} + \hat{\mathbf{g}}_h \tag{4-6}$$

where $\mathbf{K_I}$ is also 3x3 diagonal matrix

The dynamics of the errors are described by:

$$\begin{aligned}\ddot{\mathbf{e}} + \mathbf{K}_D\dot{\mathbf{e}} + \mathbf{K}_P\mathbf{e} + \mathbf{K}_I\int_0^t\mathbf{e}(x)dx &= 0 \\ \mathbf{e} &= \mathbf{q}_d - \mathbf{q}\end{aligned} \tag{4-7}$$

Figure 4-2 presents the block diagram of the Model Based PID Controller.

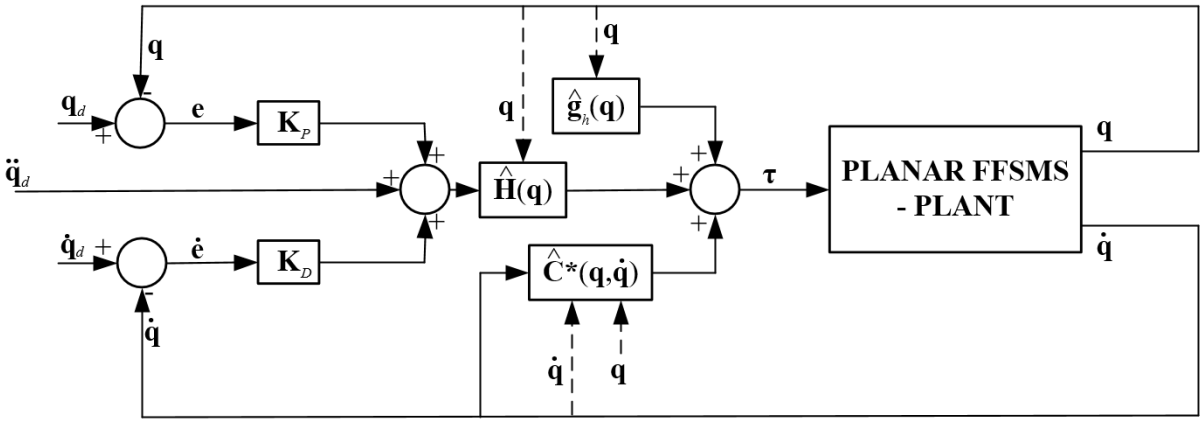

Figure 4-1. Block Diagram of the Model Based PD Controller applied to a Planar FFSMS in Joint Space.

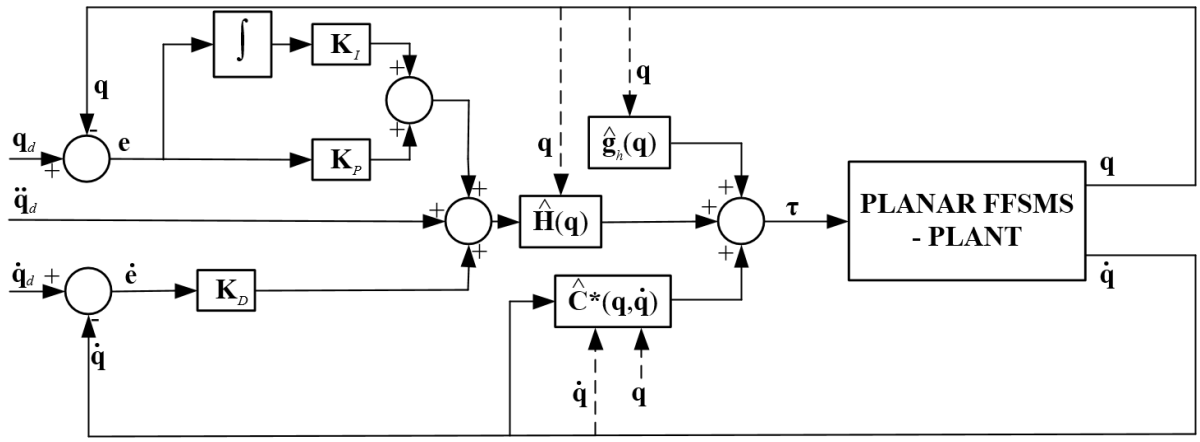

Figure 4-2. Block Diagram of the Model Based PID Controller applied to a Planar FFSMS in Joint Space.

4.2.2 Model Based PD Controller with an auxiliary MPC Input

The effectiveness of the controller presented in Section 4.2.1 depends on the accuracy of the system's parameters and matrices $\mathbf{H(q)}$, $\mathbf{C}^*(\mathbf{q},\dot{\mathbf{q}},h_{CM})$ and $\mathbf{g}_h(\mathbf{q},h_{CM})$. If these parameters are not certain, time-varying disturbances occur. These disturbances are described by the right part of Eq. (4-4). To compensate for these disturbances, an MPC is embedded into the previous Model Based PD Controller via the term $\mathbf{u}_{MPC}$. Therefore, the torques of the joints are given by:

$$\boldsymbol{\tau} = \hat{\mathbf{H}}\left[\ddot{\mathbf{q}}_d + \mathbf{K}_D\left(\dot{\mathbf{q}}_d - \dot{\mathbf{q}}\right) + \mathbf{K}_P\left(\mathbf{q}_d - \mathbf{q}\right) + \mathbf{u}_{MPC}\right] + \hat{\mathbf{C}}^*\dot{\mathbf{q}} + \hat{\mathbf{g}}_h \tag{4-8}$$

and the dynamics of the errors are described by:

$$\begin{gathered}\ddot{\mathbf{e}} + \mathbf{K}_D\dot{\mathbf{e}} + \mathbf{K}_P\mathbf{e} = \hat{\mathbf{H}}^{-1}\left(\left(\mathbf{H} - \hat{\mathbf{H}}\right)\ddot{\mathbf{q}} + \left(\mathbf{C}^* - \hat{\mathbf{C}}^*\right)\dot{\mathbf{q}} + \mathbf{g}_h - \hat{\mathbf{g}}_h\right) - \mathbf{u}_{MPC} \\ \mathbf{e} = \mathbf{q}_d - \mathbf{q}\end{gathered} \tag{4-9}$$

Figure 4-3 presents the block diagram of the Model Based PD Controller with MPC compensation.

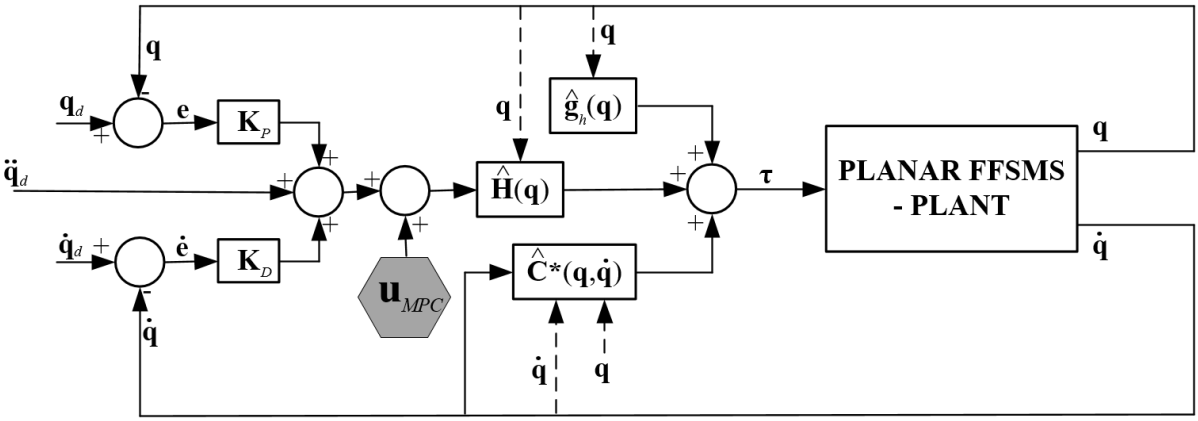

Figure 4-3. Block Diagram of the Model Based PD Controller with an auxiliary MPC Input applied to a Planar FFSMS in Joint Space.

As it was stated in Chapter 3, the application of the MPC mandates the representation of the dynamics of the system in state-space form. Considering the fact that the system is linear and decoupled and by neglecting to write the disturbances caused by the parametric uncertainties for simplification of the representation, the state-space model for each one of the three joints can be written as:

$$\begin{aligned} \dot{\mathbf{x}}_\mathbf{m}(t) &= \mathbf{A}_\mathbf{m}\mathbf{x}_\mathbf{m}(t) + \mathbf{B}_\mathbf{m}u(t) \\ y(t) &= \mathbf{C}_\mathbf{m}\mathbf{x}_\mathbf{m}(t) \end{aligned} \qquad (4\text{-}10)$$

$$with\ \ \mathbf{x}_\mathbf{m} = \begin{bmatrix} x_{m,1} \\ x_{m,2} \end{bmatrix} = \begin{bmatrix} e_i \\ \dot{e}_i \end{bmatrix},\ \mathbf{A}_\mathbf{m} = \begin{bmatrix} 0 & 1 \\ -K_{P,i} & -K_{D,i} \end{bmatrix},\ \mathbf{B}_\mathbf{m} = \begin{bmatrix} 0 \\ -1 \end{bmatrix},\ \mathbf{C}_\mathbf{m} = \begin{bmatrix} 1 & 0 \end{bmatrix},\ \ i = 1,2,3$$

For the rest of this section, the indicator i is neglected for simplification.

To implement the MPC algorithm, the augmented model of Eq. (4-10) is formed:

$$\begin{aligned} \dot{\mathbf{x}}(t) &= \mathbf{A}\mathbf{x}(t) + \mathbf{B}\dot{u}(t) \\ y(t) &= \mathbf{C}\mathbf{x}(t) \end{aligned} \qquad (4\text{-}11)$$

$$with\ \ \mathbf{x} = \begin{bmatrix} \dot{x}_{m,1} \\ \dot{x}_{m,2} \\ y \end{bmatrix},\ \mathbf{A} = \begin{bmatrix} 0 & 1 & 0 \\ -K_P & -K_D & 0 \\ 1 & 0 & 0 \end{bmatrix},\ \mathbf{B} = \begin{bmatrix} 0 \\ -1 \\ 0 \end{bmatrix},\ \mathbf{C} = \begin{bmatrix} 0 & 0 & 1 \end{bmatrix}$$

The next step is to determine the scaling factor p, the number of Laguerre functions N, the prediction horizon T_p. as well as the parameters $\mathbf{Q}$ and $\mathbf{R}$ on which the desired performance depends.

Having determined the aforementioned parameters, the methodology which was presented in Section 3.2 of Chapter 3 is followed to apply the unconstrained MPC and the methodology presented in Section 3.3 of Chapter 3 for the constrained MPC.

It is important to point out that although the desired angles, angular velocities and angular accelerations trajectories are time-dependent, the desired trajectories of the errors are constant and equal to zero. Since the equations that are used for implementation of the MPC are the equations of the errors, the desired trajectories are constant and therefore the methodology of Chapter 3 can be applied.

4.3 Design of a Controller in the Cartesian Space

Probably the most common usage of an FFSMS' manipulator involves its motion in the Cartesian Space. There are boundless occasions that the manipulator's end-effector might need to reach a desired point with a desired orientation in reference to an Inertial Frame of Reference. Besides that, in some cases, the end-effector might need to even follow a desired trajectory apart from the final position and orientation. The accomplishment of these tasks requires the measurement of the position and orientation of the end-effector as well as the base. This can be done by either using cameras which are attached to the end-effector and measure these variables with respect to another object such as another satellite or by estimating them from the equations of kinematics of the FFSMS, if the angles of the manipulator's joints and the link lengths are known. The former method is the most accurate one since the latter multiplies the disturbances in case of parametric uncertainties (the kinematics uses the parameters of the model which are uncertain).

The same procedure as the design of controller in the joint space is followed. First a Model Based PD Controller is presented and then an MPC is embedded into the controller.

4.3.1 Model Based PD & PID Controller

The methodology followed is based on the design of a Transpose Jacobian Controller. The main idea of this controller is based on the premise that the end-effector moves because a hypothetical force $\mathbf{f}$ is applied to it. This force is the result of the joints torques $\boldsymbol{\tau}$ and it is given by [21] :

$$\boldsymbol{\tau} = \mathbf{J}^T \mathbf{f} \tag{4-12}$$

where $\mathbf{J}$ is the Jacobian of the system that relates the end-effector's velocities to the joints' angular velocities and it is expressed in the inertial frame of reference. It can be extracted by solving the first part of Eq. (2-31) considering h_{CM} equals zero and by substituting $\dot{\theta}_0$ to the rest of equations. From now on, it would be considered for simplification $\mathrm{h}_{CM} = 0$, unless stated otherwise. The Jacobian is given by:

$$\mathbf{J} = \mathbf{R}_0 \mathbf{J}^* = \begin{bmatrix} \cos(\theta_0) & -\sin(\theta_0) & 0 \\ \sin(\theta_0) & \cos(\theta_0) & 0 \\ 0 & 0 & 1 \end{bmatrix} \mathbf{J}^* \tag{4-13}$$

and $\mathbf{J}^*$ is given by Eq. (2-37). By definition, the Jacobian is the matrix that is used to convert the velocities of the end effector to the angular velocities of the joints:

$$\begin{aligned} \dot{\mathbf{x}} &= \mathbf{J}\dot{\mathbf{q}} \\ \mathbf{x} &= \begin{bmatrix} x_{\mathrm{E}} & y_{\mathrm{E}} & \theta_{\mathrm{E}} \end{bmatrix}^T \end{aligned} \tag{4-14}$$

The solution of the aforementioned equation yields:

$$\dot{\mathbf{q}} = \mathbf{J}^{-1} \dot{\mathbf{x}} \tag{4-15}$$

The differentiation of Eq. (4-14) gives:

$$\ddot{\mathbf{x}} = \dot{\mathbf{J}}\dot{\mathbf{q}} + \mathbf{J}\ddot{\mathbf{q}} \tag{4-16}$$

Therefore,

$$\ddot{\mathbf{q}} = \mathbf{J}^{-1}(\ddot{\mathbf{x}} - \dot{\mathbf{J}}\dot{\mathbf{q}}) \tag{4-17}$$

Substituting Eq. (4-15) and Eq. (4-17) into the equation of dynamics of an FFSMS (Eq. (4-1)) ($\mathbf{g}_h(\mathbf{q}, h_{CM}) = 0$ because $h_{CM} = 0$) and multiplying it with the inverse transpose of the Jacobian, the equation of dynamics for the Cartesian space is given by:

$$\mathbf{H}_x(\mathbf{q}, \theta_0)\ddot{\mathbf{x}} + \mathbf{C}_x^*(\mathbf{q}, \dot{\mathbf{q}}, \theta_0, \dot{\theta}_0)\dot{\mathbf{x}} = \mathbf{f} = \mathbf{J}^{-T}\boldsymbol{\tau} \tag{4-18}$$

where:

$$\begin{aligned} \mathbf{H}_x(\mathbf{q}, \theta_0) &= \mathbf{J}^{-T}\mathbf{H}\mathbf{J}^{-1} \\ \mathbf{C}_x^*(\mathbf{q}, \dot{\mathbf{q}}, \theta_0, \dot{\theta}_0) &= \mathbf{J}^{-T}\left(\mathbf{C}^* - \mathbf{H}\mathbf{J}^{-1}\dot{\mathbf{J}}\right)\mathbf{J}^{-1} \end{aligned} \tag{4-19}$$

It is pivotal to point out here that the inertia matrix $\mathbf{H}_x$ is positive definite everywhere but at the points where Dynamic Singularities occur, since it depends on the inverse Jacobian. Dynamic Singularites have been studied in Section 2.3.2.

The design of a Model Based Controller in the Cartesian space is quite similar with the one presented for joint space. The goal of the controller is to convert the non-linear system to a decoupled linear one. This can be accomplished by using the model to compensate for the non-linear terms. Considering that the matrices $\mathbf{H}_x$ and $\mathbf{C}_x^*$ can be accurately calculated by the model, the desired trajectories of the position and orientation of the end-effector $\mathbf{x}_d(t)$, the velocities $\dot{\mathbf{x}}_d(t)$ and the accelarations $\ddot{\mathbf{x}}_d(t)$ are defined and sensors are used to measure the manipulator's joints angles $\mathbf{q}$ and angular velocities $\dot{\mathbf{q}}$, the base's rotation and angular velocity $\theta_0(t), \dot{\theta}_0(t)$, the end-effector's position and orientation $\mathbf{x}$ and velocities $\dot{\mathbf{x}}$, the Model Based PD Controller takes the form:

$$\begin{aligned} \mathbf{f} &= \hat{\mathbf{H}}_x\left[\ddot{\mathbf{x}}_d + \mathbf{K}_D\left(\dot{\mathbf{x}}_d - \dot{\mathbf{x}}\right) + \mathbf{K}_P\left(\mathbf{x}_d - \mathbf{x}\right)\right] + \hat{\mathbf{C}}_x^*\dot{\mathbf{x}} \\ \boldsymbol{\tau} &= \mathbf{J}^T\mathbf{f} \end{aligned} \tag{4-20}$$

where $\mathbf{K_D}$ and $\mathbf{K_P}$ are 3x3 diagonal matrices containing the gains of the PD part of the controller which determines the desired dynamic response of the system and the hat (^) above $\mathbf{H}$ and $\mathbf{C}^*$ indicates that they are conjectured and not perfectly known. Of course, the Jacobian matrix $\mathbf{J}$ is also an estimated matrix but the "hat" is neglected for simplification purposes.

Substituting Eq. (4-20) into Eq. (4-18) the equations of dynamics of the errors of the position and orientation are given by:

$$\begin{aligned} \ddot{\mathbf{e}}_x + \mathbf{K}_D\dot{\mathbf{e}}_x + \mathbf{K}_P\mathbf{e}_x &= \hat{\mathbf{H}}_x^{-1}\left(\left(\mathbf{H}_x - \hat{\mathbf{H}}_x\right)\ddot{\mathbf{x}} + \left(\mathbf{C}_x^* - \hat{\mathbf{C}}_x^*\right)\dot{\mathbf{x}}\right) \\ \mathbf{e}_x &= \mathbf{x}_d - \mathbf{x} \end{aligned} \tag{4-21}$$

If the matrix estimates are accurate enough, the right part of the preceding equation equals zero and the errors' dynamics are described by:

$$\begin{aligned} \ddot{\mathbf{e}}_x + \mathbf{K}_D\dot{\mathbf{e}}_x + \mathbf{K}_P\mathbf{e}_x &= 0 \\ \mathbf{e}_x &= \mathbf{x}_d - \mathbf{x} \end{aligned} \tag{4-22}$$

This equation describes a decoupled system of linear equations and if the gains are chosen suitably, the tracking error will converge to zero at the steady-state.

Figure 4-4 presents the block diagram of the Model Based PD Controller.

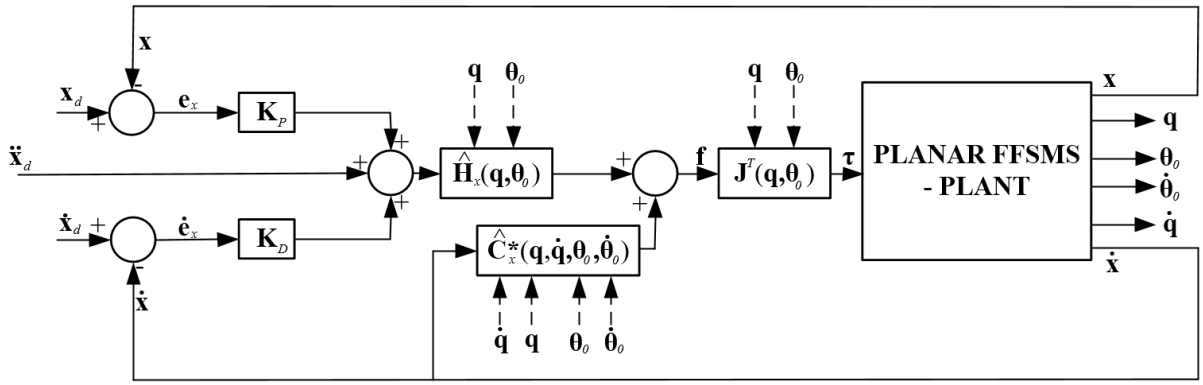

Figure 4-4. Block Diagram of the Model Based PD Controller applied to a Planar FFSMS in Cartesian Space.

The same methodology can be used for the Model Based PID Controller. The hypothetical force is given by:

$$\mathbf{f} = \hat{\mathbf{H}}_x \left[\ddot{\mathbf{x}}_d + \mathbf{K}_D \left(\dot{\mathbf{x}}_d - \dot{\mathbf{x}} \right) + \mathbf{K}_P \left(\mathbf{x}_d - \mathbf{x} \right) + \mathbf{K}_I \int_0^t \left(\mathbf{x}_d(\lambda) - \mathbf{x}(\lambda) \right) d\lambda \right] + \hat{\mathbf{C}}_x^* \dot{\mathbf{x}}$$
$$\boldsymbol{\tau} = \mathbf{J}^T \mathbf{f} \tag{4-23}$$

and the dynamics of the errors are described by:

$$\ddot{\mathbf{e}}_x + \mathbf{K}_D \dot{\mathbf{e}}_x + \mathbf{K}_P \mathbf{e}_x + \mathbf{K}_I \int_0^t \mathbf{e}_x(\lambda) d\lambda = 0$$
$$\mathbf{e}_x = \mathbf{x}_d - \mathbf{x} \tag{4-24}$$

Figure 4-5 presents the block diagram of the Model Based PID Controller.

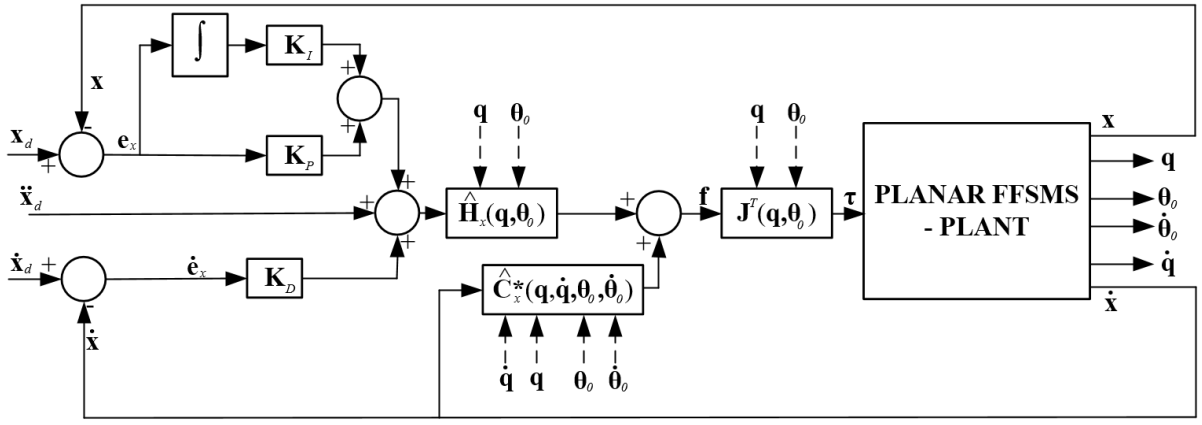

Figure 4-5. Block Diagram of the Model Based PID Controller applied to a Planar FFSMS in Cartesian Space.

4.3.2 Model Based PD Controller with an auxiliary MPC Input

Similar to the design of the controller in the joint space, an MPC, denoted by $\mathbf{u}_{MPC}$, is embedded into the Model Based PD Controller to compensate for the potential disturbances. Therefore, the hypothetical force and the torques of the joints are given by:

$$\mathbf{f} = \hat{\mathbf{H}}_x \left[\ddot{\mathbf{x}}_d + \mathbf{K}_D \left(\dot{\mathbf{x}}_d - \dot{\mathbf{x}} \right) + \mathbf{K}_P \left(\mathbf{x}_d - \mathbf{x} \right) + \mathbf{u}_{MPC} \right] + \hat{\mathbf{C}}_x^* \dot{\mathbf{x}}$$
$$\boldsymbol{\tau} = \mathbf{J}^T \mathbf{f} \tag{4-25}$$

and the dynamics of the errors are described by:

$$\ddot{\mathbf{e}}_x + \mathbf{K}_D\dot{\mathbf{e}}_x + \mathbf{K}_P\mathbf{e}_x = \hat{\mathbf{H}}_x^{-1}\left(\left(\mathbf{H}_x - \hat{\mathbf{H}}_x\right)\ddot{\mathbf{x}} + \left(\mathbf{C}_x^* - \hat{\mathbf{C}}_x^*\right)\dot{\mathbf{x}}\right) - \mathbf{u}_{MPC}$$
$$\mathbf{e}_x = \mathbf{x}_d - \mathbf{x} \tag{4-26}$$

Figure 4-6 presents the block diagram of the Model Based PD Controller with MPC.

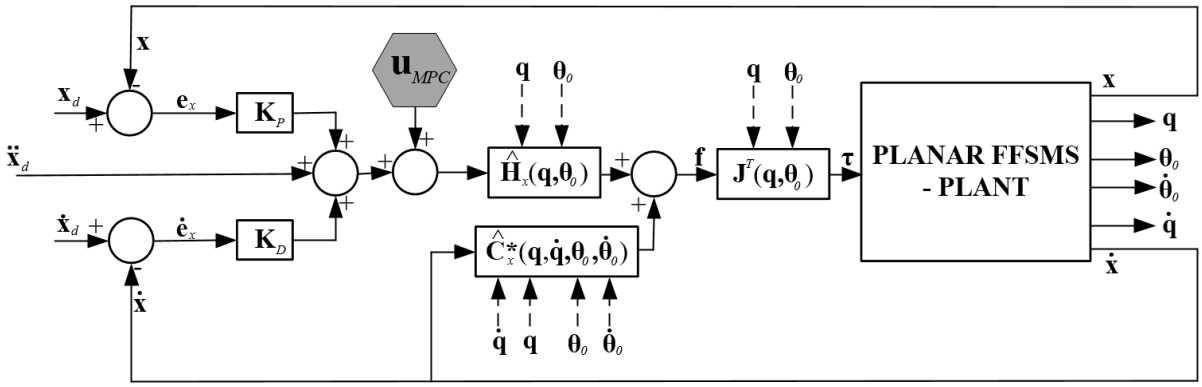

Figure 4-6. Block Diagram of the Model Based PD Controller with an auxiliary MPC Input applied to a Planar FFSMS in Cartesian Space.

As stated in Chapter 3 and presented in the design of the similar controller for motion in the joint space, the application of the MPC mandates the representation of the dynamics of the system in state-space form. Consequently, the same equations to the preceding controller is applied in this case too. Specifically, Eq. (4-10) describes the state-space model and Eq. (4-11) describes the augmented model.

The next step is to determine the scaling factor p, the number of Laguerre functions N, the prediction horizon T_p. as well as the parameters $\mathbf{Q}$ and $\mathbf{R}$ depended on the desired performance as before. Having determined the aforementioned parameters, the methodology which was presented in Section 3.2 of Chapter 3 is followed to apply the unconstrained MPC and the methodology presented in Section 3.3 of Chapter 3 for the constrained MPC.

4.4 Plant Representation - MSC Adams Simulation

Although a sole application of Matlab/Simulink can be used to simulate the performance of the aforementioned controllers implemented in an FFSMS for a plethora of different scenarios, more realistic and reliable simulations can be achieved by co-simulation of Matlab/Simulink with MSC Adams. Adams is a Multibody Dynamics software that can be used for actual representation of both the studied system and the motion that it would have depending on the forces and torques applied to it. Adams offers the ability to connect to Matlab/Simulink by extracting a “block” which can be used in Simulink which represents the plant of the system. After that, the controller is applied to the extracted plant in Simulink, offering a real-world representation.

Adams provides the ability to design the model in its environment or import it from an external design software. For the purpose of this thesis, the base and the manipulator of the FFSMS were designed in Solidworks and imported into Adams. Figure 4-7 shows the FFSMS that would be used for the simulations. The base is depicted with yellow color while the manipulator is white. The next step for the creation of the studied plant is the introduction of the connectors which describe the planar motion of the system in relation with the “ground” and the three joints of the manipulator. After that, the torques of the manipulator

are introduced as well as the measures which represent the sensors of the real model. For joint space motion, the variables that are measured from the model are the angles and angular velocities of the manipulator's joints as well as the rotation of the base: $q_1, q_2, q_3, \dot{q}_1, \dot{q}_2, \dot{q}_3, \theta_0$. For Cartesian motion, the angular velocity of the base, the position, orientation and velocities of the end-effector are also measured: $q_1, q_2, q_3, \dot{q}_1, \dot{q}_2, \dot{q}_3, \theta_0, \dot{\theta}_0, x_E, y_E, \theta_E, \dot{x}_E, \dot{y}_E, \dot{\theta}_E$. At this point, it is important to mention that each body's CM should be positioned manually because the insersion from Solidworks inserts some small discrepancies too. Finally, the model is extracted and inserted into Matlab/Simulink.

Adams offers two different modes for simulation when it is connected to Matlab/Simulink. The first one is called "Adams Discete Model" or "Co-simulation". According to this option, Matlab solves the Simulink model while Adams uses its own solver to solve Adams model. The data are exchanged periodically. The second way is called "Adams Continuous Model" or "Function Evaluation". According to this option, Matlab solves both Simulink and Adams models. The solver provided by Adams acts only as a function evaluator for Matlab integrator. Althought the former option might be more robust because Adams' solver is claimed to be better at solving complicated Adams models, it creates an algebraic loop in simulink, causing small but significant errors in the results. For this reason, the latter mode is used. However, since Continuous mode cannot provide graphical representation of the simulation, when a video is desired, Discrete mode is used.

For the following Example as well as the Scenarios presented in Chapter 5, the Adams model shown in Figure 4-7 will be used to represent the plant, unless stated otherwise.

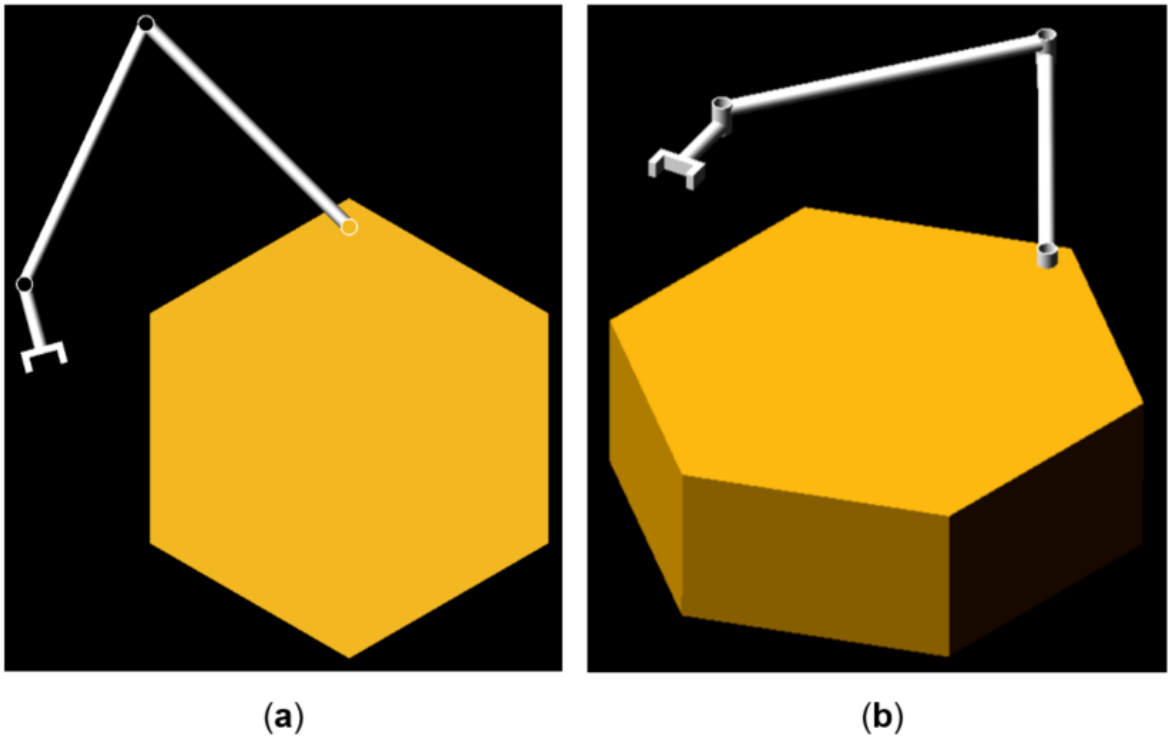

Figure 4-7. Picture of the MSC Adams Model used to represent the studied FFSMS (a) Top View, (b) Isometric View.

4.5 Example: Design of Model Based PD Controller with an auxiliary MPC Input for Motion in the Joint Space

The main purpose of this example is to manifest the co-simulation of Matlab/Simulink and MSC Adams by simulating the motion of a planar FFSMS with a 3-DoF manipulator in the joint space. Another aim of the example is to validate the application of the presented controllers. Although results would be shown for both the Model Based PID Controller and the Model Based PD Controller with an auxiliary MPC input, a comparison between these two controllers is unnecessary at this point, since disturbances, parametric uncertainties or noise is not introduced in this example. Chapter 5 contains case studies with these characteristics. Consequently, the comparison is presented there.

First, the path planning is presented to yield the desired trajectories for each joint. After that, the preceding controllers is implemented and the respective gains and poles is shown. Finally, diagrams that show the motion of the FFSMS as well as the angles' errors and torques are presented.

4.5.1 Path Planning

The control of an FFSMS in the joint space requires the determination of the desired trajectories that the manipulator's joints should follow. The base rotates freely due to the dynamic-coupling between the base and the manipulator, thus, no particular trajectory is needed for it. In this thesis, fifth power polynomials are used to be able to set the initial and the final value of the angle, the angular velocity and the angular acceleration. For each of the three joints, the polynomial for the angle is given by:

$$q_d(t) = a_0 + a_1 t + a_2 t^2 + a_3 t^3 + a_4 t^4 + a_5 t^5 \tag{4-27}$$

where the coefficients are given by the solution of the linear system (considering that the initial time is $t_0 = 0$):

$$\begin{aligned}
&q_d(t_0 = 0) = q_{d,0} \Rightarrow a_0 = q_{d,0} \\
&q_d(t_f) = q_{d,f} \Rightarrow a_0 + a_1 t_f + a_2 t_f^2 + a_3 t_f^3 + a_4 t_f^4 + a_5 t_f^5 = q_{d,f} \\
&\dot{q}_d(t_0 = 0) = \dot{q}_{d,0} \Rightarrow a_1 = \dot{q}_{d,0} \\
&\dot{q}_d(t_f) = \dot{q}_{d,f} \Rightarrow a_1 + 2a_2 t_f + 3a_3 t_f^2 + 4a_4 t_f^3 + 5a_5 t_f^4 = \dot{q}_{d,f} \\
&\ddot{q}_d(t_0 = 0) = \ddot{q}_{d,0} \Rightarrow a_2 = \ddot{q}_{d,0} \\
&\ddot{q}_d(t_f) = \ddot{q}_{d,f} \Rightarrow 2a_2 + 6a_3 t_f + 12a_4 t_f^2 + 20a_5 t_f^3 = \ddot{q}_{d,f}
\end{aligned} \tag{4-28}$$

The system was solved with the help of Matlab's command *linsolve()*. The results are shown in Appendix A. The resulted trajectories for determined initial and final angle and for initial and final angular velocity and acceleration equal to zero, which is the most usual case and the one that is used in this example, are shown in Figure 4-8.

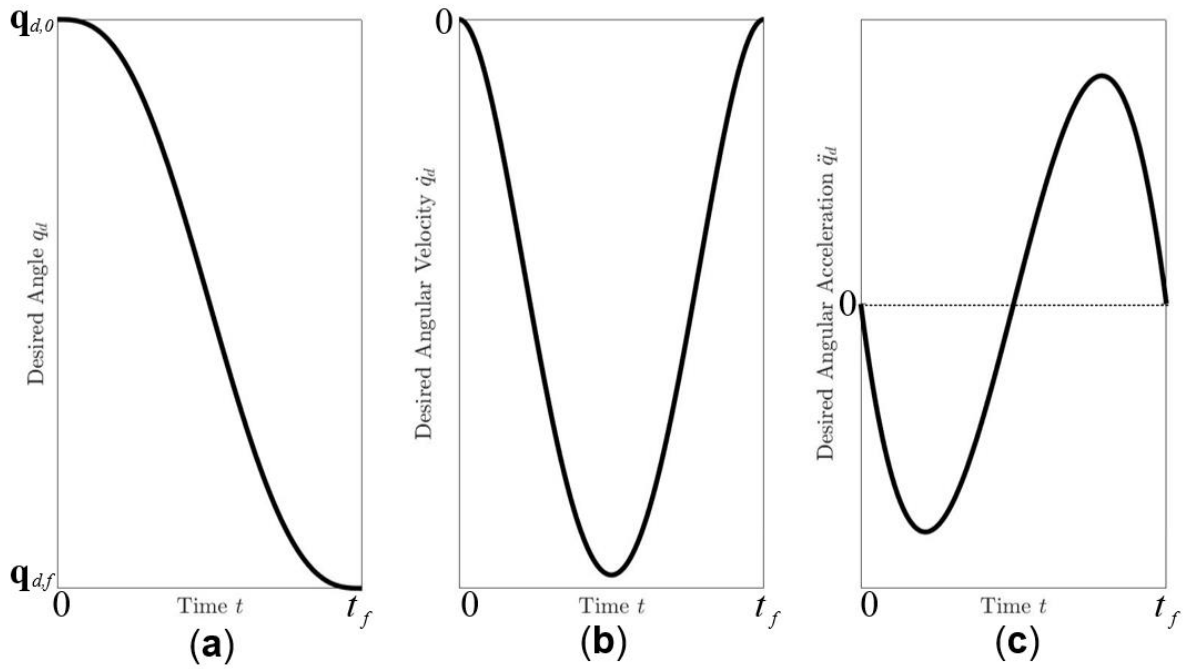

Figure 4-8. Desired Trajectories (a) Angle, (b) Angular Velocity, (c) Angular Acceleration.

In Table 4-1 the values for the initial and final angle, angular velocity and acceleration as well as the final time used in the example for each of the three joints are presented.

Table 4-1. Paremeters of the Desired Trajectories.

Joint	1st	2nd	3rd
t_f (s)	6	6	6
Initial Angle $q_{d,0}$ (deg)	45	110	40
Final Angle $q_{d,f}$ (deg)	20	70	-60
Initial Angular Velocity $\dot{q}_{d,0}$ (deg/s)	0	0	0
Final Angular Velocity $\dot{q}_{d,f}$ (deg/s)	0	0	0
Initial Angular Acceleration $\ddot{q}_{d,0}$ (deg/s^2)	0	0	0
Final Angular Acceleration $\ddot{q}_{d,f}$ (deg/s^2)	0	0	0

4.5.2 FFSMS Dynamics & Parameters

As presented in the previous sections, the effectiveness of a Model Based Controller depends mainly on the accuracy of the parameters of the FFSMS as well as the dynamical matrices. In this Section, due to the absence of disturbances and noise, the FFSMS' parameters are perfectly known and given in Table 4-2.

Table 4-2. Paremeters of the FFSMS.

Body	Mass - m_i (kg)	Moment of Inertia - I_i (kg·m^2)	Before-CM Length - l_i (m)	After-CM Length - r_i (m)
0	600	500	-	1.4
1	40	20	1	1
2	40	20	1	1
3	20	15	0.25	0.25

Nonetheless, even if the parameters of the FFSMS are known, there are still uncertainties that might occur due to the inaccurate modelling of the FFSMS. These uncertainties are defined as dynamic uncertainties. For this example as well as the scenarios presented in Chapter 5, it is considered that no dynamic uncertainties occurred, the angular momentum equals zero and the form of the matrices $\mathbf{H(q)}$ and $\mathbf{C}^*(\mathbf{q},\dot{\mathbf{q}})$ of the equations of dynamics (Eq. (4-1)) is adequately accurate and given by Eq. (2-57). For the implementation, Matlab was used to deduce the aforementioned matrices.

4.5.3 Model Based PD Controller with an Auxiliary MPC Input

The controller that is applied is given by Eq. (4-8). Considering that the matrices $\mathbf{H(q)}$ and $\mathbf{C}^*(\mathbf{q},\dot{\mathbf{q}})$ have been determined (see Section 4.5.2) and $\mathbf{g}_h(\mathbf{q},h_{CM})=0$ since $h_{CM}=0$, then, only matrices $\mathbf{K}_D$, $\mathbf{K}_P$ and the signal from the MPC $\mathbf{u}_{MPC}$ have to be defined.

By neglecting the parametric uncertainties and the MPC signal, for each of the three joints (since the system has become decoupled) Eq. (4-9) takes the form:

$$\ddot{e}_i + K_D\dot{e}_i + K_P e_i = \ddot{e}_i + 2\zeta\omega_n\dot{e}_i + \omega_n^2 e_i = 0, \quad i = 1-3 \tag{4-29}$$

where ζ is the damping ratio and was defined based on the fact that a commonly used value is $\zeta = 0.7$ and considering that the oscillation of the dynamics does not result in any impacts. ω_n is the natural frequency and was defined as $\omega_n = 7.532\text{rad/s}$. The value of the natural frequency was determined through a trial-error process until the maximum torques of the Model Based PD Controller with MPC Input and the Model Based PID Controller were adequately close. This is a very important determinant for the comparison of the two controllers and it will be analyzed thoroughly in Chapter 5. Of course, the criterion that the errors should reach zero steady-state for settling time less than 6s (the final time of the trajectory) was also taken into consideration.

Therefore, the matrices $\mathbf{K}_D$ and $\mathbf{K}_P$ are:

$$\begin{aligned}\mathbf{K}_D &= diag(10.54, 10.54, 10.54)\\ \mathbf{K}_P &= diag(56.73, 56.73, 56.73)\end{aligned} \tag{4-30}$$

As presented in Section 4.2.2, these values will be used in the augmented model of Eq. (4-11) to derive the MPC control input. Prerequisites for that is to determine also the scaling factor p, the number of Laguerre functions N, the prediction horizon T_p. as well as the parameters $\mathbf{Q}$ and $\mathbf{R}$. A good selection of the scaling factor is to set it equal to the dominant pole of the respective LQR problem [40] . By using the Matlab function *lqr()* the scaling factor was defined as $p = 5.5110$. Parameters N and T_p were determined through a number of

trials until the results were remaining adequately constant. Consequently, $\mathrm{N} = 10$ and $T_p = 6\mathrm{s}$. Finally, matrix $\mathbf{Q}$ was set equal to the transpose of the matrix of the output multiplied by the matrix of the output (see Eq. (3-24)) and $\mathbf{R}$ was set adequately small since the goal of the controller is to lessen the error and not the input signal:

$$\mathbf{Q} = \mathbf{C}^T\mathbf{C} = \begin{bmatrix} 0 & 0 & 0 \\ 0 & 0 & 0 \\ 0 & 0 & 1 \end{bmatrix} \qquad \mathbf{R} = 10^{-6} \tag{4-31}$$

Having determined the aforementioned parameters, the methodology which was presented in Section 3.2 of Chapter 3 is followed for applying the unconstrained MPC. The matrices $\mathbf{\Omega}$, $\mathbf{\Psi}$ and $\mathbf{L}(0)^T$ are calculated and used in the controller. There is no need to apply the constrained MPC since no disturbances or parametric uncertainties were introduced in this example and it only results in the increase of the computational power.

It is interesting to present also the produced gain of the MPC for the augmented model. The gain is produced by Eq. (3-31) and for this example it equals:

$$\mathbf{K}_{MPC} = \begin{bmatrix} -153.99 & -9.97 & -1000.1 \end{bmatrix} \tag{4-32}$$

To understand these values and perhaps compare them with the gains from the Model Based PID Controller presented in the next section, it has to be kept in mind that these are the gains for each joint and for the augmented model of the plant, which is of course a state-space problem.

Figure 4-9 includes snapshots of the motion of the FFSMS in the ADAMS environment for three different time-points, Figure 4-10 presents the overall motion of the FFSMS as well as the Path Independent Workspace (PIW) and the Path Dependent Workspace (PDW). It is important to point out that although the FFSMS moves into the PDW, there is no worry for dynamic singularity occurrence since the controller has been implemented in the joint space. For motion in the Cartesian space, Dynamic Singularities must be considered too.

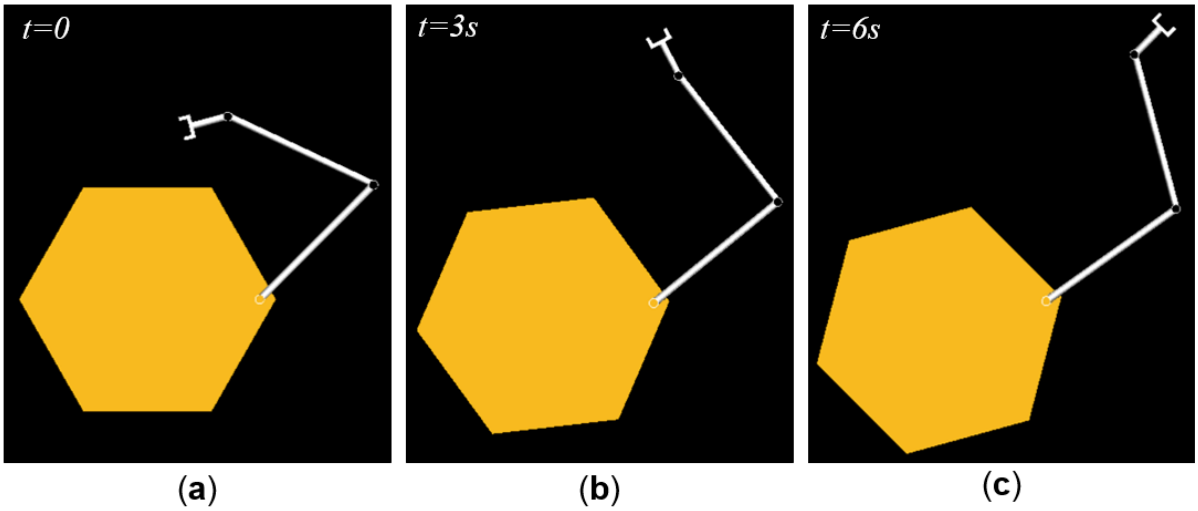

Figure 4-9. Snapshots of the Motion of the FFSMS in the ADAMS environment for three different time-points (a) t=0, (b) t=3s, (c) t=6s.

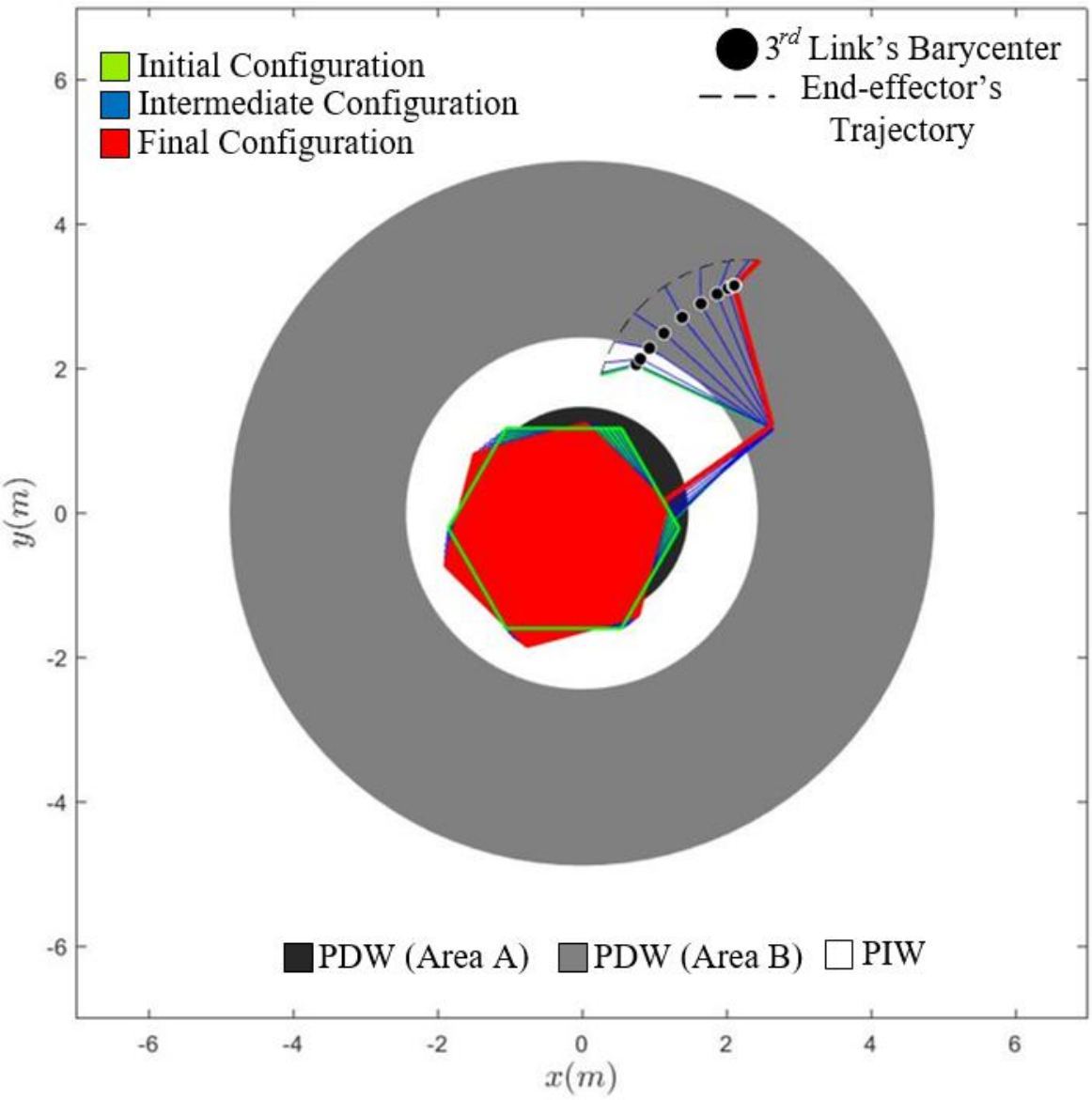

Figure 4-10. Motion of the FFSMS in the Joint Space.

Figure 4-11 presents the trajectory of the angles and angular velocities of all of three joints. It can be concluded easily that the trajectories of the angles fit almost perfectly with the desired trajectories. This can be seen also in Figure 4-12 which presents the errors of the three joints as well as the torques that have to be applied to their actuators in order the FFSMS to follow the desired path. It is obvious that the errors are about 10^{-8} which is a completely rational value since no disturbances, parametric uncertainties or noise were introduced and Adams model has an accuracy of around 10^{-8}-10^{-9} due to the number of decimal digits that can be inserted for the dynamic and geometrical parameters.

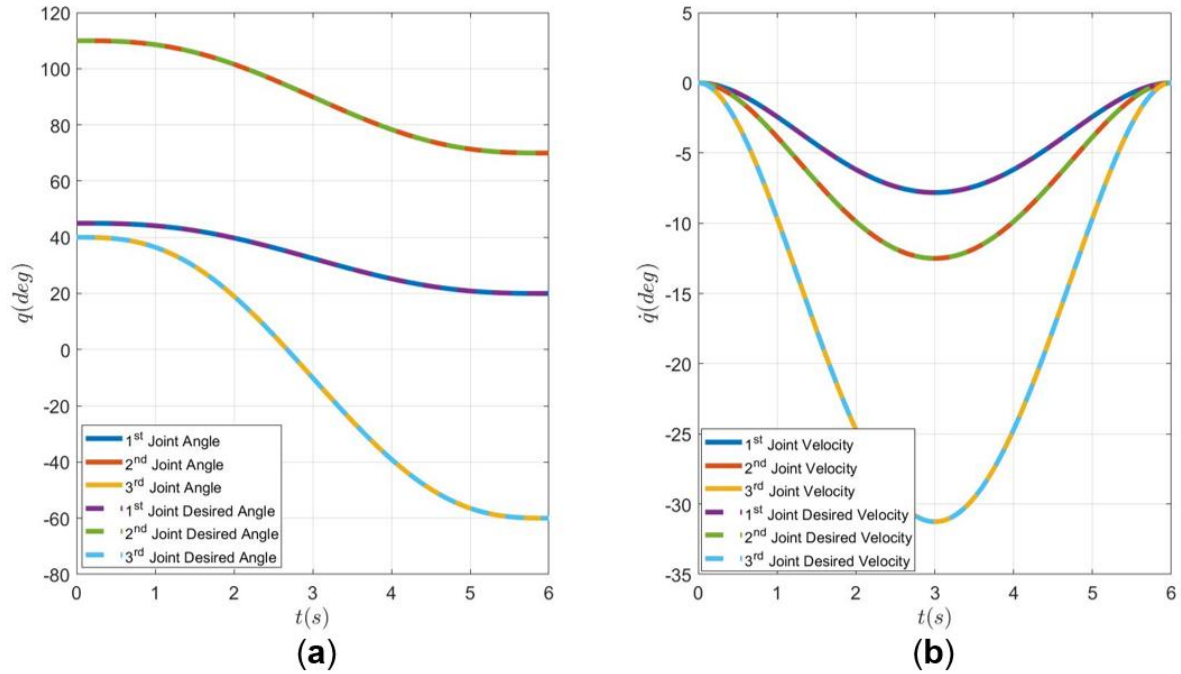

Figure 4-11. Actual and Desired Trajectories of the joints (a) Angles, (b) Velocities.

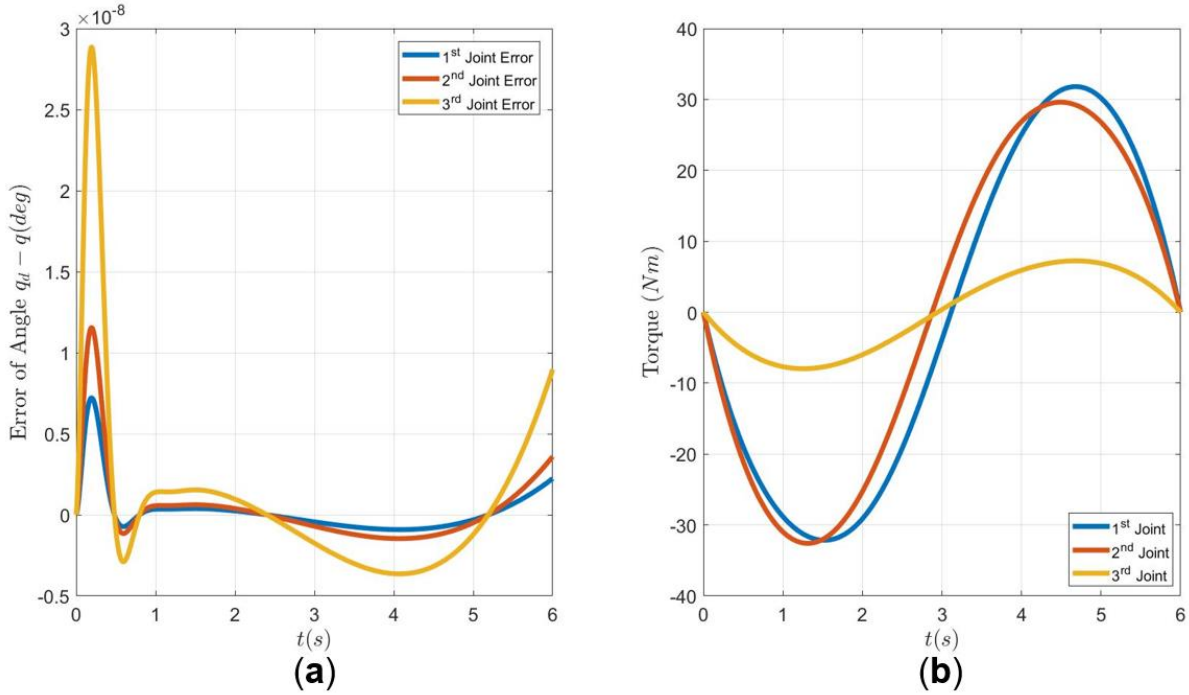

Figure 4-12. (a) Errors of Angles, (b) Applied Torques.

4.5.4 Model Based PID Controller

The controller that is applied is given by Eq. (4-6). Considering that the matrices $\mathbf{H(q)}$ and $\mathbf{C}^*(\mathbf{q},\dot{\mathbf{q}})$ have been determined (see Section 4.5.2) and $\mathbf{g}_h(\mathbf{q},h_{CM})=0$ since $h_{CM}=0$, then, only the matrices $\mathbf{K}_D$, $\mathbf{K}_P$ and $\mathbf{K}_I$ have to be defined.

The deduction of the respective characteristic equation of Eq. (4-7) for each of the three joints (since the system has become decoupled) leads to:

$$s^3 + K_D s^2 + K_P s + K_I = (s + \omega_n)(s^2 + 2\zeta\omega_n s + \omega_n^2) \Rightarrow$$
$$\Rightarrow \begin{cases} K_D = 2\zeta\omega_n + \omega_n \\ K_P = \omega_n^2 + 2\zeta\omega_n^2 \\ K_I = \omega_n^3 \end{cases} \quad (4\text{-}33)$$

where ζ is the damping ratio and was defined based on the fact that a commonly used value is $\zeta = 0.7$ and considering that the oscillation of the dynamics does not result in any impacts. ω_n is the natural frequency and was defined as $\omega_n = 7.532\text{rad/s}$. The value of the natural frequency was determined through a trial-error process until the maximum torques of the Model Based PD Controller with MPC Input and the Model Based PID Controller were adequately close. It should be pointed out again that the criterion that the angle errors should equal zero at the steady-state for settling time less than 6s was also taken into consideration.

Consequently, the matrices $\mathbf{K}_D$, $\mathbf{K}_P$ and $\mathbf{K}_I$ are:

$$\begin{aligned} \mathbf{K}_D &= diag(18.08, 18.08, 18.08) \\ \mathbf{K}_P &= diag(136.15, 136.15, 136.15) \\ \mathbf{K}_I &= diag(427.30, 427.30, 427.30) \end{aligned} \quad (4\text{-}34)$$

Figure 4-13 presents the errors of the three joints as well as the torques that have to be applied to them in order the FFSMS to follow the desired path. It is obvious that the errors are about 10^{-9} which is a reasonable value since no disturbances, parametric uncertainties or noise were introduced and Adams model has an accuracy of around 10^{-8}- 10^{-9} due to the number of decimal digits that can be inserted for the dynamic and geometrical parameters.

Since the errors are adequately low, Figure 4-9 and Figure 4-10 also present the motion of the FFSMS for the Model Based PID Controller.

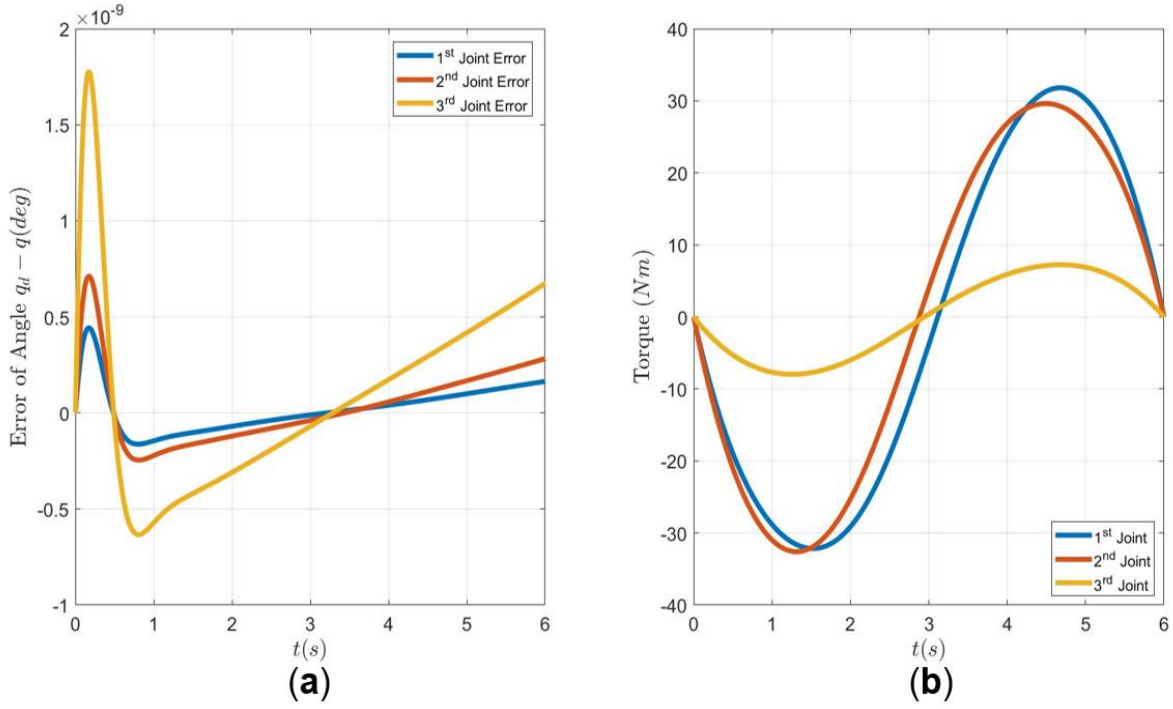

Figure 4-13. (a) Errors of Angles, (b) Applied Torques.

Finally, Figure 4-14 presents the root locus of the poles of the closed-loop system containing the Model Based PD Controller with an auxiliary MPC input as well as the poles of the Model Based PID Controller. For both systems, the absolute value of the real part of the poles is not considered high. Therefore, no problems related to noise or high values of torques are expected. Note that although someone might argue that the PID Controller was designed slower than the PD & MPC, it was observed that a different selection of the poles which would result in a faster design would require higher torques. Hence, considering the criterion that the two controllers should have the same maximum torque, the comparison between the two controllers would not be right.

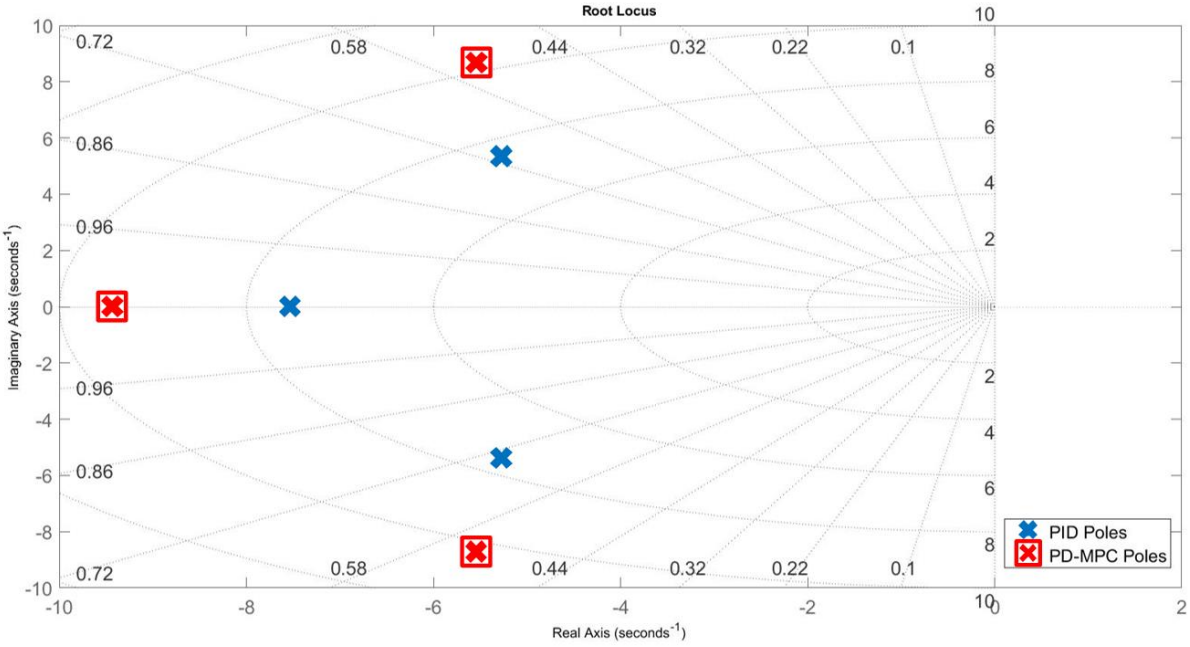

Figure 4-14. Root Locus for both the Model Based PID Controller and the Model Based PD Controller with an Auxiliary MPC Input.

5 Simulations & Case Studies

5.1 Introduction

In this Chapter, a Model Based PID Controller and a Model Based PD Controller with an auxiliary MPC input are implemented in a Free-Floating Space Manipulator System (FFSMS) for a multitude of different scenarios. The performance of the two controllers as well as their ability to tackle the various issues are compared to each other for ample different characteristics (errors, simulation time, torques). A planar FFSMS with a manipulator of 3 Degrees of Freedom (DoF) is employed for this task. For the deduction of the results, co-simulation between Matlab/Simulink and MSC Adams is performed.

The first scenario tests the performance of the two controllers when constant disturbances are present. The motion of the FFSMS is determined in the Cartesian Space since the position and orientation of the desired captured object are known. The second scenario shows the performance of the two controllers when the parameters of the FFSMS are not accurately known but estimated. Monte-Carlo simulations were performed in this scenario to manifest the behavior of the controllers for a plethora of different parametric uncertainties. The combination that resulted in the maximum errors is studied more thoroughly.

The third scenario is similar to the second since it involves parametric uncertainties. According to this case study, the object is already captured and stable but its parameters are not accurately known. Therefore, the controllers have to compensate for any errors. The motion of the FFSMS for this scenario is determined in the Joint Space. Finally, the fourth scenario studies the performance of the two controllers when the measurements involve noise. Another discrepancy of this scenario in comparison to the previous ones is that the object that the FFSMS needs to capture is not stationary but it has a known relative velocity.

The Adams model which is used as well as the design of the controllers were presented in Chapter 4. For facilitation, the data of the FFSMS are repeated in Table 5-1.

Table 5-1. Paremeters of the FFSMS.

Body	Mass - m_i (kg)	Moment of Inertia - I_i (kg·m^2)	Before-CM Length - l_i (m)	After-CM Length - r_i (m)
0	600	500	-	1.4
1	40	20	1	1
2	40	20	1	1
3	20	15	0.25	0.25

5.2 Scenario 1: Constant Disturbances

Although the effect of the friction in the FFSMS at the beginning of its lifetime might be small, as time goes by and the times that the manipulator is used increase, the friction at the joints of the manipulator may increase. This friction could be modeled satisfactorily as constant disturbances applied at each of the three joints of the manipulator.

In this scenario, the manipulator moves in Cartesian space to reach a relatively stationary target. First, the path planning is presented to yield the desired trajectories for the x and y coordinates as well as the orientation of the end-effector. After that, the Model Based PID Controller and the Model Based PD Controller with an auxiliary MPC input is implemented and compared to each other.

5.2.1 Path Planning

The control of an FFSMS in the Cartesian space requires the determination of the desired trajectories for the x and y coordinates as well as the orientation of the end-effector. In this thesis, fifth power polynomials are used to determine the initial and final value of the end-effector's variables, the velocity of them as well as their acceleration. For the position and orientation of the end-effector, the polynomials are described by:

$$\begin{aligned} x_{\mathrm{E}d}(t) &= a_0 + a_1 t + a_2 t^2 + a_3 t^3 + a_4 t^4 + a_5 t^5 \\ y_{\mathrm{E}d}(t) &= b_0 + b_1 t + b_2 t^2 + b_3 t^3 + b_4 t^4 + b_5 t^5 \\ \theta_{\mathrm{E}d}(t) &= c_0 + c_1 t + c_2 t^2 + c_3 t^3 + c_4 t^4 + c_5 t^5 \end{aligned} \tag{5-1}$$

where the coefficients are given by the solution of the three linear systems (considering that the initial time is $t_0 = 0$):

$$\begin{cases} x_{Ed}(t_0 = 0) = x_{Ed,0} \Rightarrow a_0 = x_{Ed,0} \\ x_{Ed}(t_f) = x_{Ed,f} \Rightarrow a_0 + a_1 t_f + a_2 t_f^2 + a_3 t_f^3 + a_4 t_f^4 + a_5 t_f^5 = x_{Ed,f} \\ \dot{x}_{Ed}(t_0 = 0) = \dot{x}_{Ed,0} \Rightarrow a_1 = \dot{x}_{Ed,0} \\ \dot{x}_{Ed}(t_f) = \dot{x}_{Ed,f} \Rightarrow a_1 + 2a_2 t_f + 3a_3 t_f^2 + 4a_4 t_f^3 + 5a_5 t_f^4 = \dot{x}_{Ed,f} \\ \ddot{x}_{Ed}(t_0 = 0) = \ddot{x}_{Ed,0} \Rightarrow a_2 = \ddot{x}_{Ed,0} \\ \ddot{x}_{Ed}(t_f) = \ddot{x}_{Ed,f} \Rightarrow 2a_2 + 6a_3 t_f + 12a_4 t_f^2 + 20a_5 t_f^3 = \ddot{x}_{Ed,f} \end{cases} \tag{5-2}$$

$$\begin{cases} y_{Ed}(t_0 = 0) = y_{Ed,0} \Rightarrow b_0 = y_{Ed,0} \\ y_{Ed}(t_f) = y_{Ed,f} \Rightarrow b_0 + b_1 t_f + b_2 t_f^2 + b_3 t_f^3 + b_4 t_f^4 + b_5 t_f^5 = y_{Ed,f} \\ \dot{y}_{Ed}(t_0 = 0) = \dot{y}_{Ed,0} \Rightarrow b_1 = \dot{y}_{Ed,0} \\ \dot{y}_{Ed}(t_f) = \dot{y}_{Ed,f} \Rightarrow b_1 + 2b_2 t_f + 3b_3 t_f^2 + 4b_4 t_f^3 + 5b_5 t_f^4 = \dot{y}_{Ed,f} \\ \ddot{y}_{Ed}(t_0 = 0) = \ddot{y}_{Ed,0} \Rightarrow b_2 = \ddot{y}_{Ed,0} \\ \ddot{y}_{Ed}(t_f) = \ddot{y}_{Ed,f} \Rightarrow 2b_2 + 6b_3 t_f + 12b_4 t_f^2 + 20b_5 t_f^3 = \ddot{y}_{Ed,f} \end{cases} \tag{5-3}$$

$$\begin{cases} \theta_{Ed}(t_0 = 0) = \theta_{Ed,0} \Rightarrow c_0 = \theta_{Ed,0} \\ \theta_{Ed}(t_f) = \theta_{Ed,f} \Rightarrow c_0 + c_1 t_f + c_2 t_f^2 + c_3 t_f^3 + c_4 t_f^4 + c_5 t_f^5 = \theta_{Ed,f} \\ \dot{\theta}_{Ed}(t_0 = 0) = \dot{\theta}_{Ed,0} \Rightarrow c_1 = \dot{\theta}_{Ed,0} \\ \dot{\theta}_{Ed}(t_f) = \dot{\theta}_{Ed,f} \Rightarrow c_1 + 2c_2 t_f + 3c_3 t_f^2 + 4c_4 t_f^3 + 5c_5 t_f^4 = \dot{\theta}_{Ed,f} \\ \ddot{\theta}_{Ed}(t_0 = 0) = \ddot{\theta}_{Ed,0} \Rightarrow c_2 = \ddot{\theta}_{Ed,0} \\ \ddot{\theta}_{Ed}(t_f) = \ddot{\theta}_{Ed,f} \Rightarrow 2c_2 + 6c_3 t_f + 12c_4 t_f^2 + 20c_5 t_f^3 = \ddot{\theta}_{Ed,f} \end{cases} \tag{5-4}$$

The system was solved with the help of Matlab's command *linsolve()*. The results are shown in Appendix A. The resulted trajectories for preset initial and final coordinates and orientation of the end-effector and for initial and final first and second derivatives of them equal to zero, which is the most usual case and the one that is used in this scenario, are shown in Figure 5-1.

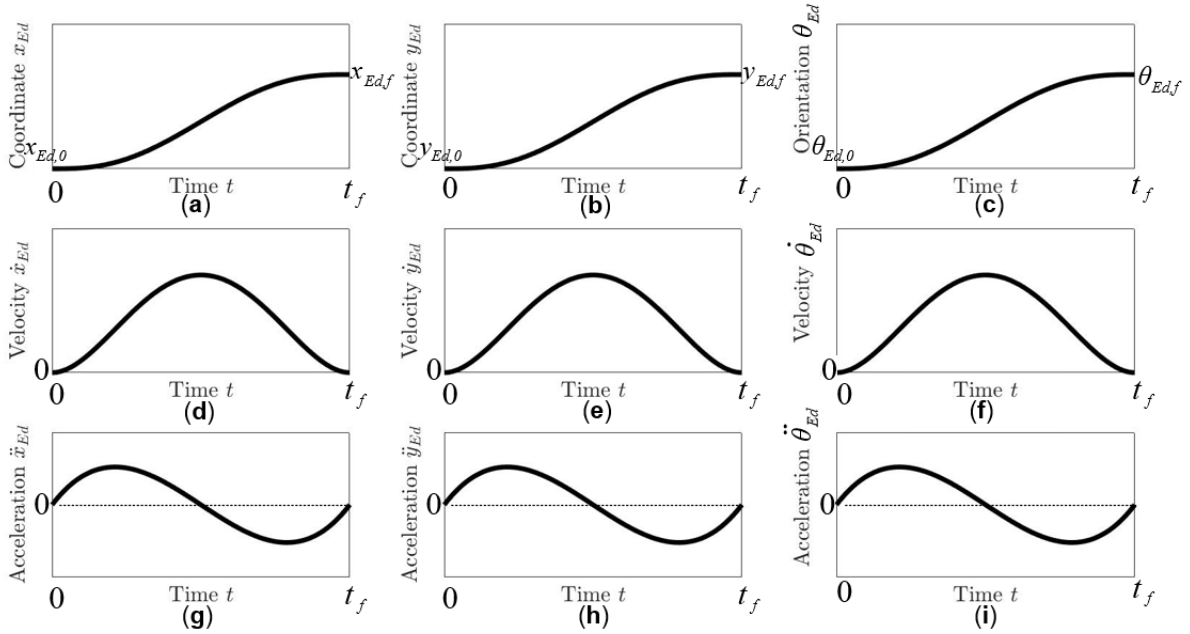

Figure 5-1. End-Effector's Desired Trajectories (a) Horizontal Position, (b) Vertical Position, (c) Orientation, (d) Horizontal Velocity, (e) Vertical Velocity (f) Angular Velocity, (g) Horizontal Acceleration, (h) Vertical Acceleration, (i) Angular Acceleration.

In Table 5-2 the values of the initial and final coordinates and orientation of the end-effector, its velocities and accelerations as well as the final time that is used in the scenario are presented. It is pivotal to clarify that the coordinates are measured from the FFSMS' Center of Mass (CM).

Table 5-2. Paremeters of the Desired Trajectories.

	x_E (m)	y_E (m)	θ_E (deg)
t_f (s)	6	6	6
Initial Value	0.2675	1.9220	195
Final Value	-2	1.8	170
1st Derivative's Initial Value	0	0	0
1st Derivative's Final Value	0	0	0
2nd Derivative's Initial Value	0	0	0
2nd Derivative's Final Value	0	0	0

5.2.2 Model Based PID Controller vs Model Based PD Controller with an Auxiliary MPC Input

For both controllers, the parameters of the FFSMS are given in Table 5-1 and considered known with adequate accuracy. The angular momentum is considered zero ($h_{CM}=0$). As presented in Chapter 4, the motion in the Cartesian space and the formation of a Transpose Jacobian Controller mandate the value of the matrices $\mathbf{H_x(q)}$ and $\mathbf{C}_x^*(\mathbf{q},\dot{\mathbf{q}})$. These matrices are given by Eq. (4-19) and they depend on the matrices $\mathbf{H(q)}$ and $\mathbf{C}^*(\mathbf{q},\dot{\mathbf{q}})$ as well as the Jacobian matrices $\mathbf{J}$ given by Eq. (4-13) and the derivative of the Jacobian $\dot{\mathbf{J}}$.

The disturbances act on the actuators of the manipulator. The values of the disturbances introduced in this scenario are:

$$\mathbf{d}=\begin{bmatrix}12 & 6 & 4\end{bmatrix}^T\ (Nm) \tag{5-5}$$

The values of the disturbances might be considered rather high for a realistic scenario. These values were chosen primarily to manifest clearly the different performance of the two compared controllers.

Figure 5-2 presents the block diagram of the system for both controllers.

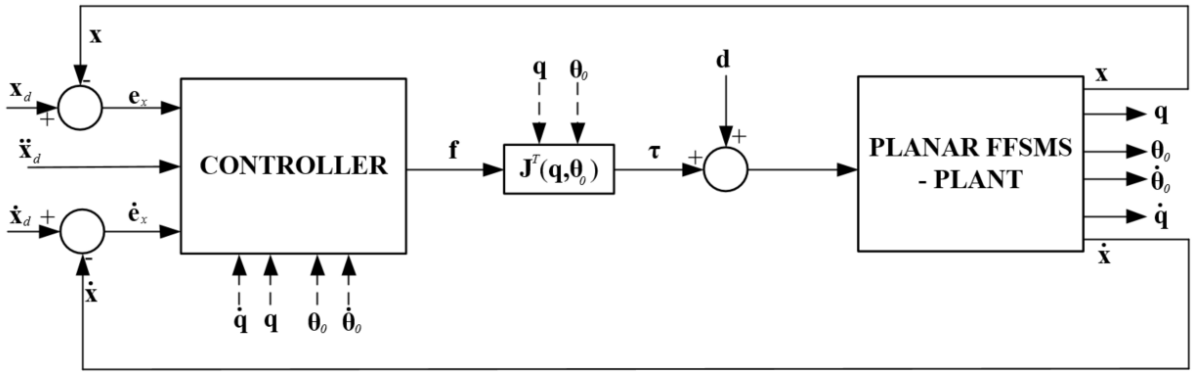

Figure 5-2. Block Diagram of the 1st Scenario.

The Model Based PID Controller is given by Eq. (4-23) and is repeated here for convenience:

$$\begin{aligned}\mathbf{f}&=\mathbf{H}_x\left[\ddot{\mathbf{x}}_d+\mathbf{K}_D\left(\dot{\mathbf{x}}_d-\dot{\mathbf{x}}\right)+\mathbf{K}_P\left(\mathbf{x}_d-\mathbf{x}\right)+\mathbf{K}_I\int_0^t\left(\mathbf{x}_d(\lambda)-\mathbf{x}(\lambda)\right)d\lambda\right]+\mathbf{C}_x^*\dot{\mathbf{x}}\\ \boldsymbol{\tau}&=\mathbf{J}^T\mathbf{f}\end{aligned} \tag{5-6}$$

As it was mentioned earlier, it is considered that the matrices $\mathbf{H_x(q)}$ and $\mathbf{C}_x^*(\mathbf{q},\dot{\mathbf{q}})$ are known and $h_{CM}=0$. Therefore, the only matrices that have to be defined are $\mathbf{K}_D$, $\mathbf{K}_P$ and $\mathbf{K}_I$.

The deduction of the respective characteristic equation of Eq. (4-24) for each of the three variables of the end-effector (x-coordinate, y-coordinate, orientation) results in:

$$\begin{aligned}&s^3+K_Ds^2+K_Ps+K_I=\left(s+\omega_n\right)\left(s^2+2\zeta\omega_ns+\omega_n^2\right)\Rightarrow\\ &\Rightarrow\begin{cases}K_D=2\zeta\omega_n+\omega_n\\ K_P=\omega_n^2+2\zeta\omega_n^2\\ K_I=\omega_n^3\end{cases}\end{aligned} \tag{5-7}$$

where ζ is the damping ratio and was defined based on the fact that a commonly used value is $\zeta=0.7$ and considering that the oscillation of the dynamics does not result in any impacts. ω_n is the natural frequency and was defined as $\omega_n=7.532\text{rad/s}$. The value of the natural

frequency was determined through a trial-error process until the maximum torques of the Model Based PD Controller with MPC Input and the Model Based PID Controller were adequately close and by considering the criterion that the errors of the position and orientation of the end-effector compared to the desired trajectories equal approximately zero at the desired settling time (6s) (for set-point input).

Consequently, the matrices $\mathbf{K}_D$, $\mathbf{K}_P$ and $\mathbf{K}_I$ are:

$$\begin{aligned}\mathbf{K}_D &= diag(18.08, 18.08, 18.08)\\ \mathbf{K}_P &= diag(136.15, 136.15, 136.15)\\ \mathbf{K}_I &= diag(427.30, 427.30, 427.30)\end{aligned} \tag{5-8}$$

It is evident that the integral gain $\mathbf{K}_I$ is quite larger than the other gains. This is rational since it was defined as the third power of the natural frequency (see Eq. (5-7)). Besides that, the definition of the integral gain is that it compensates for changing system dynamics, which is the main criterion that will be used for the comparison of the two controllers. In other words, the PID Controller needs to be designed with large integral gain in order to compete with the PD & MPC Controller.

The Model Based PD Controller with an Auxiliary MPC Input is given by Eq. (4-25) and is repeated here for convenience:

$$\begin{aligned}\mathbf{f}_{MPC} &= \mathbf{H}_x\left[\ddot{\mathbf{x}}_d + \mathbf{K}_{D,MPC}\left(\dot{\mathbf{x}}_d - \dot{\mathbf{x}}\right) + \mathbf{K}_{P,MPC}\left(\mathbf{x}_d - \mathbf{x}\right) + \mathbf{u}_{MPC}\right] + \mathbf{C}_x^*\dot{\mathbf{x}}\\ \boldsymbol{\tau}_{MPC} &= \mathbf{J}^T\mathbf{f}_{MPC}\end{aligned} \tag{5-9}$$

By neglecting the parametric uncertainties and the MPC signal for now, the characteristic equation, that results for each of the end-effector's variables (since the system has become decoupled) from Eq. (4-26), takes the form:

$$s^2 + K_{D,MPC}s + K_{P,MPC} = s^2 + 2\zeta\omega_n s + \omega_n^2 \tag{5-10}$$

where ζ and ω_n have been previously defined for the Model Based PID Controller.

Therefore, the matrices $\mathbf{K}_{D,MPC}$ and $\mathbf{K}_{P,MPC}$ are:

$$\begin{aligned}K_{D,MPC} &= diag(10.54, 10.54, 10.54)\\ K_{P,MPC} &= diag(56.73, 56.73, 56.73)\end{aligned} \tag{5-11}$$

As presented in Section 4.2.2, these values are used in the augmented model of Eq. (4-11) to derive the MPC control input. Prerequisites is to determine the scaling factor p, the number of Laguerre functions N, the prediction horizon T_p, and the parameters $\mathbf{Q}$ and $\mathbf{R}$.

Following the footsteps of Section 4.2.2, a good selection of the scaling factor is to set it equal to the dominant pole of the respective LQR problem [40] . By using the Matlab function *lqr()* the scaling factor was defined as $p = 5.5110$. Parameters N and T_p were determined through a number of trials until the results were remaining adequately constant. Consequently, $\mathrm{N} = 10$ and $T_p = 6$s. Finally, matrix $\mathbf{Q}$ was set equal to the transpose of the matrix of the output multiplied by the matrix of the output and $\mathbf{R}$ was set adequately small since the goal of the controller is to lessen the error and not the input signal:

$$\mathbf{Q} = \mathbf{C}^T\mathbf{C} = \begin{bmatrix} 0 & 0 & 0 \\ 0 & 0 & 0 \\ 0 & 0 & 1 \end{bmatrix} \qquad \mathbf{R} = 10^{-6} \tag{5-12}$$

Having determined the aforementioned parameters, the methodology which was presented in Section 3.2 is followed to apply the unconstrained MPC. The matrices $\mathbf{\Omega}$, $\mathbf{\Psi}$ and $\mathbf{L}(0)^T$ are calculated and used in the controller. For the constrained MPC, the methodology presented in Section 3.3 is applied. For this task, the maximum and minimum values for the output and/or input should also be given to the controller. Results containing the performance of constrained MPC are presented next.

Figure 5-3 includes snapshots of the motion of the FFSMS in the ADAMS environment for three different time-points and for top view and isometric view. The white line depicts the trajectory of the end-effector. Although the manipulator seems to pass above the base, this is not a problem for our studied model since the base and the manipulator are not on the same plane but on parallel ones. However, the case of them being on the same plane requires a different path planning method. This does not affect the results of the controllers' comparison.

Figure 5-4 presents the overall motion of the FFSMS as well as the Path Independent Workspace (PIW) and the Path Dependent Workspace (PDW). It is evident that the barycenter of the third link is moving in the PIW to avoid Dynamic Singularities (see Section 2.3.2). For evaluation of the motion, Figure 5-5 presents the determinant of the Jacobian (see Eq. (2-38)) which does not take values close to zero, hence, there is no worry for Dynamic Singularities. These figures are extracted from the performance of both controllers since the errors, that the controllers yield, are quite small (see Figure 5-7).

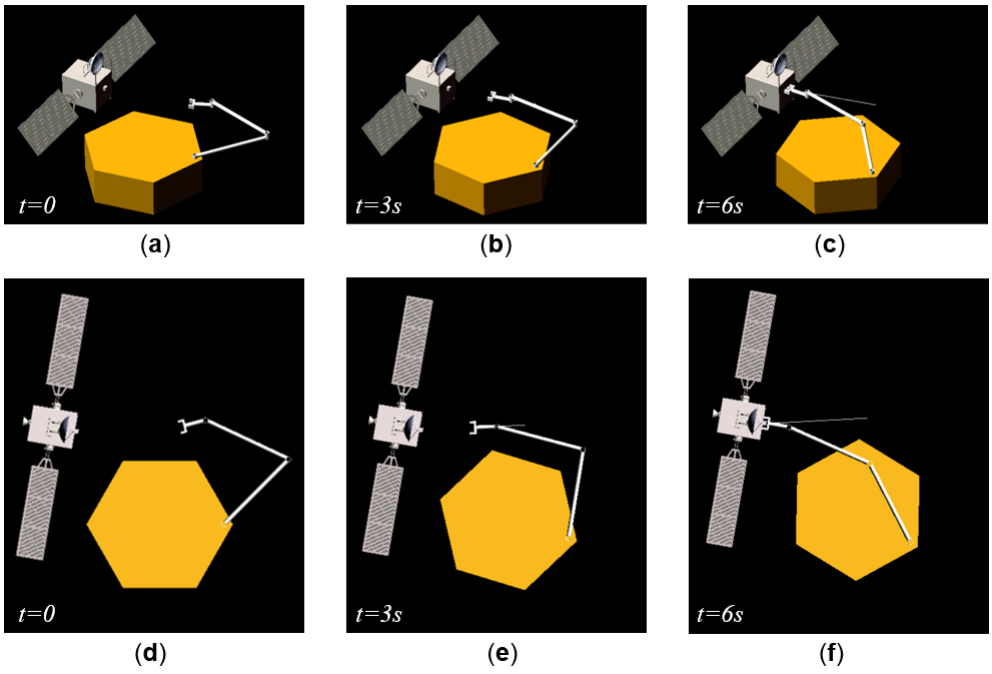

Figure 5-3. Snapshots of the Motion of the FFSMS in the ADAMS environment for three different time-points and two different views for the 1st Scenario (a) Isometric View (t=0), (b) Isometric View (t=3s), (c) Isometric View (t=6s), (d) Top View (t=0), (e) Top View (t=3s), (c) Top View (t=6s).

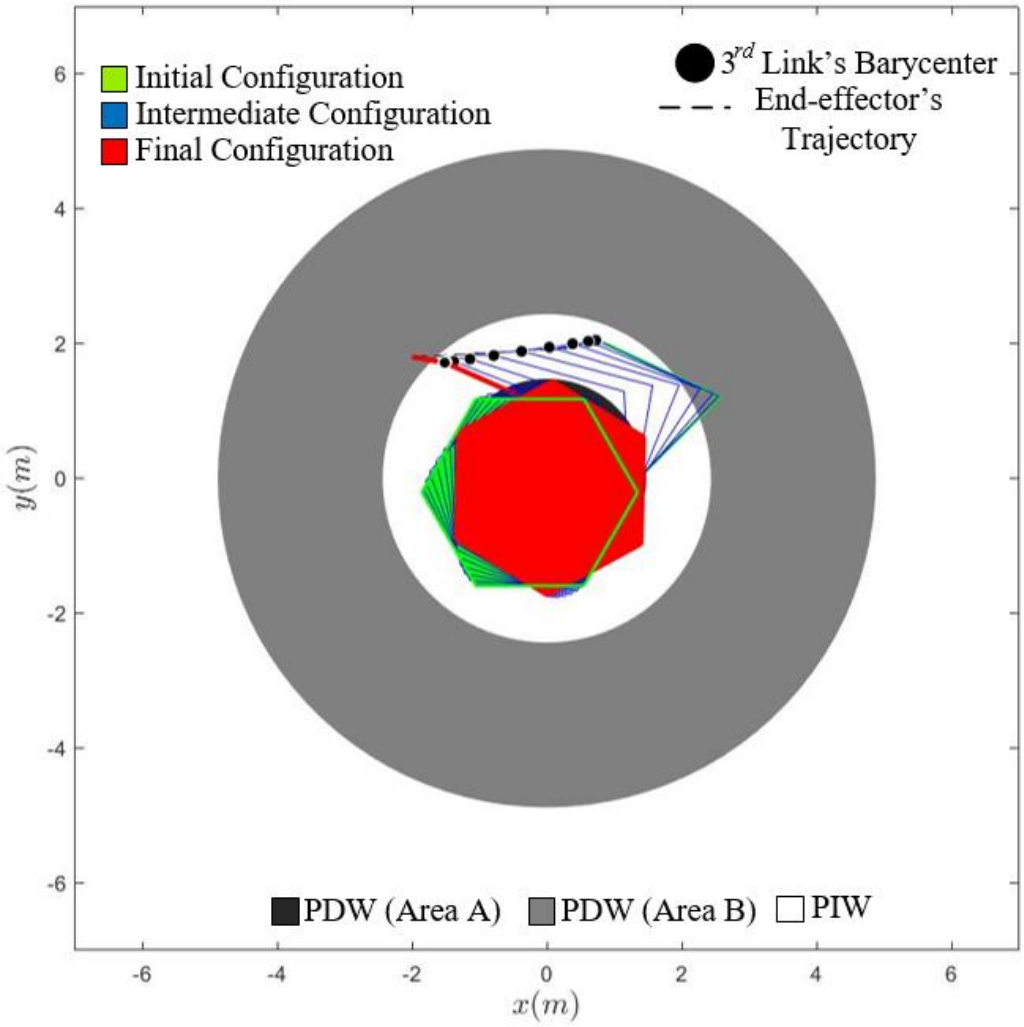

Figure 5-4. Motion of the FFSMS in the Cartesian Space for the 1st Scenario.

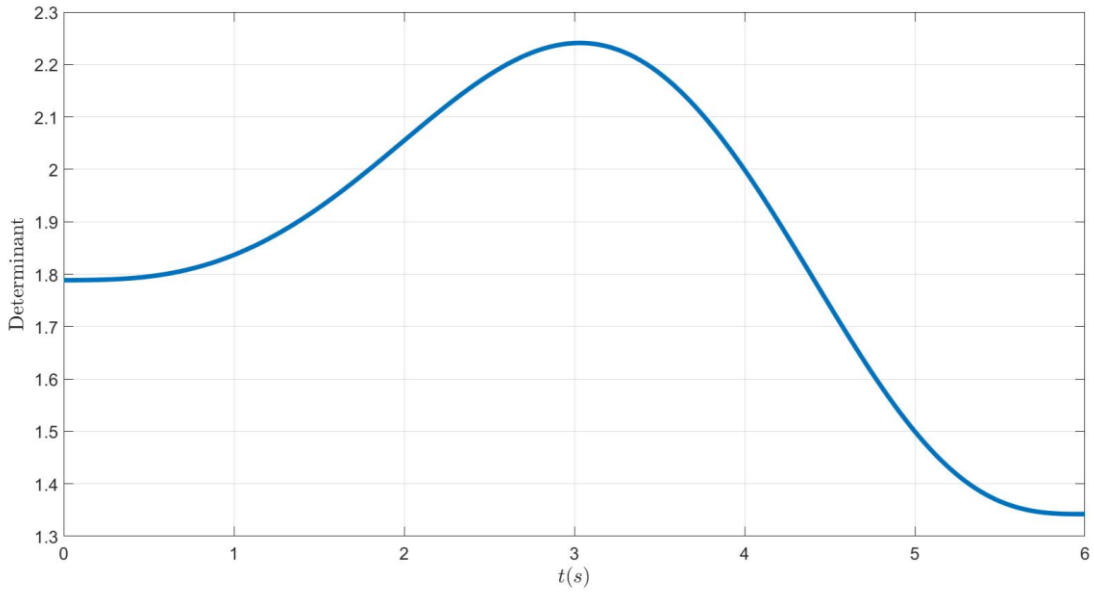

Figure 5-5. Determinant given by Eq. (2-38) for the 1st Scenario.

Figure 5-6 presents the end-effector trajectories in the x, y coordinate and its orientation trajectory. These diagrams are for both controllers since the errors of these variables are small enough for both of them. These errors are presented in Figure 5-7. It is obvious that the controller with the auxiliary MPC input has better results than the other controller in all three variables. In particular, the controller with the MPC input achieved:

- 43% reduction of the x-Coordinate error
- 43% reduction of the y-Coordinate error
- 43% reduction of the orientation error

It should be clarified that the criterion that the two controllers should reach 2% of the steady-state at about 6s is also satisfied for both controllers since the errors of the Model Based PID Controller are lower than 10^{-5} which is considered low enough for motion in the Cartesian space and the errors of the Model Based PD with an auxiliary MPC input are lower than 10^{-6} at about 6 seconds.

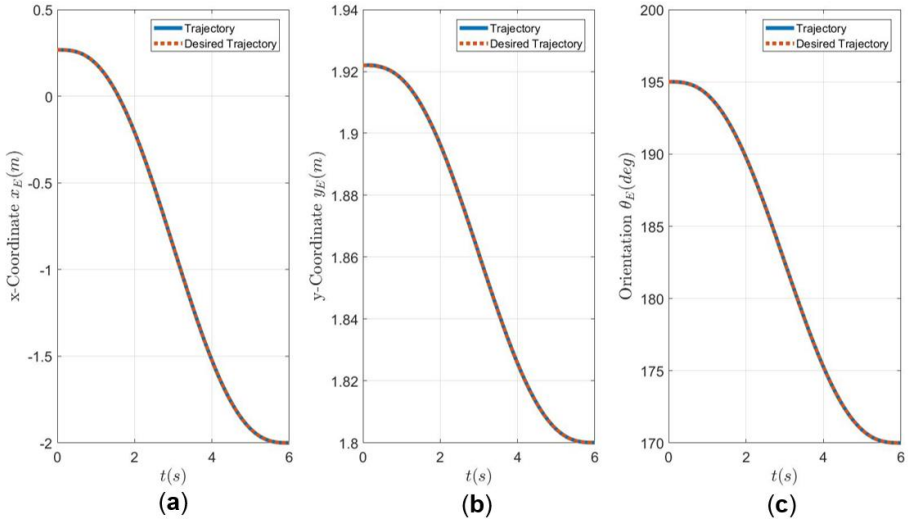

Figure 5-6. Actual and Desired Trajectories of the End-Effector (a) x-Coordinate, (b) y-Coordinate, (c) Orientation.

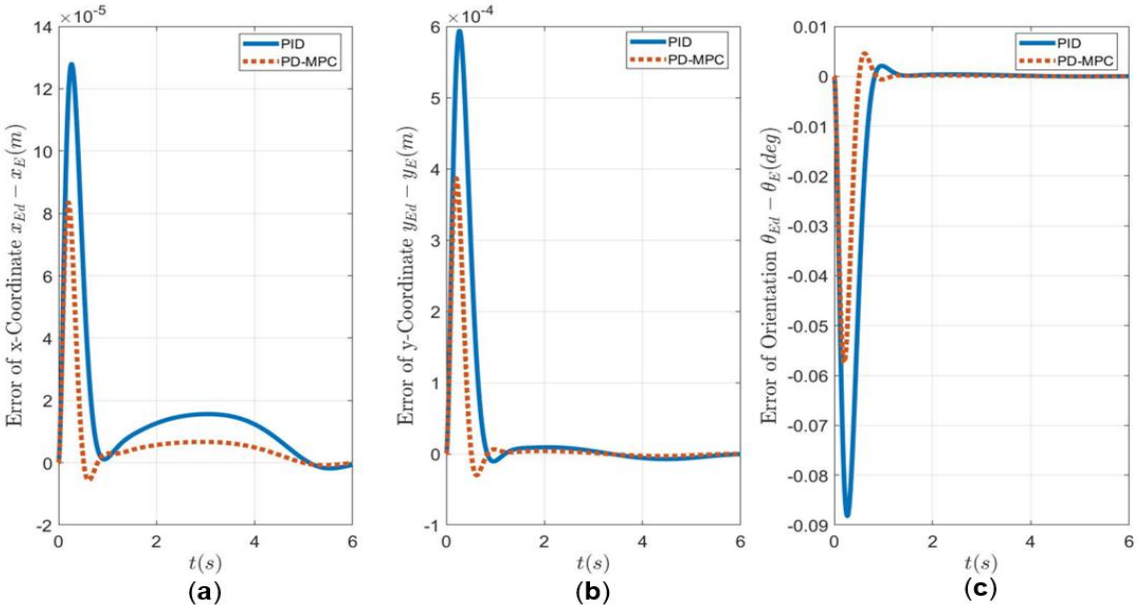

Figure 5-7. Error of the Actual and the Desired Value of the End-Effector's variables for the 1st Scenario (a) x-Coordinate, (b) y-Coordinate, (c) Orientation.

Figure 5-8 presents the torques that are applied to the joints of the manipulator. As it was mentioned earlier, the torques have to be close enough in order for the comparison of them to be considered valid. In other words, this means that the MPC does not require additionally control effort to achieve better results but it only distributes the torques better. The maximum torque of the first two joints is almost identical while the torque of the third joint manifest a 2% increase for the controller with the MPC input, which is considered negligible.

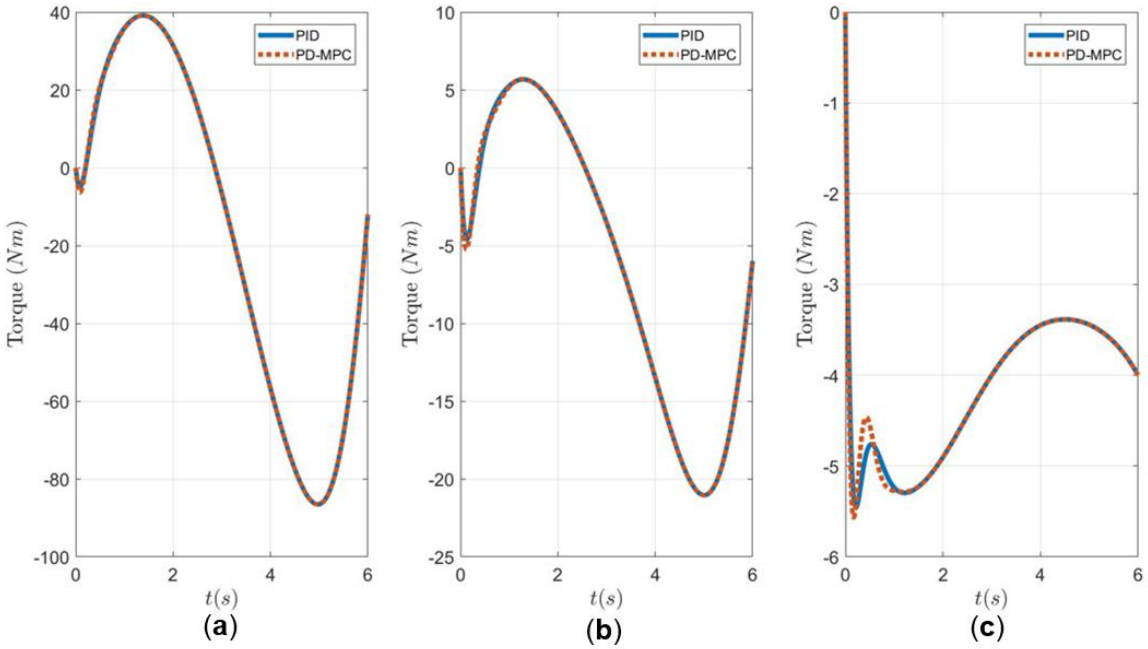

Figure 5-8. Torques of the Joints of the Manipulator applied in the 1st Scenario (a) 1st Joint, (b) 2nd Joint (c) 3rd Joint.

No constraints were introduced on the MPC controller presented in the preceding diagrams. As mentioned in Chapter 3, better results can be obtained if output constraints are inserted in the design of the controller. One of the benefits of MPC is the easy introduction of the constraints regardless of the time of the simulation. Since MPC optimizes the performance for each time-step, the constraints can be inserted and stopped regardless of the time. After a plethora of simulations, it was noticed that the errors are reduced significantly if the constraints presented below are inserted from the beginning of the simulation until the time-step $t = 0.01\text{s}$. If the constraints were not removed at that time-step, they would just slow the algorithm since it would not converge because of the enormous torques that it would require or the output constraints would just become inactive.

$$\begin{aligned} \mathbf{x}_{\max} &= \begin{bmatrix} 10^{-6} & 10^{-6} & 10^{-4}\pi/180 \end{bmatrix}^T \\ \mathbf{x}_{\min} &= -\mathbf{x}_{\max} \end{aligned} \tag{5-13}$$

However, because the output constraints contain the risk of rising significantly the joints' torques, input constraints on the MPC signal u_{MPC} were also introduced. So, if the signal exceeds these values, they become active:

$$\begin{aligned} \mathbf{u}_{\max} &= \begin{bmatrix} 0.5 & 0.5 & 0.5 \end{bmatrix}^T \\ \mathbf{u}_{\min} &= -\mathbf{u}_{\max} \end{aligned} \tag{5-14}$$

Figure 5-9 presents the errors when the preceding constraints are inserted in the MPC algorithm. It is obvious that the results are significantly better not only from the Model Based PID Controller but also from the Model Based PD Controller with unconstrained MPC. In particular, the Model Based PD Controller with MPC with output constraints achieves (in comparison with the Model Based PID Controller):

- 90% reduction of the x-Coordinate error
- 80% reduction of the y-Coordinate error
- 96% reduction of the orientation error

Apart from that, the criterion that the two controllers have to reach 2% steady-state at about 6s is again satisfied.

Figure 5-10 depicts the torques of the controllers. Note that this controller mandates the torques to achieve a considerably high value in small time duration. This might be a problem for the actuators of the manipulator and hence a problem for future examination. It is evident that these controllers also satisfied the criterion for equal maximum power that their joints' actuators could provide.

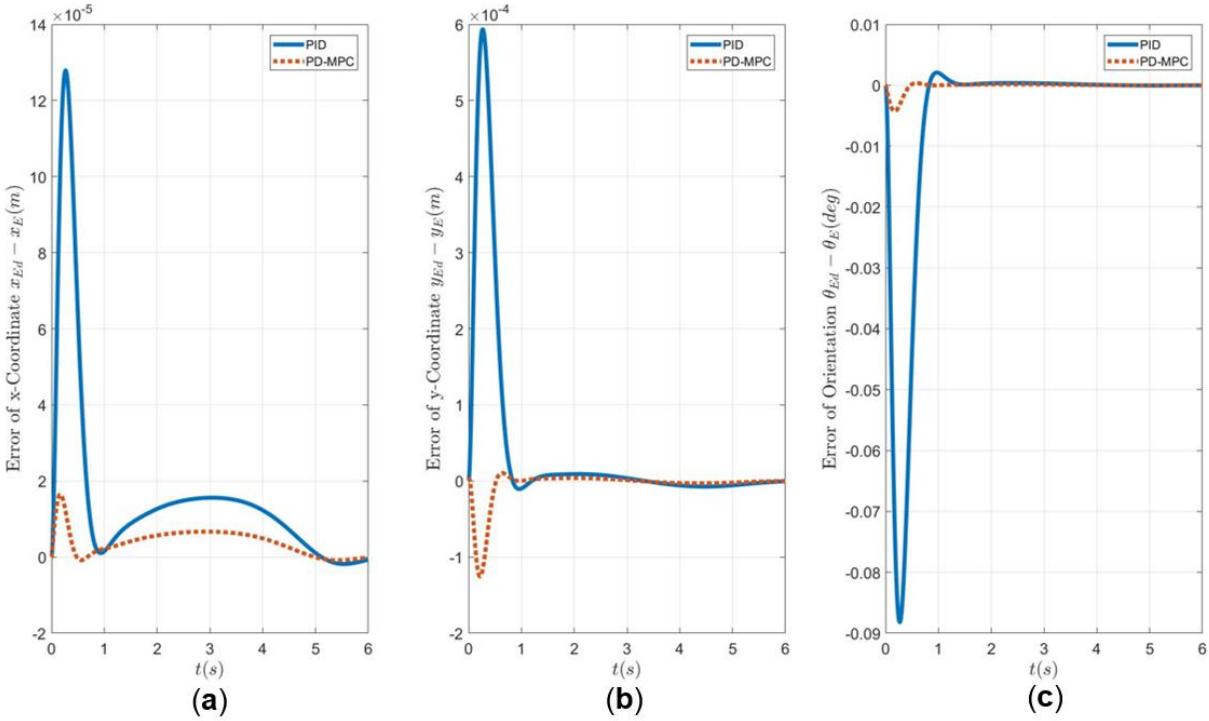

Figure 5-9. Error of the Actual and the Desired Value of the End-Effector's variables for the 1st Scenario using Constraints on the MPC (a) x-Coordinate, (b) y-Coordinate, (c) Orientation.

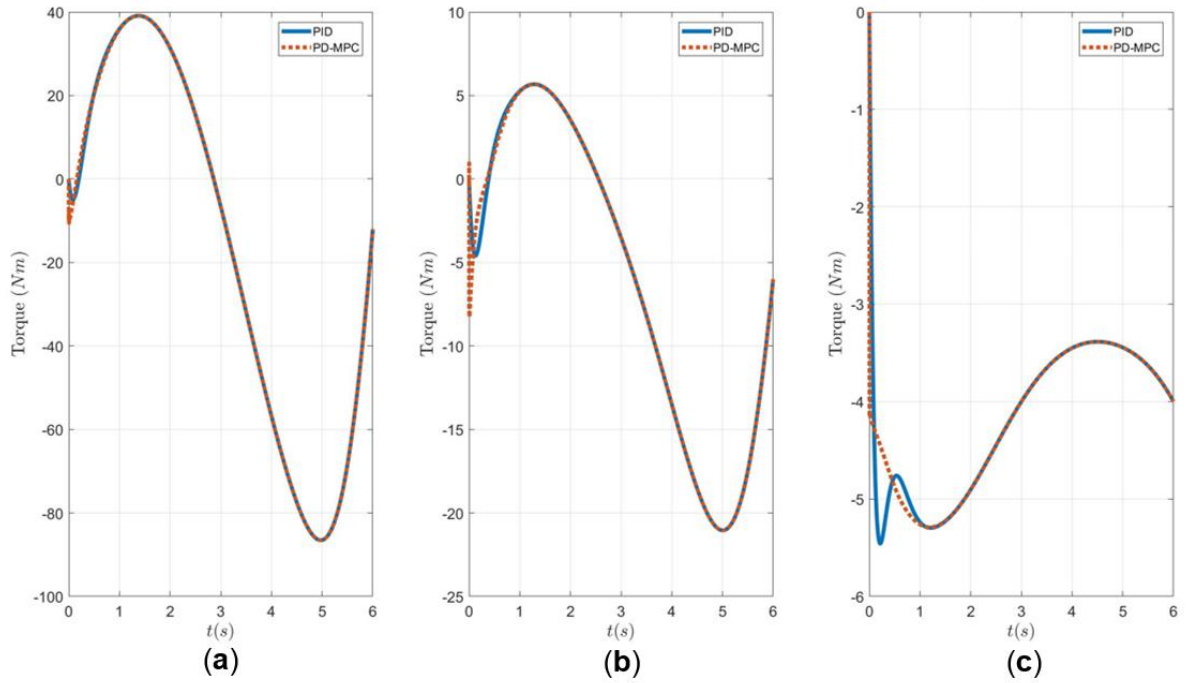

Figure 5-10. Torques of the Joints of the Manipulator applied in the 1st Scenario using Constraints on the MPC (a) 1st Joint, (b) 2nd Joint (c) 3rd Joint.

Finally, the controllers should be compared based on the computational power that they require which is proportionate to the duration of the simulation. Considering that the unconstrained MPC requires most of its computations to run off-line, its computational power should not exceed significantly the simple PID Controller. However, the MPC with constraints requires loops of the Hildreth's algorithm (see Section 3.3.1) to run during the simulation. Consequently, it shall require more computational power.

Through ample simulations using Matlab/Simulink and Adams and on the same computer, it was concluded that the average duration of the simulation (including the time required to present the results in the environment of Matlab/Simulink) when Model Based PID Controller is applied is 79s. The Model Based PD Controller with MPC without constraints takes about 82s and the Model Based PD Controller with MPC with constraints takes about 82s too. Although, it was expected that the latter would require more time, this extra duration is miniscule since the constraints are introduced only for 0.01s.

5.3 Scenario 2: Parametric Uncertainties

In this Section, the Scenario of parametric uncertainties is presented. As mentioned in Chapter 1, it is very common for the parameters of an FFSMS to deviate from the nominal/manufacturing dimensions due to the extreme alterations of temperature throughout its lifetime. This can cause significant errors to the lengths of the manipulator as well as the base. Besides that, small collisions with other objects that float into space and the reduction of the base's mass due to its fuel consumption can cause divergence of the joints' mass and the mass of the base respectively. It is veritable that the fuel would be consumed at a known rate. Nonetheless, an abnormality of the actuators might cause excessive and uncertain fuel consumption which would result in significant uncertainty regarding the mass of the base. It

is evident that the preceding controllers have to perform successfully and counterbalance these errors.

Firstly, a Monte-Carlo simulation is performed for a wide range of parametric uncertainties to investigate the performance of both controllers and to indicate the parameter that cause the highest errors of the end-effector's position and orientation. Secondly, a more scrutinous analysis would be performed using the parameters with the highest errors. Besides the unconstrained MPC, the case of the Model Based PD Controller with MPC input with constraints is presented too.

5.3.1 Sensitivity Analysis & Monte-Carlo Simulation

A Monte-Carlo simulation (or Monte-Carlo method) is a simulation that is repeated using a wide range of different parameters. The parameters are obtained using random sampling and statistical analysis [30] . For this case, the samples are taken based on the following parameter variation:

$$\begin{aligned} &0.95l_{i,nominal} \le l_i \le 1.05l_{i,nominal} \quad i=1-3 \\ &0.95r_{i,nominal} \le r_i \le 1.05r_{i,nominal} \quad i=1-3 \\ &0.95m_{i,nominal} \le m_i \le 1.05m_{i,nominal} \quad i=1-3 \\ &0.80m_{0,nominal} \le m_0 \le 1.05m_{0,nominal} \end{aligned} \tag{5-15}$$

The argument behind this selection was presented in Section 5.3. It is also important to note that the moment of inertia of each part was chosen to vary proportionally with the variance of its respective mass.

To acquire the samples, the Sensitivity Analysis package of Matlab/Simulink was used. The sample of the statistics of each variance of Eq. (5-15) was selected to be uniform (same possibility for each value). There were chosen 200 different combinations.

The model that was used is almost the same with the one studied in Scenario 1. The only difference is that an analytical representation of the plant was used, substituting the Adams model, to save computational power. The values of the end-effector's position, orientation as well as their velocities were obtained using inverse kinematics. The nominal values of these parameters were used for the equations of the inverse kinematics since in reality these values would be obtained through sensors and cameras.

The nominal values of the FFSMS parameters are given in Table 5-1. For the determination of the desired trajectory, 5th polynomials were used and their values are presented in Table 5-2. The torques of the Model Based PID Controller are given by Eq. (5-6) and the gains of each joint are given by Eq. (5-8). The torques of the Model Based PD Controller with an auxiliary MPC input are given by Eq. (5-9) and the respective gains are given by Eq. (5-11). The rest of the required parameters of the MPC can be found in Scenario 1.

The results of the 200 simulations performed are displayed in Figure 5-11. The errors of the position and orientation of the end-effector are shown. Diagrams (a), (b) and (c) depict the results when the Model Based PID Controller is implemented while diagrams (d), (e) and (f) depict the results when the Model Based PD Controller with an MPC Input is implemented. It is clear that the latter improves significantly the results by minimizing the error. Table 5-3 shows the maximum errors for each controller as well as the values of the FFSMS' parameters that result in these values. It is obvious that the maximum for each of

the three variables is a result of a different combination of the FFSMS' parameters. However, it was observed that the y-coordinate's error varies almost proportionally with the orientation's error while the x-coordinate error is inversely proportional. Finally, it can be concluded that the values do not converge to zero in 6s. Nevertheless, as it would be presented in the following Section, the integration of constraints in the MPC can result in a partial solution to this problem.

Figure 5-12 shows which parameter has the most impact for each one of the three errors. These results were obtained using the Sensitivity Analysis tool of Matlab/Simulink. It can be concluded that for each of the three errors, different parameters are the most influential. In these tornado diagrams, correlation indicates how a model parameter and the cost function output are correlated, partial correlation shows how these are correlated while removing the effects of the rest parameters and finally standardized regressions shows to what extent the parameters have a linear influence on the cost function.

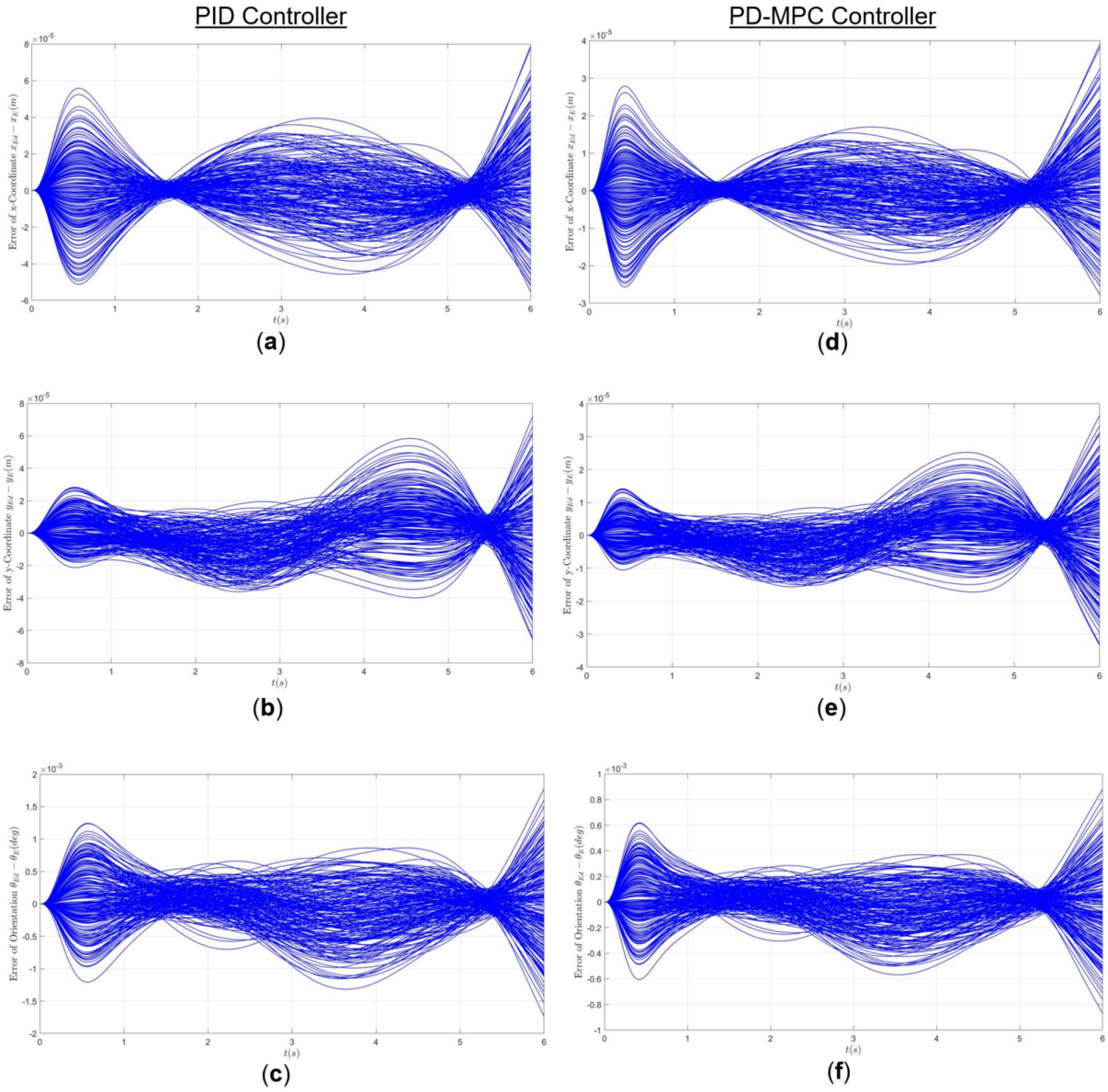

Figure 5-11. Errors of the End-Effector's Position & Orientation using Monte-Carlo Simulation for the 200 Different Random Samples. (a), (b) and (c): Model Based PID Controller, (d), (e) and (f): Model Based PD Controller with MPC Input.

Table 5-3. Maximum Errors performing Monte-Carlo Simulation and their Model Parameters.

	$x_{E,d} - x_d$	$y_{E,d} - y_d$	$\theta_{E,d} - \theta_d$
Max_{PID}	$7.919 \cdot 10^{-5}$	$7.176 \cdot 10^{-5}$	$18 \cdot 10^{-4}$
Max_{PD-MPC}	$3.925 \cdot 10^{-5}$	$3.645 \cdot 10^{-5}$	$8.818 \cdot 10^{-4}$
m_0 (kg)	540.9	595.1	510.7
(m_1, m_2, m_3) (kg)	(39.81, 41.80, 20.98)	(38.65, 41.51, 20.77)	(38.61, 40.82, 20.93)
r_0 (m)	1.384	1.376	1.364
(r_1, r_2, r_3) (m)	(1.019, 1.046, 0.2576)	(0.9631, 1.046, 0.2534)	(1.016, 1.042, 0.2511)
(l_1, l_2, l_3) (m)	(1.042, 0.993, 0.244)	(0.9611, 1.037, 0.2552)	(0.9631, 1.049, 0.2405)

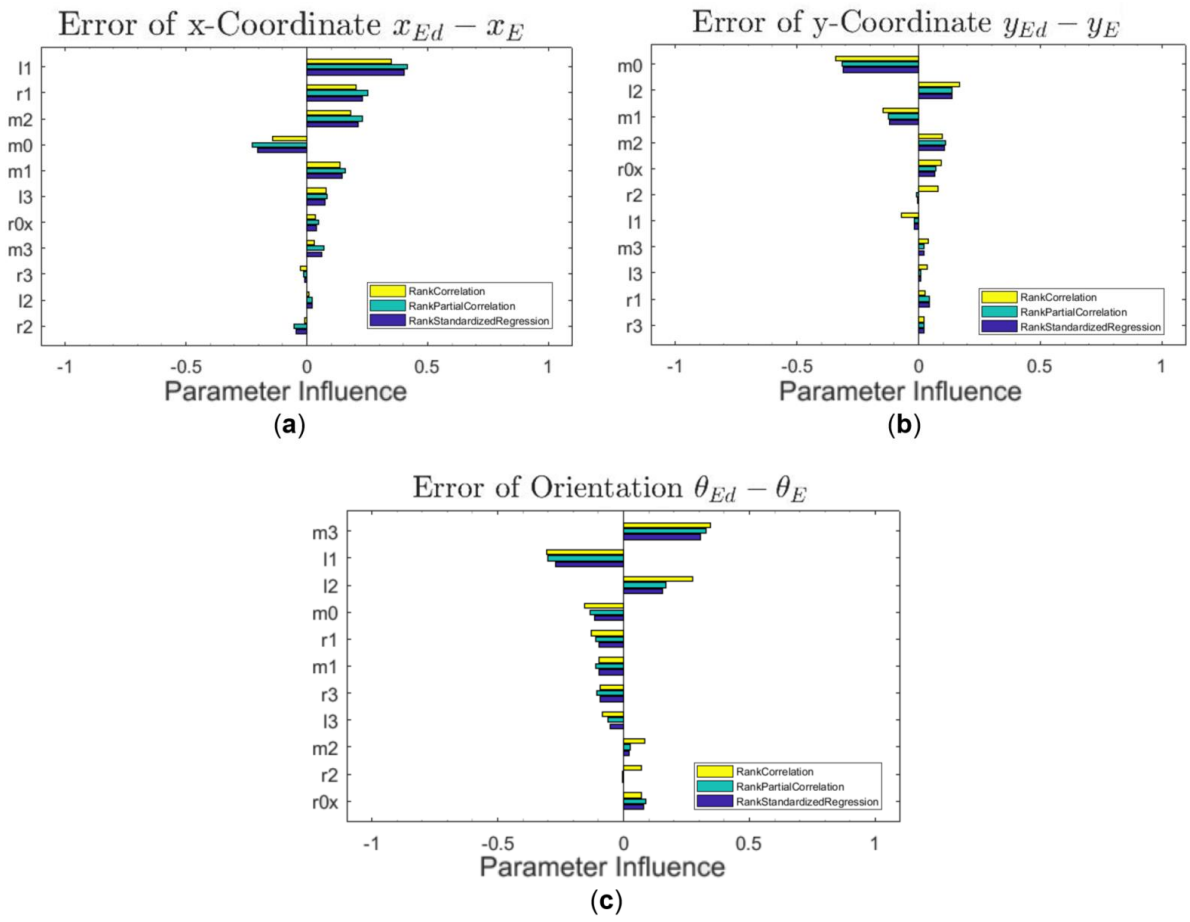

Figure 5-12. Parameter Influence on the Position & Orientation of the End-Effector.

5.3.2 Model Based PID Controller vs Model Based PD Controller with an Auxiliary MPC Input

It is interesting to investigate more thoroughly the performance of the controllers for the model parameters that result in the maximum incongruities. In this section, the parameters that result in the maximum error of the end-effector's x-coordinate are regarded as the approximate (known) parameters of the model (see Table 5-3). However, the Adams model that is used for the plant contains the nominal values of the parameters (see Table 5-1).

Figure 5-13 presents the errors of the x-coordinate, the y-coordinate and the orientation of the end-effector. It is obvious that the controller with the auxiliary MPC input has better results than the simple PID Controller in all three variables. In particular, the controller with the MPC input achieved:

- 50% reduction of the x-Coordinate error
- 57% reduction of the y-Coordinate error
- 57% reduction of the orientation error

Note that the criterion that the two controllers should reach 2% of the steady-state at about 6s is not satisfied for neither of the controllers, despite the fact that MPC has lower errors at 6s. The reason behind this phenomenon is the fact that the disturbances, that the parametric uncertainties produce, vary with time.

Figure 5-14 presents the torques that are applied to the actuators of the manipulator. As mentioned earlier, the applied torques have to be close enough in order for the comparison of them to be considered valid. In other words, this means that the MPC does not require additional control effort to achieve better results but it only distributes the torques better. This criterion is satisfied perfectly.

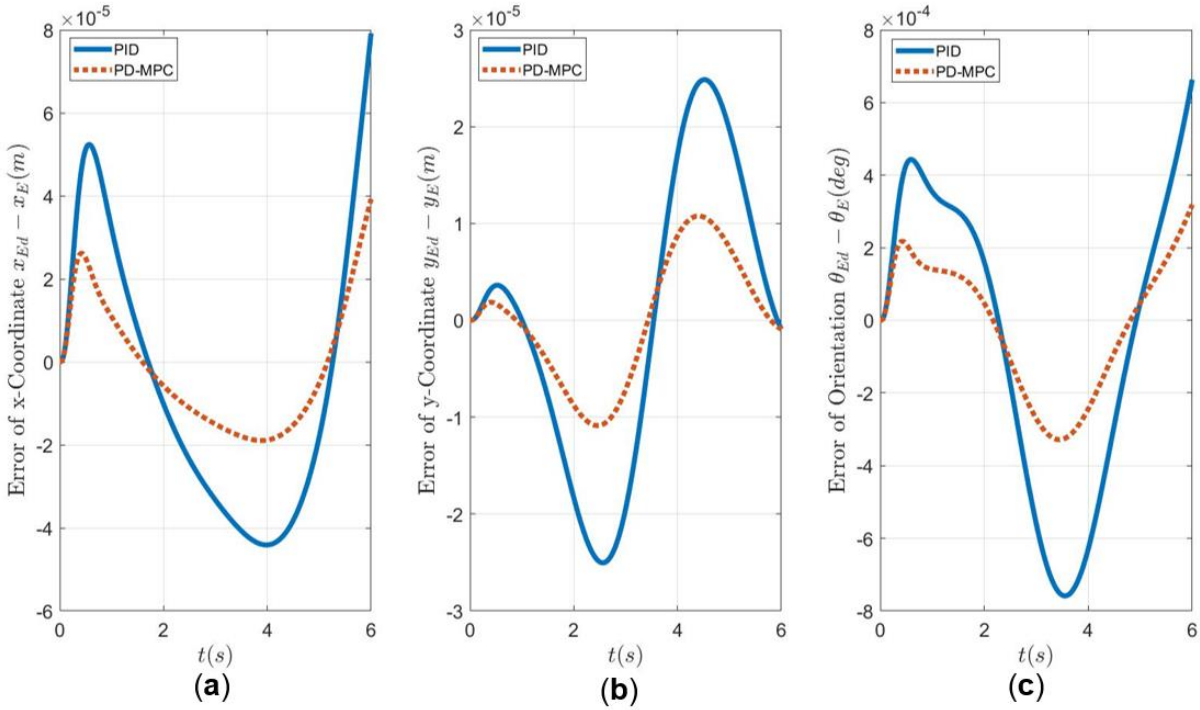

Figure 5-13. Error of the Actual and the Desired Value of the End-Effector's variables for the 2nd Scenario (a) x-Coordinate, (b) y-Coordinate, (c) Orientation.

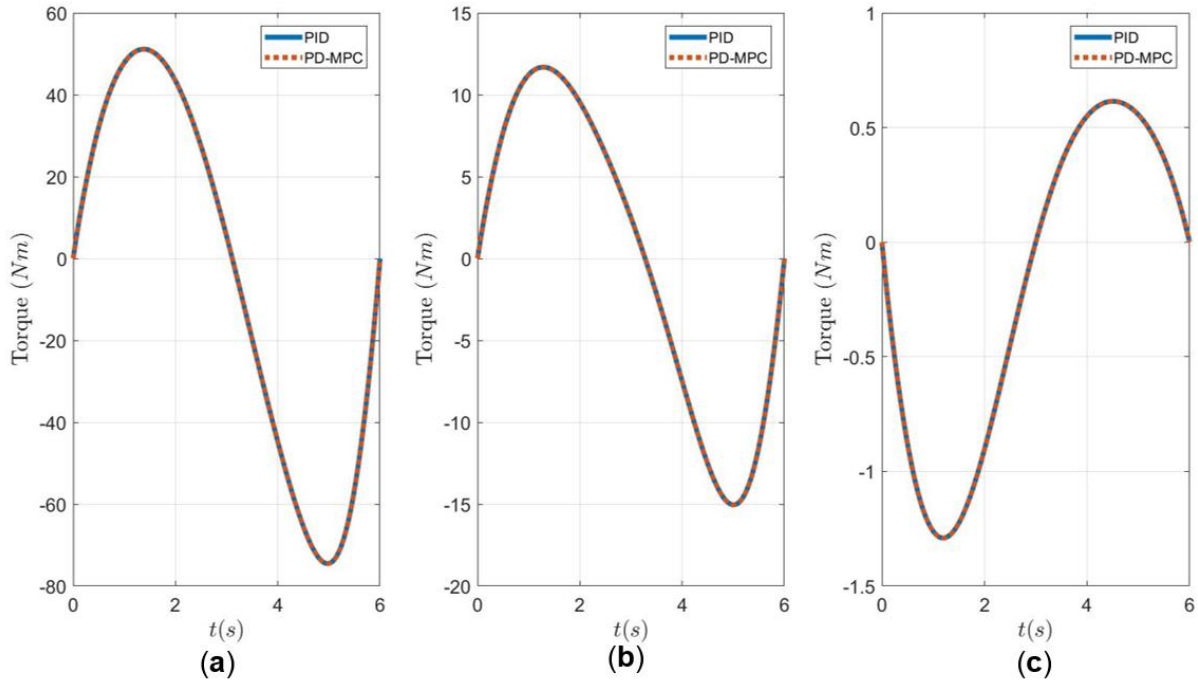

Figure 5-14. Torques of the Joints of the Manipulator applied in the 2nd Scenario (a) 1st Joint, (b) 2nd Joint (c) 3rd Joint.

To achieve a partial convergence of the errors at the steady-state, constraints were integrated on the MPC. In particular, the constraints were inserted after the time-step t = 4.5s and until the end of the simulation. These output/error constraints are:

$$\mathbf{x}_{\max} = \begin{bmatrix} 5\cdot10^{-6} & 5\cdot10^{-6} & 5\cdot10^{-6}\pi/180 \end{bmatrix}^T$$
$$\mathbf{x}_{\min} = -\mathbf{x}_{\max} \tag{5-16}$$

However, because the output constraints contain the risk of surge of the joints' torques, input constraints on the MPC signal u_{MPC} were also introduced. So, if the signal exceeds these values, they become active:

$$\mathbf{u}_{\max} = \begin{bmatrix} 2 & 2 & 2 \end{bmatrix}^T$$
$$\mathbf{u}_{\min} = -\mathbf{u}_{\max} \tag{5-17}$$

Figure 5-15 presents the errors when the preceding constraints are inserted in the MPC algorithm. It can be seen that the orientation converges smoothly to zero. However, the error of the x-coordinate does not, despite the fact that at some point it tries to. At that point, the input constraints become active because it would result in significant increase of the torques which would might lead to instability. Finally, the Model Based PD Controller with MPC with output constraints achieves (in comparison with the Model Based PID Controller):

- 50% reduction of the x-Coordinate error
- 57% reduction of the y-Coordinate error
- 57% reduction of the orientation error

Figure 5-16 depicts the torques of the controllers. The two controllers manifest a 4% deviation for the first and second joint, a percentage that can be considered negligible.

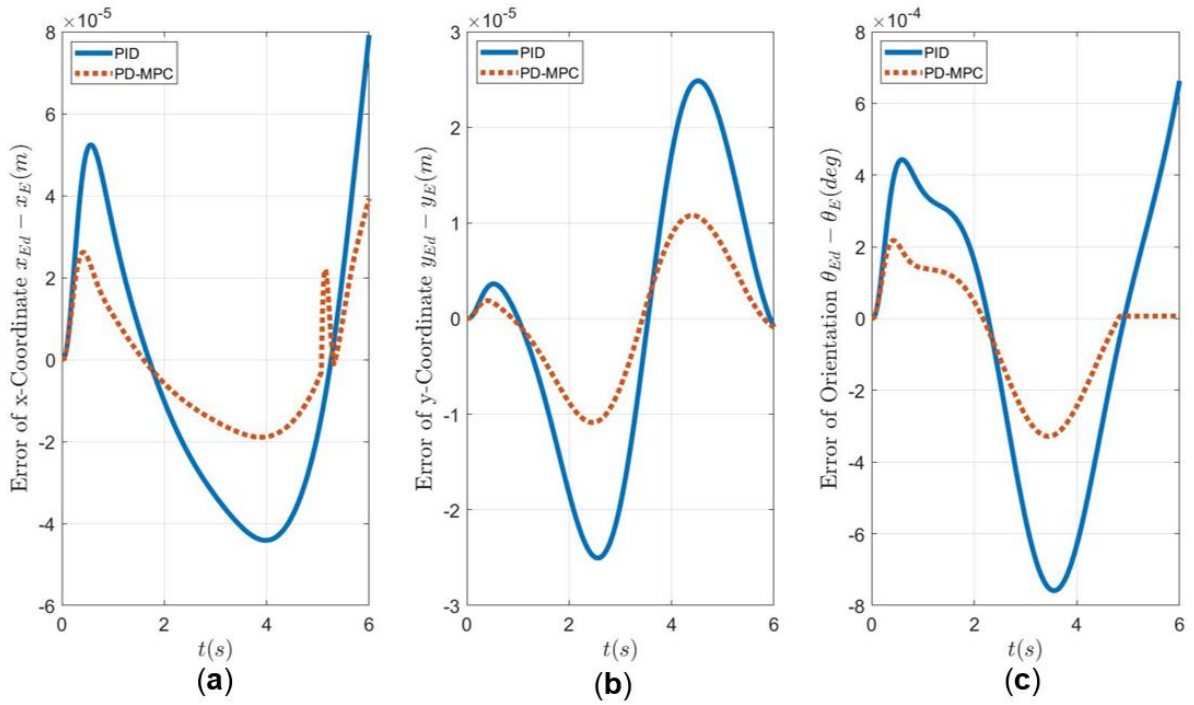

Figure 5-15. Error of the Actual and the Desired Value of the End-Effector's variables for the 2nd Scenario using Constraints on the MPC (a) x-Coordinate, (b) y-Coordinate, (c) Orientation.

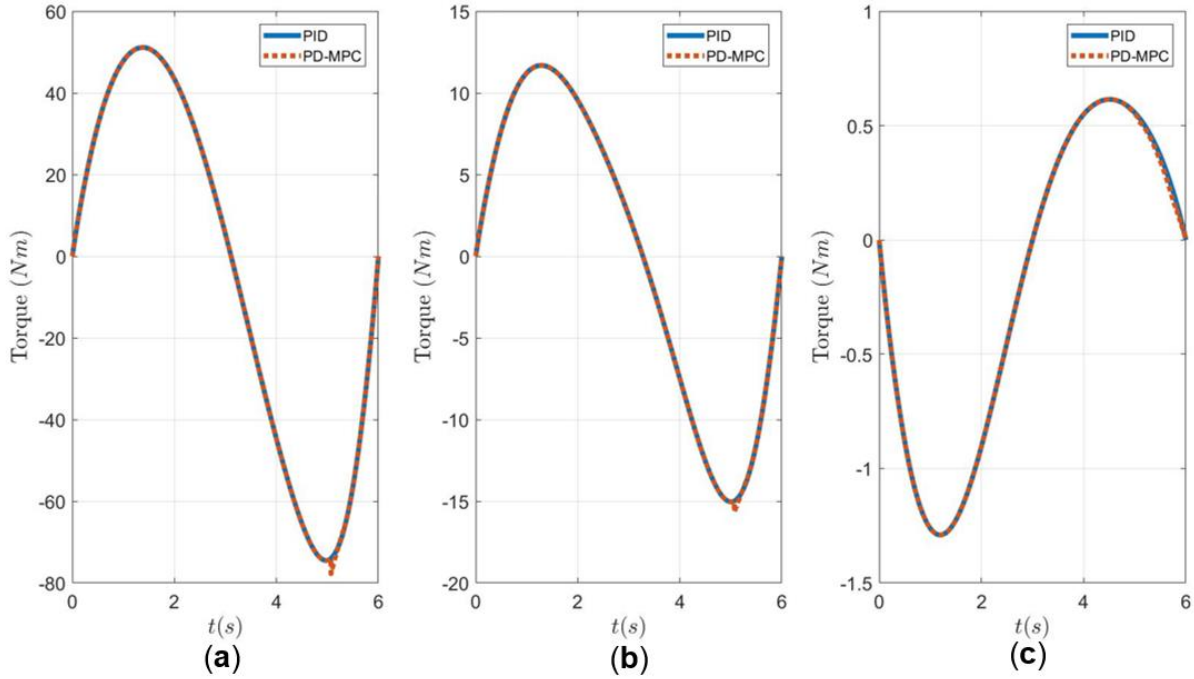

Figure 5-16. Torques of the Joints of the Manipulator applied in the 2nd Scenario using Constraints on the MPC (a) 1st Joint, (b) 2nd Joint (c) 3rd Joint.

5.4 Scenario 3: Position Captured Object of Unknown Mass

The main cause of an FFSMS is to capture and move an object which floats in space. Although rough data of the object might be known from the period of time that it was functioning or can be acquired through cameras and sensors of the FFSMS, the actual values of the object's parameters would probably have a deviation from the known parameters. In this scenario, the position of a captured object with undefined mass, inertia as well as position of its Center of Mass (CM) would be presented. The stabilization of the object, which is the previous stage of an on-orbit servicing mission (see Chapter 1), is considered accomplished. This scenario is expected to show similar behavior with Scenario 2 since the captured object would be regarded as an extension of the 3rd link. Therefore, the parametric uncertainty of the captured object is considered as a parametric uncertainty of the 3rd link. In contrast to the preceding scenarios, in this scenario the FFSMS moves in the joint space and not in the Cartesian space.

The variable m_s is used for the mass of the captured object, I_s for the Inertia of the captured object, and r_s for the distance between the CM of the 3rd link and the CM of the captured object. The mass of the unified 3rd link and captured object is given by:

$$m_3^{'} = m_3 + m_s \tag{5-18}$$

The inertia of the unified 3rd link and captured object with respect to the position of its CM, by implementing Steiner's theorem, is given by:

$$I_3^{'} = I_3 + I_s + m_3\left(l_3^{'} - l_3\right)^2 + m_s r_3^{'2} \tag{5-19}$$

where $l_3^{'}$ is the distance between the 3rd joint and the new CM, $r_3^{'}$ is the distance between the new CM and the CM of the captured object and they are given by:

$$\begin{aligned} l_3^{'} &= \frac{m_3 l_3 + m_s\left(l_3 + r_s\right)}{m_3 + m_s} \\ r_3^{'} &= r_s + l_3 - l_3^{'} \end{aligned} \tag{5-20}$$

The values of these variables that will be used in the simulation are presented in Table 5-4. The rest of the parameters of the FFSMS are presented in Table 5-1.

Table 5-4. Parameters of the Captured Object.

Captured Object	Nominal Value	Estimated Value
Mass m_s (kg)	200	220
Moment of Inertia I_s (kg·m^2)	100	110
Distance r_s (m)	0.8	0.76

5.4.1 Path Planning

As previously mentioned, the control of the FFSMS is performed in the joint space. Fifth power polynomials are used for the determination of the desired trajectories. They are given by Eq. (4-27) - (4-28) and presented in Figure 4-8.

In Table 5-5 the values of the initial and final angle, angular velocity and acceleration as well as the final time that is used in this scenario for each of the three joints are presented.

Table 5-5. Paremeters of the Desired Trajectories for the 3rd Scenario.

Joint	1st	2nd	3rd
t_f (s)	6	6	6
Initial Angle $q_{d,0}$ (deg)	45	110	-60
Final Angle $q_{d,f}$ (deg)	20	60	-70
Initial Angular Velocity $\dot{q}_{d,0}$ (deg/s)	0	0	0
Final Angular Velocity $\dot{q}_{d,f}$ (deg/s)	0	0	0
Initial Angular Acceleration $\ddot{q}_{d,0}$ (deg/s^2)	0	0	0
Final Angular Acceleration $\ddot{q}_{d,f}$ (deg/s^2)	0	0	0

5.4.2 Model Based PID Controller vs Model Based PD Controller with an Auxiliary MPC Input

The torques of the Model Based PID Controller are given by Eq. (4-6) (with the assumption that the angular momentum is considered zero ($h_{CM}=0$)) and the gains of each joint are given by Eq. (4-34). The torques of the Model Based PD Controller with an auxiliary MPC input are given by Eq. (4-8) and the respective gains are given by Eq. (4-30). The argument for selecting these gains can be found in Section 4.5. The rest of the required parameters of the MPC are:

$$\begin{aligned} p &= 5.5110 \\ N &= 10 \\ T_p &= 6s \\ \mathbf{Q} = \mathbf{C}^T\mathbf{C} &= \begin{bmatrix} 0 & 0 & 0 \\ 0 & 0 & 0 \\ 0 & 0 & 1 \end{bmatrix} \\ \mathbf{R} &= 10^{-6} \end{aligned} \tag{5-21}$$

There are no output constraints integrated in the MPC design since it was observed that no particular benefit can be acquired from them.

Figure 5-17 contains snapshots of the motion of the FFSMS in the ADAMS environment for three different time-points and for top and isometric view. The path planning was conducted in the joint space. Hence, there is no concern for Dynamic Singularities. The figure presents the motion when either of the controllers is applied since the errors of both controllers are quite small (see Figure 5-18).

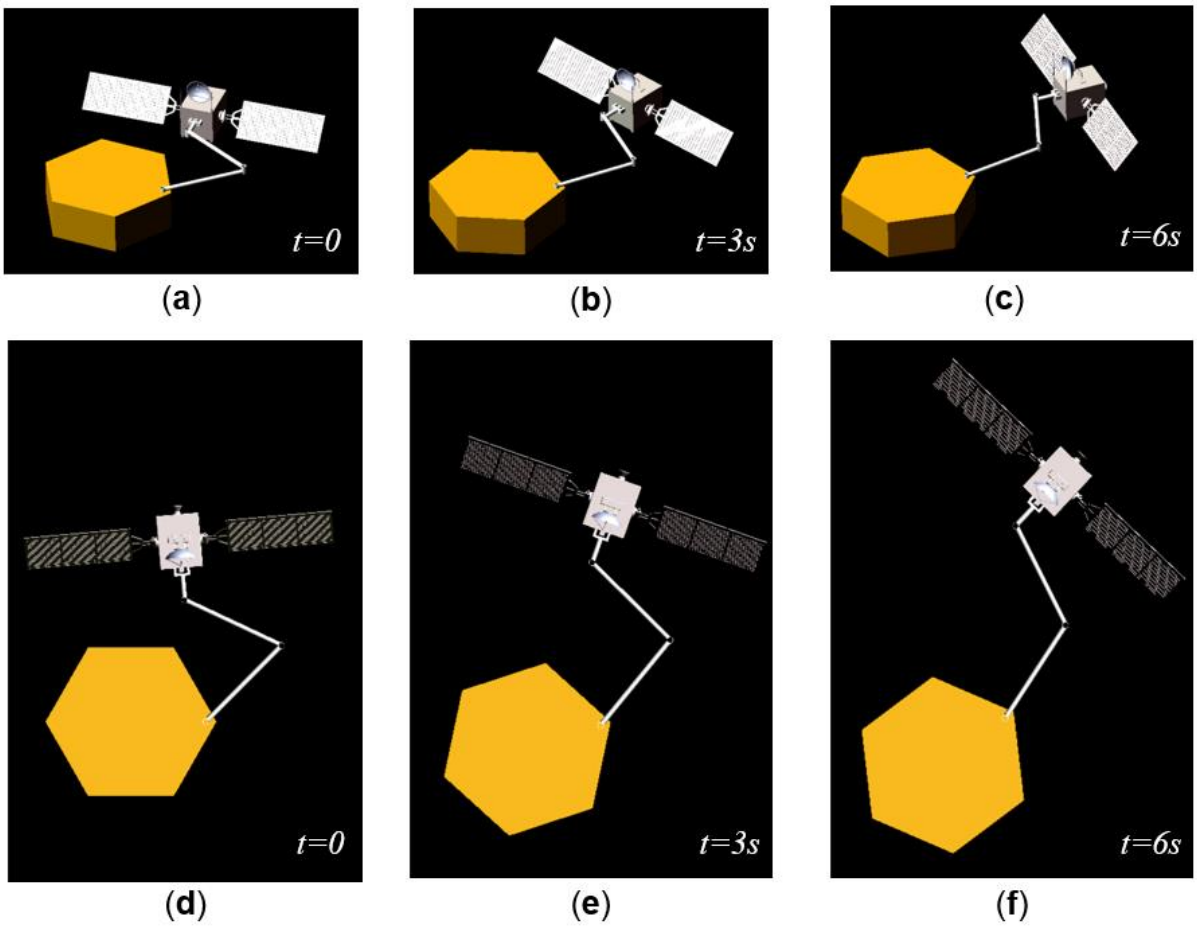

Figure 5-17. Snapshots of the Motion of the FFSMS in the ADAMS environment for three different time-points and two different views for the 3rd Scenario (a) Isometric View (t=0), (b) Isometric View (t=3s), (c) Isometric View (t=6s), (d) Top View (t=0), (e) Top View (t=3s), (c) Top View (t=6s).

Figure 5-18 presents the errors of the angles of the manipulator's joints in comparison with the desired trajectory. It is obvious that the controller with the auxiliary MPC input has better results than the simple PID Controller in all three variables. In particular, the controller with the MPC input achieved:

- 52% reduction of the error of the 1st joint's angle
- 52% reduction of the error of the 2nd joint's angle
- 56% reduction of the error of the 3rd joint's angle

Similarly to the 2nd Scenario, the criterion that the two controllers should reach 2% of the steady-state at about 6s is not satisfied for neither of the controllers, albeit MPC has lower errors at 6s. The reason behind this phenomenon is the fact that the disturbances, that the parametric uncertainties produce, vary with time.

Figure 5-19 presents the torques that are applied to the manipulator joints. The torques that the two controllers produce are almost identical. It is obvious that the values of the torques are much higher than the torques of the previous scenarios. This is completely reasonable since the manipulator has to move a quite large object.

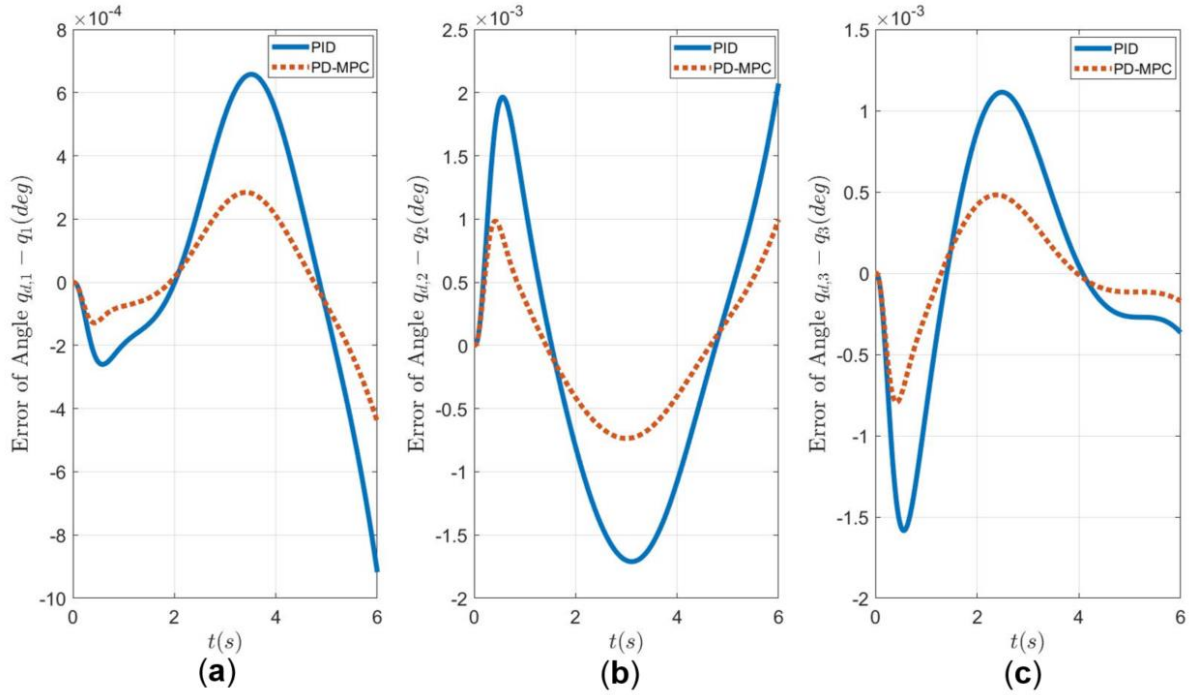

Figure 5-18. Error of the Actual and the Desired Value of the Joints' Angles for the 3rd Scenario (a) 1st Joint, (b) 2nd Joint, (c) 3rd Joint.

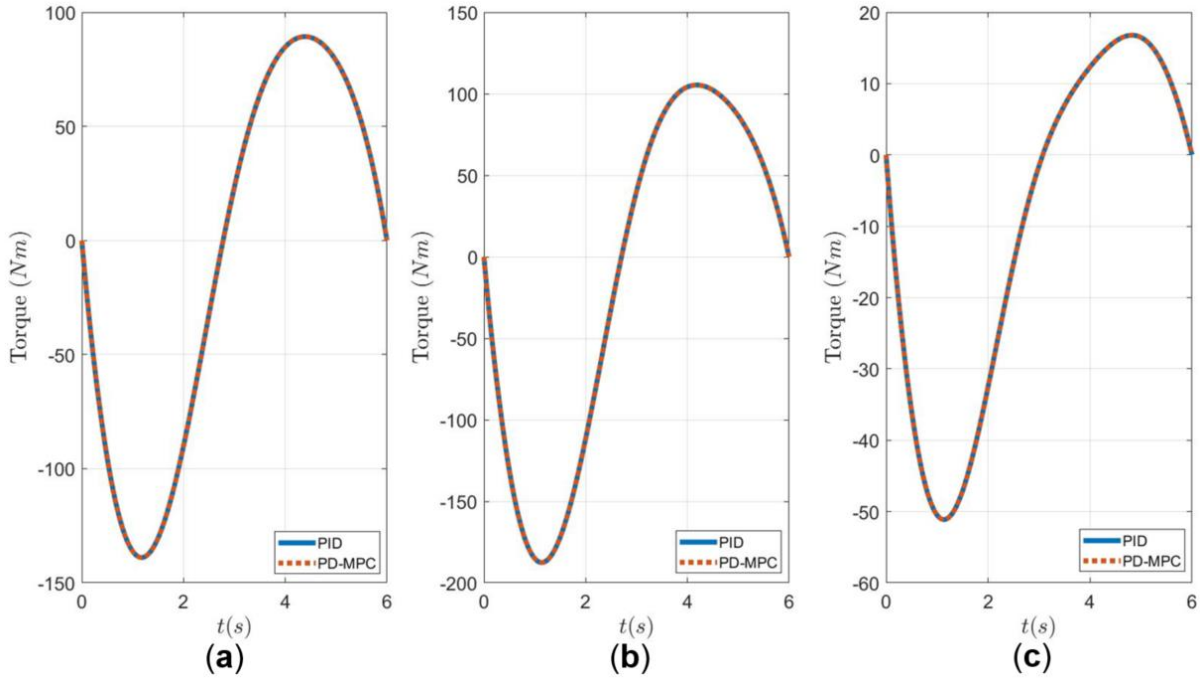

Figure 5-19. Torques of the Joints of the Manipulator applied in the 3rd Scenario (a) 1st Joint, (b) 2nd Joint (c) 3rd Joint.

5.5 Scenario 4: Noise

The successful control of an FFSMS requires the accurate measurement of a variety of process variables. However, the sensors that are used for this task provide the output with a level of sensor noise. Noise consists of arbitrary variations of sensor signal which are unrelated to variations in the input. In this Section, the Scenario of noise is presented.

The primal objective of this scenario is to compare the performance of the Model Based PID Controller to the Model Based PD Controller with an auxiliary MPC input. Consequently, observers or state estimation filters are not required in the design. A more realistic approach needs the insertion of such components. However, they requires the discretization of the model as well as the implementation of a non-linear observer or filter (e.g., an Extended Kalman Filter [11]). This deviates from the main focus of this thesis, but it is an interesting area for future research.

The two controllers are compared with respect to the errors of the end-effector's position and orientation, the errors of end-effector's velocities as well as their torques. As it was previously mentioned in this chapter, actuators may not be able to perform sudden changes in their torques, which might be needed to compensate for the noise. Therefore, according to this criterion, the controller which requires the lower rate of change of torques is the most suitable choice.

The process variables which are regarded as the ones containing noise are: $q_1, q_2, q_3, \dot{q}_1, \dot{q}_2, \dot{q}_3, \theta_0, \dot{\theta}_0, x_E, y_E, \theta_E, \dot{x}_E, \dot{y}_E, \dot{\theta}_E$. Figure 5-20 presents the block diagram of the system for both controllers. The noise is considered to be normally distributed with a zero mean and variance $\sigma^2 = 10^{-10}$ or $\sigma^2 = 10^{-8}$ (where σ is the standard deviation).

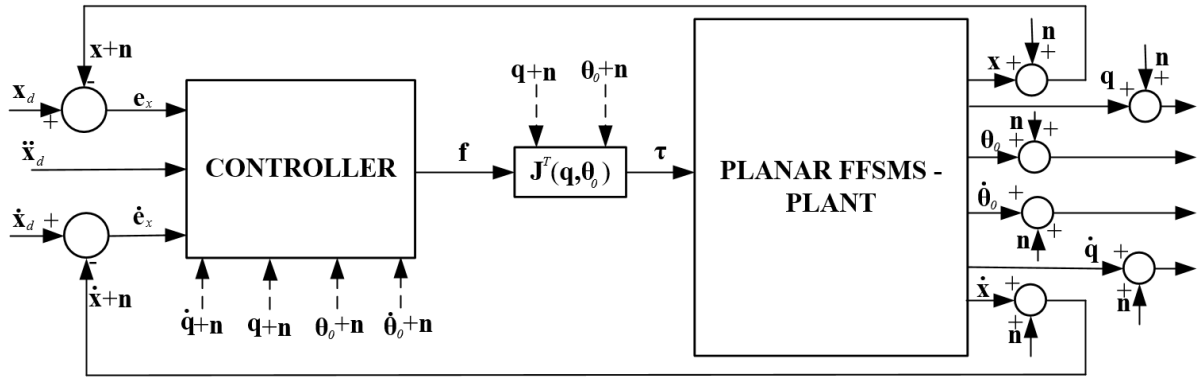

Figure 5-20. Block Diagram of the 4th Scenario.

5.5.1 Path Planning – Moving Target

In contrast to Scenarios 1 and 2, for this scenario the captured object-target was selected to have a constant relative velocity in respect to the FFSMS. The parameters of the moving target (specifically for the captured point) are shown in Table 5-6.

Table 5-6. Parameters of the Moving Target.

Moving Target	Value of Velocity v (m/s)	Slope of Velocity (deg)	Position (x, y) (m)
Time $t = 0$	0.05	-10	(-2.30, 1.85)
Time $t = 6$s	0.05	-10	(-2, 1.8)

The motion of the target mandates the final velocities of the end-effector to be non-zero and equal to the velocity of the target. Although fifth polynomials like the ones presented in Scenario 1 were used for the determination of the desired trajectories (see Eq. (5-1)-(5-4)), the parameters of the trajectories are different. They are presented in Table 5-7. It can be seen that the end-effector's final position and velocity are equal to the ones of the target.

Table 5-7. Paremeters of the Desired Trajectories for the 4th Scenario.

	x_E (m)	y_E (m)	θ_E (deg)
t_f (s)	6	6	6
Initial Value	0.2675	1.9220	195
Final Value	-2	1.8	170
1st Derivative's Initial Value	0	0	0
1st Derivative's Final Value	0.0492 (v·cos(-10))	-0.0087 (v·sin(-10))	0
2nd Derivative's Initial Value	0	0	0
2nd Derivative's Final Value	0	0	0

5.5.2 Model Based PID Controller vs Model Based PD Controller with an Auxiliary MPC Input

For both controllers, the parameters of the FFSMS are given in Table 5-1 and considered known with adequate accuracy. The angular momentum is considered zero $(h_{CM} = 0)$. The torques of the Model Based PID Controller are given by Eq. (5-6) and the gains of each joint are given by Eq. (5-8). The torques of the Model Based PD Controller with an auxiliary MPC input are given by Eq. (5-9) and the respective gains are given by Eq. (5-11). The rest of the required parameters of the MPC can be found in Scenario 1.

Figure 5-21 includes snapshots of the motion of the FFSMS in the ADAMS environment for three different time-points and for top view and isometric view. The white line depicts the trajectory of the end-effector. This figure is similar to Figure 5-3 since the velocity of the target is quite low. However, the motion of the target can be witnessed through a closer observation. Figure 5-4 and Figure 5-5 depict the motion of the FFSMS and the determinant for this scenario, since the final position and orientation of the FFSMS remained the same.

Two different cases are studied to show the performance of the two controllers when noise is inserted in the design. Both cases consist of a normally distributed noise with a mean value equal to zero. However, the noise in the first case has a variance $\sigma^2 = 10^{-10}$ while the second has a variance $\sigma^2 = 10^{-8}$. These values were chosen through various trials to show the value of noise that starts to affect the controllers. Prior to the comparisson of the two controllers, Figure 5-22 presents the trajectories of the end-effector's velocities for the first case and for both controllers (since as it is shown in Figure 5-23 the errors for both controllers are quite small). It is evident that the final values of the linear velocity are the ones presented in Table 5-7.

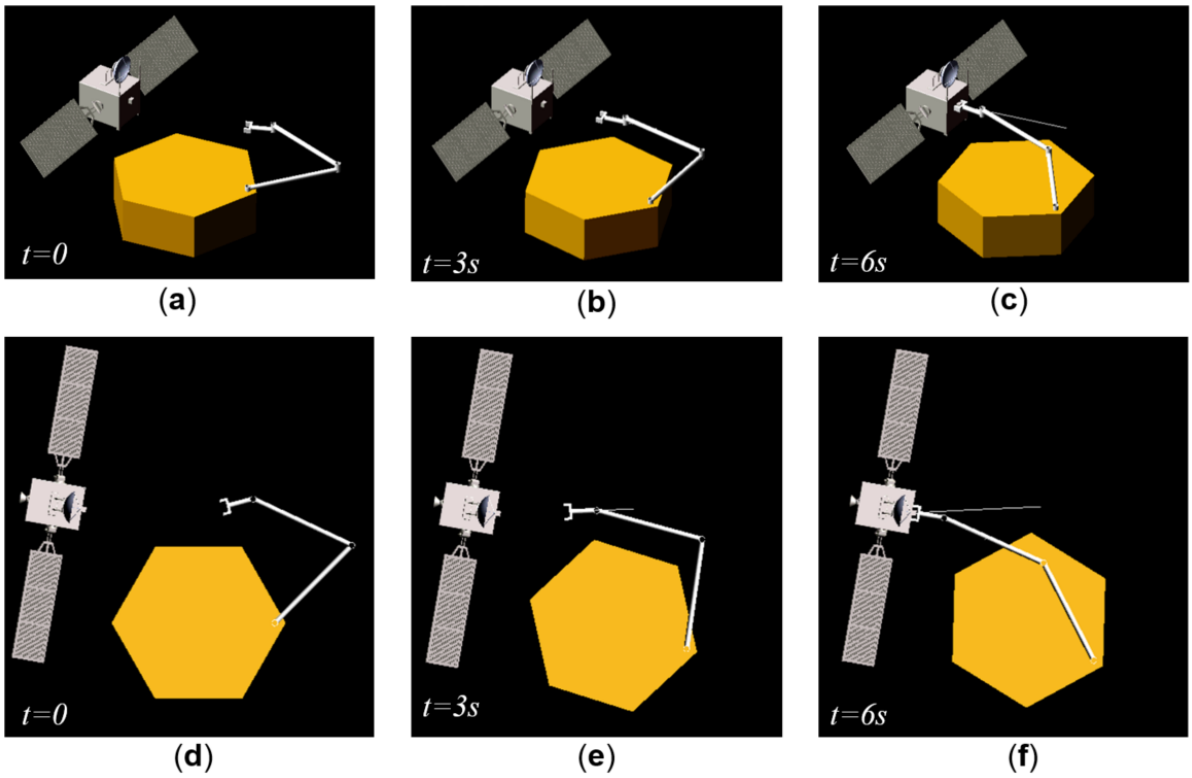

Figure 5-21. Snapshots of the Motion of the FFSMS in the ADAMS environment for three different time-points and two different views for the 4th Scenario (a) Isometric View (t=0), (b) Isometric View (t=3s), (c) Isometric View (t=6s), (d) Top View (t=0), (e) Top View (t=3s), (c) Top View (t=6s).

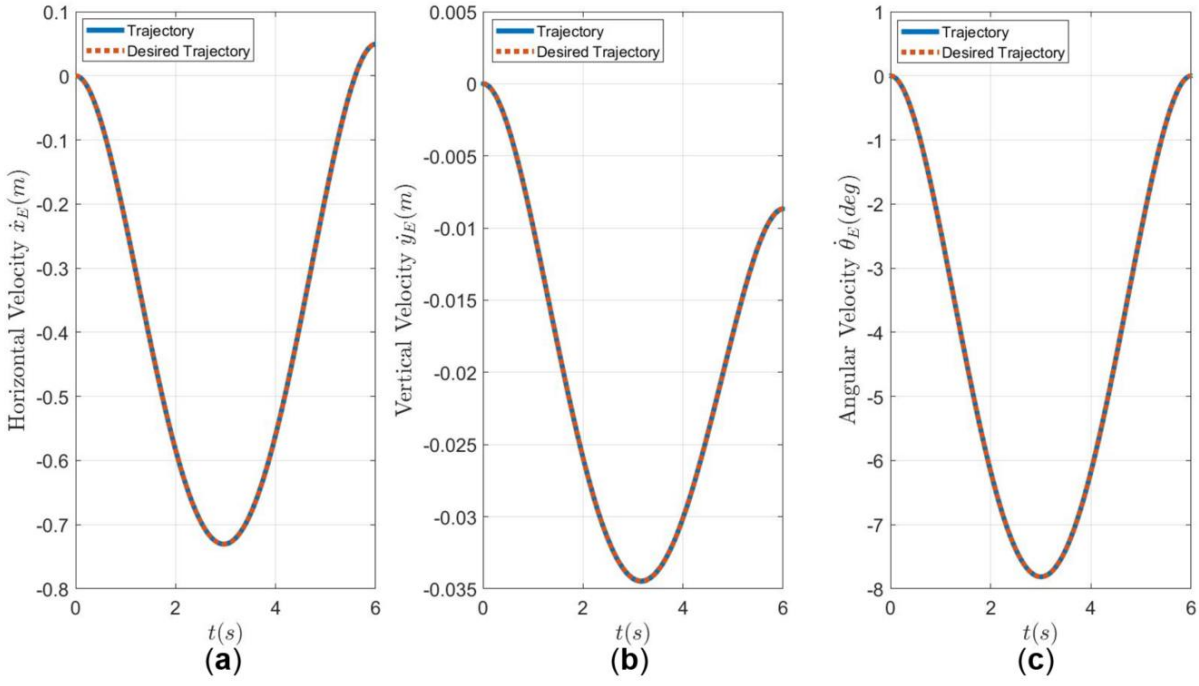

Figure 5-22. Actual and Desired Trajectories of the End-Effector (a) Horizontal Velocity, (b) Vertical Velocity, (c) Angular Velocity.

Figure 5-23 presents the errors of the end-effector's position, orientation and velocities in comparison with the desired trajectory for the case of noise with variance $\sigma^2 = 10^{-10}$. Figure 5-24 presents the torques that are applied in the joints. It can be concluded that both

controllers perform in a similar way for this level of noise. The final errors of the position, orientation and velocities of the end-effector are low enough in order for the manipulator to capture the target. Besides that, the diagram of the torques proves that this variance of noise is the threshold above which the noise starts to have a profound effect on the performance.

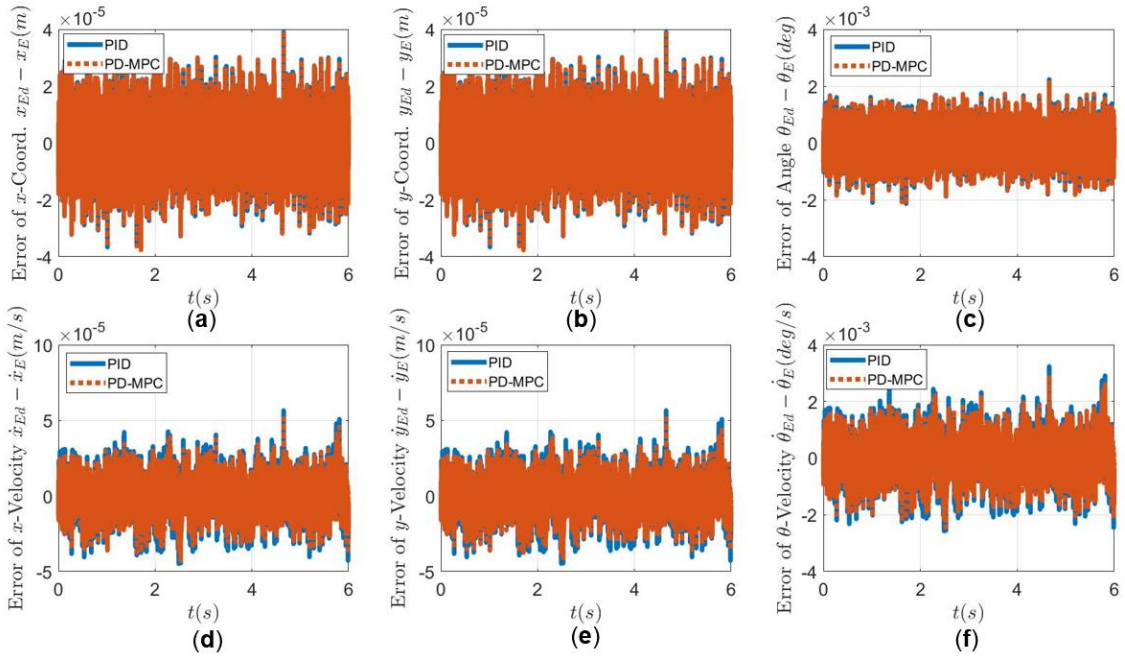

Figure 5-23. Error of the Actual and the Desired Value of the End-Effector's variables for the 4th Scenario and for Noise with Variance 10^{-10} (a) x-Coordinate, (b) y-Coordinate, (c) Orientation, (d) Horizontal Velocity, (e) Vertical Velocity, (f) Angular Velocity.

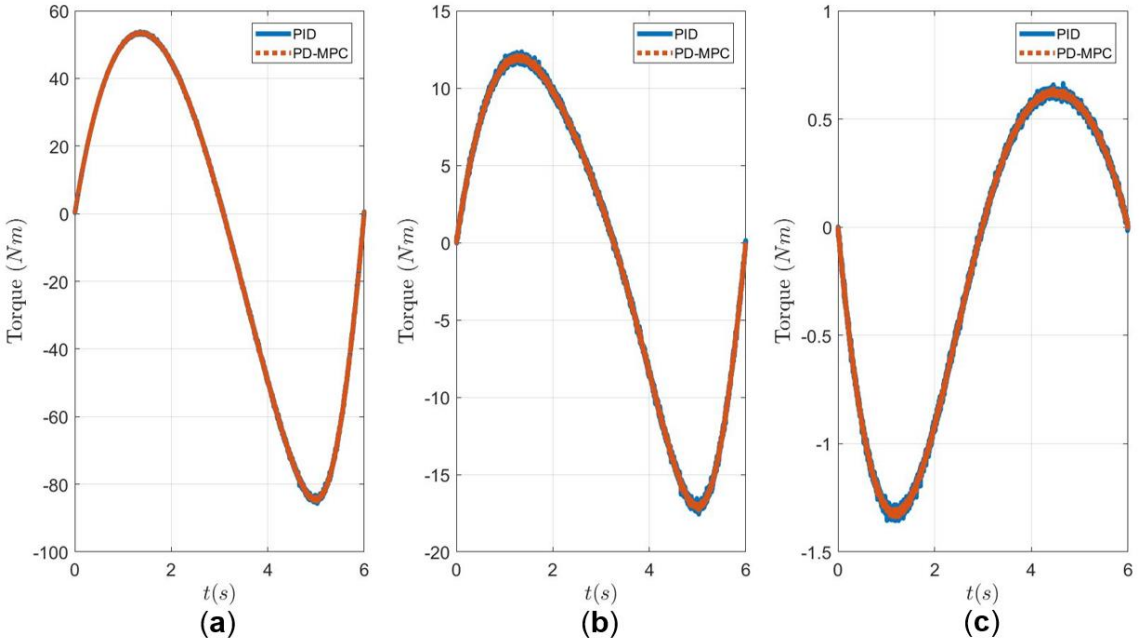

Figure 5-24. Torques of the Joints of the Manipulator applied in the 4th Scenario and for Noise with Variance 10^{-10} (a) 1st Joint, (b) 2nd Joint (c) 3rd Joint.

Figure 5-25 displays the errors of the end-effector's position, orientation and velocities in comparison with the desired trajectory for the case of noise with variance $\sigma^2 = 10^{-8}$. Figure

5-26 displays the torques that are applied in the joints. It can be concluded that both controllers manifest similar behavior regarding the errors compared with the desired trajectory. As expected, the errors are higher by a factor of 10 compared with the previous case. The errors can still be considered as low enough for the FFSMS to accomplish each goal. However, the Model Based PID Controller requires more sudden changes of the torques to achieve the same level of error. This is another benefit of the Model Based PD Controller with MPC input.

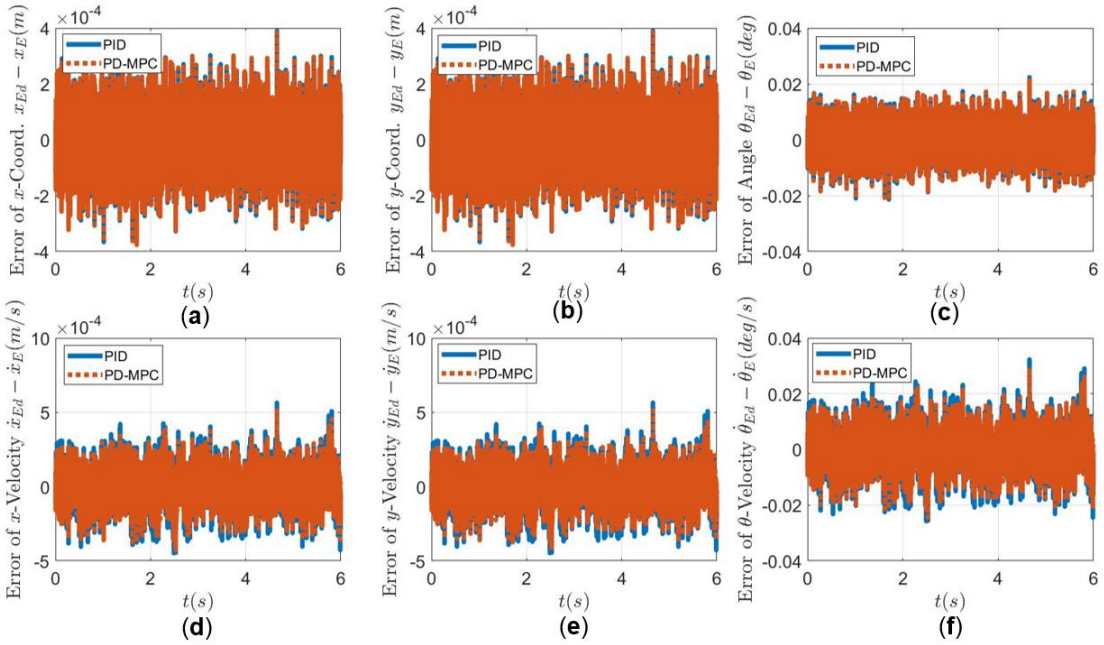

Figure 5-25. Error of the Actual and the Desired Value of the End-Effector's variables for the 4th Scenario and for Noise with Variance 10^{-8} (a) x-Coordinate, (b) y-Coordinate, (c) Orientation, (d) Horizontal Velocity, (e) Vertical Velocity, (f) Angular Velocity.

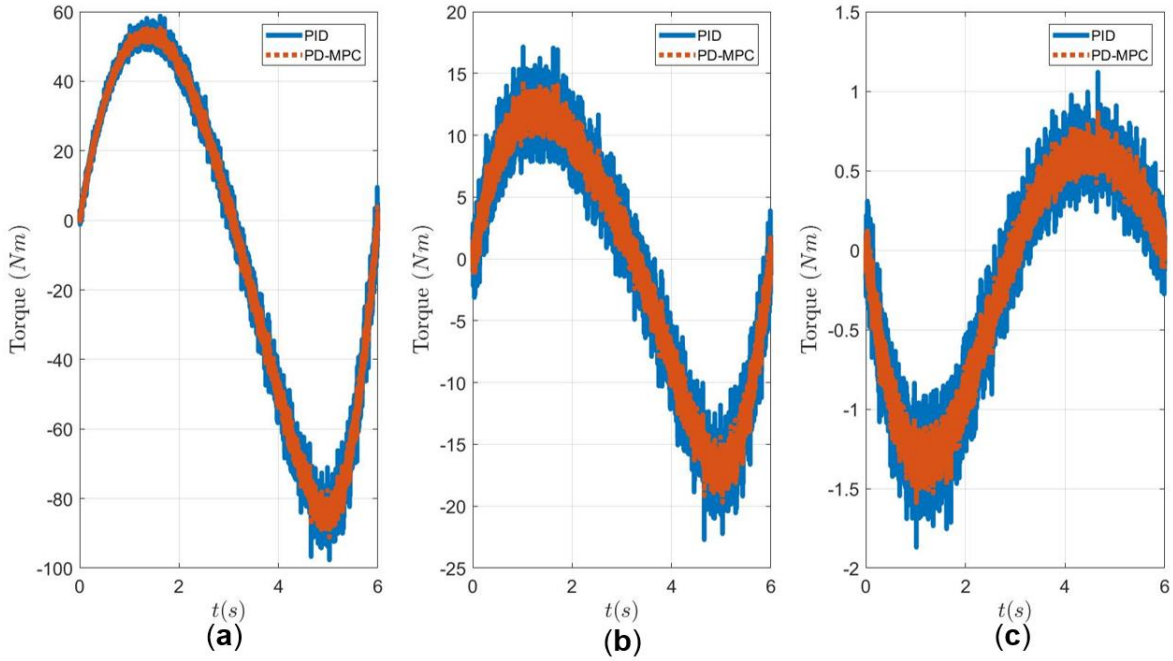

Figure 5-26. Torques of the Joints of the Manipulator applied in the 4th Scenario and for Noise with Variance 10^{-8} (a) 1st Joint, (b) 2nd Joint (c) 3rd Joint.

6 Conclusion & Future Work

The preceding study and comparison of the Model Based PID Controller and the Model Based PD Controller with an auxiliary MPC Input has engendered a variety of noteworthy results. This chapter contains the major findings that have been deduced throughout the thesis as well as proposals for future work.

6.1 Conclusion

The main purpose of the thesis was to study the performance of an FFSMS when an MPC is implemented for a plethora of different realistic scenarios. This was illustrated through a comparison with a regular PID Controller to highlight potential shortcomings or benefits.

In Chapter 2, the dynamics, kinematics and differential kinematics were described. It was shown that an FFSMS contains strong non-linearities. Consequently, a controller needs to overcome this impediment. Besides that, it was shown that singularities might occur in more positions compared to a manipulator with a fixed base due to the dynamic coupling between the base of the FFSMS and the manipulator. This constitutes an extra limit to the path planning of the FFSMS.

In Chapter 3, the MPC was described extensively. The simplicity of its implementation as well as the easy incorporation of constraints were shown. Although the input constraints are quite safe to activate, immense attention should be given when output constraints are active. Output constraints tend to cause severe nonlinearities which lead to close-loop oscillation or instability. Therefore, input constraints should be set as a priority, in case the output constraints request the control signal to surge. Apart from that, MPC also gives the benefit of setting constraints only for a specific duration. This can also constitute a solution to the dangers of implementing output constraints.

In Chapter 4, the implementation of the Model Based PID Controller and the Model Based PD Controller with an auxiliary MPC Input for the control of an FFSMS was described. A Model Based Controller is required to compensate for the non-linearities of the FFSMS. The MSC Adams model that was used as the representation of the simulation's plant was also presented. Although Adams provides a distinct visual representation of the model, attention should be given on the model's parameters and properties, since they might cause errors during the simulation (e.g., small discrepancies of Markers' position or a mode which causes algebraic loop in Matlab/Simulink). It was also validated that MSC Adams offers an accuracy of 10^{-8} for the FFSMS' angles.

In Chapter 5, different realistic scenarios that might occur through the operations of an FFSMS were presented. The two controllers were compared according to their performance in these scenarios. The first scenario contained an FFSMS whose actuators were subject to constant disturbances. The motion of the FFSMS was designed in the Cartesian space to capture a relatively stationary target. The MPC manifested significantly better behavior in compensating for the disturbances while the maximum torques of the two controllers were equal. Note that a faster design of PID is possible. However, it would result in higher maximum torques, hence an invalid comparison. Additionally, constraints were introduced in the MPC for a short time interval at the beginning of the simulation which improved the results even more. However, the sudden changes, that the satisfaction of the output

constraints required, might not be able to be performed by an actuator. Results about the computational power of the control laws were also obtained for this scenario. It was shown that both control laws require about the same amount of time to perform the task.

The second scenario presented the problem of parametric uncertainties. A Monte-Carlo simulation was performed for 200 different combinations of the FFSMS parameters. In all of them, the MPC showed better performance than the PID. However, none of them achieved convergence of the errors at the steady-state. This is partially reasonable since the disturbances, that the parametric uncertainties cause, vary with time. Nonetheless, by integrating output constraints in the MPC, it was shown that the MPC is able to achieve sufficient convergence of the orientation of the end-effector. Apart from that, the performed sensitivity analysis showed that that the y-coordinate's error varies almost proportionally with the orientation's error while the x-coordinate error is inversely proportional. The third scenario included the position of a captured object with undefined parameters. The path was planned in the joint space. This scenario manifested similar behavior to the second scenario, since the captured object can be regarded as an extension of the third link.

The fourth and final scenario presented the performance of the controllers when the process variables are measured with a known level of noise. Two different cases were studied, one with a noise of variance 10^{-10} and one with variance 10^{-8}. The former case did not affect significantly the performance of the controllers. However, the latter caused profound variation of the torques. It was shown that in this scenario too, the MPC has an advantage since it produces the same level of errors with the smaller variations of torques.

Consequently, considering all the previous arguments, one might conclude that a Model Based PD Controller with an auxiliary MPC input is better in many respects than a Model Based PID Controller. Indubitably, the former manifested better behavior in all the aforementioned case studies and it is quite simple to implement. Nonetheless, it is not as simple as a PID Controller. Therefore, the selection depends on the criteria set by the potential user.

6.2 Future Work

This thesis can become the impetus for further research since boundless questions have been raised throughout the conduction of the research.

To begin with, many assumptions have been made for this study. The angular momentum was considered zero, the manipulator was considered rigid and the study was performed for planar motions. However, in real life, angular momentum might be accumulated in an FFSMS and the base's control system might not be able to counterbalance it. Therefore, the FFSMS has to move in the presence of angular momentum. Besides that, to capture a target, the manipulator probably has to move in the three-dimensional space and its links have to be considered flexible due to their low mass and high lengths.

A realistic scenario also requires Cartesian motion of the FFSMS in the Path Dependent Workspace as well as the implementation of observers or state estimation filter to compensate for the process variables' noise. Various techniques have been proposed to avoid dynamic singularities which could be integrated in the design of the controllers [21] . Keeping also in mind that FFSMS contains severe non-linearities, observers or filters have to be competent to perform regardless of them. This task requires the controller to be

designed in the discrete time and not in the continuous as it was presented in this thesis. Inserting one of these components and discretizing the controller opens the way for implementation of the controller on a real robotic simulator like the one that the Control Systems Lab of NTUA possess.

Furthermore, the whole study was performed for Free-Floating robots. It is also interesting to study Free-Flying robots. During this phase, the thrusters are on-off, hence, they cannot produce continuous control signal.

Finally, as far as the MPC is concerned, the controller can be compared with other controllers to study further its advantages and disadvantages. To adduce a pertinent example, it can be compared to an H-infinity controller or even an adaptive controller. However, an adaptive controller, although it might prove to be very efficient in compensating for parametric uncertainties, it might not be able to be applied in an FFSMS due to the number and advanced technology of required sensors. Apart from that, different types of MPC can also be studied. For example, robust MPC like the min-max MPC is considered to compensate efficiently for bounded disturbances.

7 Bibliography

[1] Allwright, J. C., and Papavasiliou, G. C., “On linear programming and robust model-predictive control using impulse-responses,” *Systems & Control Letters*, 18(2), February 1992, pp. 159–164. DOI:10.1016/0167-6911(92)90020-s.

[2] Caccavale, F., and Siciliano, B., “Kinematic Control of Redundant Free-floating Robotic Systems”, *Advanced Robotics*, Vol. 15, No. 4, 2001, pp. 429-448.

[3] Camacho, E. F., and Bordons, C., “Model Predictive Control,” *Advanced Textbooks in Control and Signal Processing*, Springer-Verlag London, 2007. DOI: 10.1007/978-0-85729-398-5.

[4] Campo, P. J., and Morari, M., “Robust model predictive control,” *1987 American Control Conference*, 10-12 June, 1987, Minneapolis, USA, pp. 1021– 1026. DOI: 10.23919/ACC.1987.4789462.

[5] Cutler, C. R., and Ramaker, B. L., “Dynamic matrix control - A computer control algorithm,” *IEEE Transactions on Automatic Control*, Vol. 17, 1979. DOI: 10.1109/JACC.1980.4232009.

[6] Dai, L., Yu, Y., Zhai, D., Huang, T., and Xia, Y., “Robust Model Predictive Tracking Control for Robot Manipulators With Disturbances,” *IEEE Transactions on Industrial Electronics*, Vol. 68, 07 April, 2020, pp. 4288-4297. DOI: 10.1109/TIE.2020.2984986

[7] Garcia, C.E., Prett, D.M., and Morari, M., “Model Predictive Control: Theory and Practice-a Survey,” *Automatica*, 25(3), May, 1989, pp. 335–348.

[8] Gomez-Ortega, J., and Camacho, E. F., “Neural network MBPC for mobile robot path tracking,” *Robotics and Computer-Integrated Manufacturing*, 11(4), December, 1994, pp. 271–278. DOI:10.1016/0736-5845(95)00003-8.

[9] Gossner, J. R., Kouvaritakis, B., and Rossiter, J. A., “Stable generalized predictive control with constraints and bounded disturbances,” *Automatica*, 33(4), April, 1997, pp. 551–568. DOI:10.1016/s0005-1098(96)00214-2.

[10] Hildreth, C., “A quadratic programming procedure,” *Naval Research Logistics Quarterly*, 4(1), pp. 79–85. DOI:10.1002/nav.3800040113

[11] Julier, S. J., and Uhlmann, J. K., "Unscented filtering and nonlinear estimation," *Proceedings of the IEEE*, 92(3), pp. 401–422. DOI:10.1109/jproc.2003.823141. (2004).

[12] Kayastha S., Shi, L., Katupitiya, J., and Pearce, G., “Nonlinear model predictive control of a planar three-link space manipulator,". *2017 11th Asian Control Conference (ASCC)*, 17-20 December, 2017, Gold Coast, QLD, Australia. DOI: 10.1109/ASCC.2017.8287244.

[13] Kothare, M. V., Balakrishnan, V., and Morari, M. “Robust constrained model predictive control using linear matrix inequalities,” *Automatica*, 32(10), October, 1996, pp. 1361–1379. DOI:10.1016/0005-1098(96)00063-5.

[14] Kuhn, H. W., and Tucker, A. W., "Nonlinear Programming," *Second Berkeley Symposium on Mathematical Statistics and Probability*, University of California Press, 1950.

[15] Langson, W., Chryssochoos, I., Raković, S. V., and Mayne, D. Q. “Robust model predictive control using tubes,” *Automatica*, 40(1), January, 2004, pp. 125–133. DOI: 10.1016/j.automatica.2003.08.009

[16] Lee, Y. W., *Statistical Theory of Communication*, John Wiley and Sons, New York, 1960.

[17] Lucia, S., Finkler, T., Basak, D., and Engell, S., “A new Robust NMPC Scheme and its Application to a Semi-batch Reactor Example,” *IFAC Proceedings Volumes*, 45(15), July, 2012, pp. 69–74. DOI:10.3182/20120710-4-sg-2026.00035.

[18] Maasoumya, M., Razmara, M., Shahbakhti, M., and Sangiovanni Vincentelli, A., "Handling model uncertainty in model predictive control for energy efficient buildings," *Energy and Buildings*, Vol. 77, July, 2014, pp. 377-392.

[19] Marruedo, D. L., Alamo, T., and Camacho, E. F., "Stability analysis of systems with bounded additive uncertainties based on invariant sets: Stability and feasibility of MPC," *Proceedings of the 2002 American Control Conference (IEEE Cat. No.CH37301)*, 8-10 May, 2002, Anchorage, USA. DOI: 10.1109/acc.2002.1024831

[20] Meirovitch, L., *Methods of Analytical Dynamics*, McGraw Hill, New York, 1970.

[21] Nanos, K., "Dynamics, Trajectory Planning, and Control of Space Robotic Systems in the Presence of Angular Momentum and Flexibilities," *PhD Thesis*, Department of Mechanical Engineering, NTUA, Athens, 2015.

[22] Nanos, K. and Papadopoulos, E., "On the Dynamics and Control of Flexible Joint Space Manipulators," *Control Engineering Practice*, vol. 45, December, 2015, pp. 230-243.

[23] Nanos, K. and Papadopoulos, E., "On the Dynamics and Control of Free-floating Space Manipulator Systems in the Presence of Angular Momentum," *Frontiers: Robotics & AI - Space Robotics*, June 29, 2017. DOI: 10.3389/frobt.2017.00026.

[24] Oda, M., "Space robot experiments on NASDA's ETS-VII satellite preliminary overview of the experiment results," *Proceedings 1999 IEEE International Conference on Robotics and Automation*, Detroit, MI, USA, May 10-15, 1999. DOI: 10.1109/ROBOT.1999.772555.

[25] Ogilvie, A., Allport, J., Hannah, M., and Lymer, J., "Autonomous Satellite Servicing Using the Orbital Express Demonstration Manipulator System," *Proceedings of the 9th International Symposium on Artificial Intelligence, Robotics and Automation in Space*, iSAIRAS, 2008.

[26] Papadopoulos, E., "On the Dynamics and Control of Space Manipulators," *PhD Thesis*, Department of Mechanical Engineering, MIT, October, 1990.

[27] Papadopoulos, E., and Dubowsky, S., "Coordinated Manipulator/Spacecraft Motion Control for Space Robotic Systems," *IEEE International Conference on Robotics and Automation (ICRA '91)*, Vol. 2, April 9-11, 1991, Sacramento, CA, pp.1696-1701.

[28] Papadopoulos, E., and Dubowsky, S., "Dynamic Singularities of Free-Floating Space Manipulators," *ASME Journal of Dynamic Systems, Measurement, and Control*, Vol. 115, No. 1, March, 1993, pp. 44-52.

[29] Papadopoulos, E., and Dubowsky, S., "On the Nature of Control Algorithms for FreeFloating Space Manipulators," *IEEE Transactions on Robotics and Automation*, Vol. 7, No.6, December, 1991, pp. 750-758.

[30] Raychaudhuri, S., "Introduction to Monte Carlo simulation," *Proceedings of the 2008 Winter Simulation Conference*, Miami, Florida, USA, December 7-10. DOI: 10.1109/wsc.2008.4736059.

[31] Rekleitis, I., Martin, E., Rouleau, G., L'Archeveque, R., Parsa, K., and Depuis, E., "Autonomous Capture of a Tumbling Satellite," *Journal of Field Robotics, Special Issue on Space Robotics*, 24(4), 2007, pp. 275-296.

[32] Richalet, J., Rault, A., Testud, J. L., and Papon, J. "Model algorithmic control of industrial processes," *IFAC Proceedings Volumes*, 10(16), 1977, pp. 103–120. DOI:10.1016/s1474-6670(17)69513-2.

[33] Richalet, J., Rault, A., Testud, J. L., and Papon, J. "Model Predictive Heuristic Control: Application to Industrial Processes," *Automatica*, 14(5), September, 1978, pp. 413–428.

[34] Richards, A., and How, J., "Performance evaluation of rendezvous using model predictive control," *AIAA Guidance, Navigation and Control Conference and Exhibit*, Austin, Texas, August 11–14, 2003. DOI: 10.2514/6.2003-5507.

[35] Richards, A., and How, J., “Robust Stable Model Predictive Control with Constraint Tightening,” *2006 American Control Conference*, 14-16 June, 2006, Minneapolis, USA. DOI: 10.1109/ACC.2006.1656440.

[36] Rybus T., Seweryn K., and Sasiadek J.Z. “Control System for Free-Floating Space Manipulator Based on Nonlinear Model Predictive Control (NMPC),” *Journal of Intelligent and Robotic Systems 85*, 2017, pp. 491-509.

[37] Rybus T., Seweryn K., and Sasiadek J. Z., “Nonlinear Model Predictive Control (NMPC) for Free-Floating Space Manipulator," *Aerospace Robotics III. GeoPlanet: Earth and Planetary Sciences*. Springer, November, 2018, pp. 17-29.

[38] Ullah, M. I., Ajwad, S. A., Irfan, M., Iqbal, J., “MPC and H-Infinity Based Feedback Control of Non-Linear Robotic Manipulator,” *International Conference on Frontiers of Information Technology (FIT)*, Islamabad, Pakistan, 19-21 December, 2016. DOI: 10.1109/FIT.2016.033.

[39] Umetani, Y., and Yoshida, K., “Resolved Motion Rate Control of Space Manipulators with Generalized Jacobian Matrix,” *IEEE Transactions on Robotics and Automation*, Vol. 5, No. 3, June, 1989, pp. 303-314.

[40] Wang, L., *Model Predictive Control System Design and Implementation Using MATLAB*, Springer-Verlag, London, UK, 2009.

Appendix A – Matlab Algorithms

Path Planning (Example pg53)

```
    t_vect = [1; t; t^2; t^3; t^4;
t^5];
    t_vectdot = [0; 1; 2*t; 3*t^2;
4*t^3; 5*t^4];
    t_vectdot2 = [0; 0; 2; 6*t;
12*t^2; 20*t^3];

    Coeff1 = [qd1_0, qd1dot_0,
qd1dot2_0/2, -(20*qd1_0 - 20*qd1_f +
12*qd1dot_0*tf + 8*qd1dot_f*tf -
qd1dot2_f*tf^2 +
3*qd1dot2_0*tf^2)/(2*tf^3), (30*qd1_0
- 30*qd1_f + 16*qd1dot_0*tf +
14*qd1dot_f*tf - 2*qd1dot2_f*tf^2 +
3*qd1dot2_0*tf^2)/(2*tf^4), -(12*qd1_0
- 12*qd1_f + 6*qd1dot_0*tf +
6*qd1dot_f*tf - qd1dot2_f*tf^2 +
qd1dot2_0*tf^2)/(2*tf^5)];
    qd1 = Coeff1*t_vect;
    qd1dot = Coeff1*t_vectdot;
    qd1dot2 = Coeff1*t_vectdot2;

    Coeff2 = [qd2_0, qd2dot_0,
qd2dot2_0/2, -(20*qd2_0 - 20*qd2_f +
12*qd2dot_0*tf + 8*qd2dot_f*tf -
qd2dot2_f*tf^2 +
3*qd2dot2_0*tf^2)/(2*tf^3), (30*qd2_0
- 30*qd2_f + 16*qd2dot_0*tf +
14*qd2dot_f*tf - 2*qd2dot2_f*tf^2 +
3*qd2dot2_0*tf^2)/(2*tf^4), -(12*qd2_0
- 12*qd2_f + 6*qd2dot_0*tf +
6*qd2dot_f*tf - qd2dot2_f*tf^2 +
qd2dot2_0*tf^2)/(2*tf^5)];
    qd2 = Coeff2*t_vect;
    qd2dot = Coeff2*t_vectdot;
    qd2dot2 = Coeff2*t_vectdot2;

    Coeff3 = [qd3_0, qd3dot_0,
qd3dot2_0/2, -(20*qd3_0 - 20*qd3_f +
12*qd3dot_0*tf + 8*qd3dot_f*tf -
qd3dot2_f*tf^2 +
3*qd3dot2_0*tf^2)/(2*tf^3), (30*qd3_0
- 30*qd3_f + 16*qd3dot_0*tf +
14*qd3dot_f*tf - 2*qd3dot2_f*tf^2 +
3*qd3dot2_0*tf^2)/(2*tf^4), -(12*qd3_0
- 12*qd3_f + 6*qd3dot_0*tf +
6*qd3dot_f*tf - qd3dot2_f*tf^2 +
qd3dot2_0*tf^2)/(2*tf^5)];
    qd3 = Coeff3*t_vect;
    qd3dot = Coeff3*t_vectdot;
    qd3dot2 = Coeff3*t_vectdot2;
```

Path Planning (Scenario 1 pg62)

```
    t_vect = [1; t; t^2; t^3; t^4;
t^5];
    t_vectdot = [0; 1; 2*t; 3*t^2;
4*t^3; 5*t^4];
    t_vectdot2 = [0; 0; 2; 6*t;
12*t^2; 20*t^3];

    Coeff1 = [xd_0, xddot_0,
xddot2_0/2, -(20*xd_0 - 20*xd_f +
12*xddot_0*tf + 8*xddot_f*tf -
xddot2_f*tf^2 +
3*xddot2_0*tf^2)/(2*tf^3), (30*xd_0 -
30*xd_f + 16*xddot_0*tf +
14*xddot_f*tf - 2*xddot2_f*tf^2 +
3*xddot2_0*tf^2)/(2*tf^4), -(12*xd_0 -
12*xd_f + 6*xddot_0*tf + 6*xddot_f*tf
- xddot2_f*tf^2 +
xddot2_0*tf^2)/(2*tf^5)];
    xd = Coeff1*t_vect;
    xddot = Coeff1*t_vectdot;
    xddot2 = Coeff1*t_vectdot2;

    Coeff2 = [yd_0, yddot_0,
yddot2_0/2, -(20*yd_0 - 20*yd_f +
12*yddot_0*tf + 8*yddot_f*tf -
yddot2_f*tf^2 +
3*yddot2_0*tf^2)/(2*tf^3), (30*yd_0 -
30*yd_f + 16*yddot_0*tf +
14*yddot_f*tf - 2*yddot2_f*tf^2 +
3*yddot2_0*tf^2)/(2*tf^4), -(12*yd_0 -
12*yd_f + 6*yddot_0*tf + 6*yddot_f*tf
- yddot2_f*tf^2 +
yddot2_0*tf^2)/(2*tf^5)];
    yd = Coeff2*t_vect;
    yddot = Coeff2*t_vectdot;
    yddot2 = Coeff2*t_vectdot2;

    Coeff3 = [thEd_0, thEddot_0,
thEddot2_0/2, -(20*thEd_0 - 20*thEd_f
+ 12*thEddot_0*tf + 8*thEddot_f*tf -
thEddot2_f*tf^2 +
3*thEddot2_0*tf^2)/(2*tf^3),
(30*thEd_0 - 30*thEd_f +
16*thEddot_0*tf + 14*thEddot_f*tf -
2*thEddot2_f*tf^2 +
3*thEddot2_0*tf^2)/(2*tf^4), -
(12*thEd_0 - 12*thEd_f +
6*thEddot_0*tf + 6*thEddot_f*tf -
thEddot2_f*tf^2 +
thEddot2_0*tf^2)/(2*tf^5)];
    thEd = Coeff3*t_vect;
    thEddot = Coeff3*t_vectdot;
    thEddot2 = Coeff3*t_vectdot2;
```

ΕΘΝΙΚΟ ΜΕΤΣΟΒΙΟ ΠΟΛΥΤΕΧΝΕΙΟ
ΣΧΟΛΗ ΜΗΧΑΝΟΛΟΓΩΝ ΜΗΧΑΝΙΚΩΝ
ΤΟΜΕΑΣ Μ.Κ. & Α.Ε.
Εργαστήριο Αυτομάτου Ελέγχου

Εκτενής Περίληψη Διπλωματικής Εργασίας

Προβλεπτικός Έλεγχος για Διαστημικά Ρομποτικά Συστήματα με Παραμετρική Αβεβαιότητα & Υποκείμενα σε Διαταραχές

Ευάγγελος Ψωμιάδης

Επιβλέπων Καθηγητής: Ε. Γ. Παπαδόπουλος

ΑΘΗΝΑ 2021

1 Εισαγωγή

Η συνεχής και ανησυχητική αύξηση του αριθμού των δορυφόρων εκτός λειτουργίας που βρίσκονται σε τροχιά γύρω από τη Γη (τα αποκαλούμενα διαστημικά σκουπίδια) έχει αποτελέσει έναυσμα για την οργάνωση αποστολών και την ανάπτυξη συστημάτων τα οποία θα είναι ικανά να αντιμετωπίσουν το πρόβλημα. Τα συστήματα αυτά θα πρέπει να είναι σε θέση να πιάσουν, να τροφοδοτήσουν με καύσιμο, να επισκευάσουν ή ακόμη και να αλλάξουν την ήδη υπάρχουσα τροχιά ενός σώματος (π.χ. δορυφόρος). Δεδομένης της επικινδυνότητας μίας επανδρωμένης αποστολής, τα Διαστημικά Ρομποτικά Συστήματα (ΔΡΣ) είναι η καταλληλότερη επιλογή.

Ένα ΔΡΣ αποτελείται από δύο βασικά μέρη, τη βάση και τους ρομποτικούς βραχίονες. Κάθε ένα από αυτά έχει τους δικούς του επενεργητές και σύστημα ελέγχου. Λόγω της δυναμικής σύζευξης μεταξύ τους, η κίνηση του ενός επηρεάζει την κίνηση του άλλου. Σε αυτή τη διπλωματική θα μελετηθεί ένα επίπεδο ρομποτικό σύστημα με ένα βραχίονα τριών βαθμών ελευθερίας. Το σύστημα θα είναι ελεύθερα αιωρούμενο, δηλαδή οι επενεργητές της βάσης θα βρίσκονται εκτός λειτουργίας έτσι ώστε να μην επηρεάζουν την κίνηση του ρομποτικού βραχίονα. Βασικός σκοπός της εργασίας είναι η μελέτη της λειτουργίας ενός τέτοιου συστήματος υποκείμενο σε διάφορες διαταραχές με την χρήση Προβλεπτικού Ελέγχου (Model Predictive Control). Για τον λόγο αυτό, τα αποτελέσματα θα συγκριθούν με τα αντίστοιχα αποτελέσματα ενός κλασικού PID Ελέγχου.

Η παρούσα διπλωματική εργασία αποτελείται από έξι κεφάλαια. Το πρώτο κεφάλαιο αποτελείται από την εισαγωγή και την βιβλιογραφική ανασκόπηση. Μία σύντομη αναφορά σε σημαντικές δημοσιεύσεις σχετικές με την δυναμική και τον έλεγχο των ΔΡΣ καθώς και των γενικότερων εφαρμογών του Προβλεπτικού Ελέγχου παρατίθεται σε αυτό το κεφάλαιο. Το δεύτερο κεφάλαιο περιέχει τη κινηματική, αντίστροφη κινηματική και τη δυναμική μελέτη των Ελεύθερων Αιωρούμενων ΔΡΣ. Οι προκύπτουσες εξισώσεις είναι θεμελιώδεις για τον έλεγχο του συστήματος. Στο τρίτο κεφάλαιο περιγράφεται ο Προβλεπτικός Έλεγχος που θα εφαρμοστεί. Παρατίθεται όλη η θεωρία και η μεθοδολογία που απαιτείται για την εφαρμογή του. Ιδιαίτερη προσοχή δίνεται στην εφαρμογή περιορισμών (εισόδων ή/και εξόδων), ένα βασικό πλεονέκτημα του Προβλεπτικού Ελέγχου.

Στο τέταρτο κεφάλαιο παρουσιάζεται η εφαρμογή του Προβλεπτικού Ελέγχου στο Ελεύθερα Αιωρούμενο ΔΡΣ. Η μη γραμμικότητα του συστήματος απαιτεί την γραμμικοποίηση του μοντέλου πριν την εφαρμογή του. Αυτό επιτυγχάνεται μέσω της χρήση Ελέγχου Βασιζόμενου στο Μοντέλο. Μετά τη γραμμικοποίησή του, εφαρμόζεται ο έλεγχος και στο χώρο των αρθρώσεων αλλά και στο Καρτεσιανό επίπεδο. Επιπλέον, παρατίθεται ο σχεδιασμός του PID Ελέγχου ο οποίος θα είναι χρήσιμος για την σύγκριση.

Στο πέμπτο κεφάλαιο παρουσιάζονται οι προσομοιώσεις και τα διάφορα σενάρια που μελετήθηκαν. Το πρώτο σενάριο περιέχει την σύγκριση των δύο αναφερόμενων ελέγχων για κίνηση στον Καρτεσιανό χώρο, όταν ο στόχος είναι σταθερός και ενώ εφαρμόζονται σταθερές διαταραχές στους επενεργητές του βραχίονα. Το δεύτερο σενάριο έχει τον ίδιο σχεδιασμό τροχιάς με το πρώτο μόνο που σε αυτό οι παράμετροι του μοντέλου (μήκη, μάζες και ροπές αδράνειας) δεν είναι ακριβώς γνωστές. Το σενάριο αυτό περιέχει επίσης προσομοίωση Monte-Carlo. Στο τρίτο σενάριο το ΔΡΣ έχει πιάσει και σταθεροποιήσει ήδη τον στόχο, του οποίου οι παράμετροι δεν είναι ακριβείς, και επιθυμεί να κινηθεί στο χώρο των αρθρώσεων. Το πέμπτο σενάριο παρουσιάζει την απόδοση των νόμων ελέγχου όταν

εμπεριέχεται θόρυβος στις μετρήσεις. Σε αυτό το σενάριο επίσης, ο στόχος δεν θεωρείται σταθερός αλλά κινείται με σταθερή σχετική ταχύτητα.

Στο έκτο και τελευταίο κεφάλαιο αναφέρονται τα συμπεράσματα της εργασίας καθώς και οι προτάσεις για μελλοντική έρευνα.

2 Κινηματική & Δυναμική Ελεύθερων Αιωρούμενων Διαστημικών Ρομποτικών Συστημάτων

Ο έλεγχος και συγκεκριμένα ο Έλεγχος Βασισμένος στο Μοντέλο απαιτεί ακριβή γνώση της κινηματικής και δυναμικής του συστήματος. Το σύστημα που μελετάται στη παρούσα διπλωματική είναι ένα Ελεύθερα Αιωρούμενο ΔΡΣ με ένα βραχίονα με 3 βαθμούς ελευθερίας. Το μελετούμενο σύστημα φαίνεται στο Σχήμα 2-1. Η μελέτη γίνεται με βάση τις προϋποθέσεις ότι οι εξωτερικές δυνάμεις που ενεργούν στο ΔΡΣ (π.χ. δύναμη από το μαγνητικό και βαρυτικό πεδίο της Γης ή αντίσταση της ατμόσφαιρας) θεωρούνται μηδενικές ή αμελητέες. Η γραμμική ορμή και η στροφορμή του ΔΡΣ θεωρούνται επίσης μηδενικές.

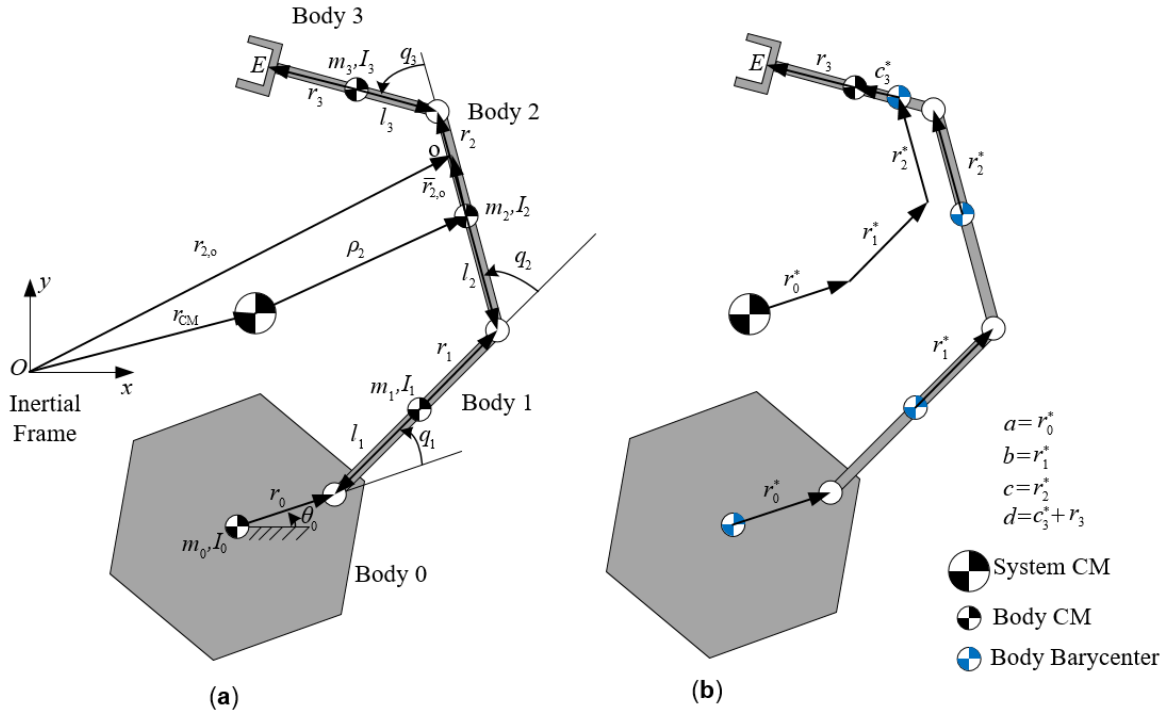

Σχήμα 2-1. Επίπεδο Ελεύθερα Αιωρούμενο ΔΡΣ με Ρομποτικό Βραχίονα 3 Βαθμών Ελευθερίας (a) Γεωμετρικές & Δυναμικές Παράμετροι (b) Παράμετροι των Βαρύκεντρων.

Λαμβάνοντας υπόψη αυτές τις προϋποθέσεις, η θέση και η περιστροφή του τελικού σημείου δράσης του βραχίονα δίνεται από:

$$\begin{aligned} x_E &= a\,\mathrm{c}_{\theta_o} + b\,\mathrm{c}_{\theta_o+q_1} + c\,\mathrm{c}_{\theta_o+q_1+q_2} + d\,\mathrm{c}_{\theta_o+q_1+q_2+q_3} \\ y_E &= a\,\mathrm{s}_{\theta_o} + b\,\mathrm{s}_{\theta_o+q_1} + c\,\mathrm{s}_{\theta_o+q_1+q_2} + d\,\mathrm{s}_{\theta_o+q_1+q_2+q_3} \\ \theta_E &= \theta_o + q_1 + q_2 + q_3 \end{aligned} \tag{2-1}$$

όπου:

$$
\begin{aligned}
a &= \frac{m_0 r_0}{M} \\
b &= \frac{m_0 l_1 + (m_0 + m_1) r_1}{M} \\
c &= \frac{(m_0 + m_1) l_2 + (m_0 + m_1 + m_2) r_2}{M} \\
d &= \frac{(m_0 + m_1 + m_2) l_3}{M} + r_3 \\
M &= m_0 + m_1 + m_2 + m_3
\end{aligned}
\tag{2-2}
$$

Η αντίστροφη κινηματική προκύπτει με την αντιστροφή των παραπάνω εξισώσεων ως προς τις γωνίες των αρθρώσεων.

Η γραμμική ταχύτητα του τελικού σημείου δράσης δίνεται από:

$$
\begin{aligned}
\dot{\mathbf{r}}_E &= \mathbf{R}_0 \left({}^0\mathbf{j}_{11} \dot{\theta}_0 + {}^0\mathbf{J}_{12} \dot{\mathbf{q}} \right) \\
\mathbf{R_0}(\theta_0) &= \begin{bmatrix} \mathrm{c}_{\theta_o} & -\mathrm{s}_{\theta_o} \\ \mathrm{s}_{\theta_o} & \mathrm{c}_{\theta_o} \end{bmatrix} \\
{}^0\mathbf{j}_{11}(\mathbf{q}) &= \begin{bmatrix} -\left(b\,\mathrm{s}_{q_1} + c\,\mathrm{s}_{q_1+q_2} + d\,\mathrm{s}_{q_1+q_2+q_3} \right) \\ a + b\,\mathrm{c}_{q_1} + c\,\mathrm{c}_{q_1+q_2} + d\,\mathrm{c}_{q_1+q_2+q_3} \end{bmatrix} \\
{}^0\mathbf{J}_{12}(\mathbf{q}) &= \begin{bmatrix} -\left(b\,\mathrm{s}_{q_1} + c\,\mathrm{s}_{q_1+q_2} + d\,\mathrm{s}_{q_1+q_2+q_3} \right) & -\left(c\,\mathrm{s}_{q_1+q_2} + d\,\mathrm{s}_{q_1+q_2+q_3} \right) & -d\,\mathrm{s}_{q_1+q_2+q_3} \\ b\,\mathrm{c}_{q_1} + c\,\mathrm{c}_{q_1+q_2} + d\,\mathrm{c}_{q_1+q_2+q_3} & c\,\mathrm{c}_{q_1+q_2} + d\,\mathrm{c}_{q_1+q_2+q_3} & d\,\mathrm{c}_{q_1+q_2+q_3} \end{bmatrix}
\end{aligned}
\tag{2-3}
$$

όπου θ_0 είναι η γωνία περιστροφής της βάσης και $\mathbf{q} = [q_1\ q_2\ q_3]^{\mathrm{T}}$.

Η γωνιακή ταχύτητα του τελικού σημείου δράσης δίνεται από:

$$
\begin{aligned}
\dot{\theta}_{\mathrm{E}} &= \dot{\theta}_0 + {}^0\mathbf{j}_{22} \dot{\mathbf{q}} \\
{}^0\mathbf{j}_{22}(\mathbf{q}) &= \begin{bmatrix} 1 & 1 & 1 \end{bmatrix}
\end{aligned}
\tag{2-4}
$$

Λόγω της ύπαρξης της γωνίας περιστροφής της βάσης ως μεταβλητή, απαιτείται μία ακόμη εξίσωση για να επιλυθεί το πρόβλημα. Αυτή η εξίσωση δίνεται από την αρχή διατήρηση της στροφορμής σύμφωνα με την οποία:

$$
h_{CM} = {}^0D \dot{\theta}_0 + {}^0\mathbf{D}_q \dot{\mathbf{q}} \tag{2-5}
$$

με:

$$
\begin{aligned}
{}^0D &= {}^0D_0 + {}^0D_1 + {}^0D_2 + {}^0D_3 \\
{}^0\mathbf{D}_q &= \begin{bmatrix} {}^0D_1 + {}^0D_2 + {}^0D_3 & {}^0D_2 + {}^0D_3 & {}^0D_3 \end{bmatrix} \\
{}^0D_0 &= a_{00} + a_{01}\,\mathrm{c}_{q_1} + a_{02}\,\mathrm{c}_{q_1+q_2} + a m_3 l_3\,\mathrm{c}_{q_1+q_2+q_3} \\
{}^0D_1 &= a_{01}\,\mathrm{c}_{q_1} + a_{11} + a_{12}\,\mathrm{c}_{q_2} + b m_3 l_3\,\mathrm{c}_{q_2+q_3} \\
{}^0D_2 &= a_{02}\,\mathrm{c}_{q_1+q_2} + a_{12}\,\mathrm{c}_{q_2} + a_{22} + c m_3 l_3\,\mathrm{c}_{q_3} \\
{}^0D_3 &= a_{33} + c m_3 l_3\,\mathrm{c}_{q_3} + b m_3 l_3\,\mathrm{c}_{q_2+q_3} + a m_3 l_3\,\mathrm{c}_{q_1+q_2+q_3}
\end{aligned}
\tag{2-6}
$$

όπου a, b και c δίνονται από Εξ. (2-2) και:

$$
\begin{aligned}
a_{00} &= I_0 + \frac{m_0\left(m_1+m_2+m_3\right)r_0^2}{M} \\
a_{01} &= \frac{m_0 r_0\left[l_1\left(m_1+m_2+m_3\right)+r_1\left(m_2+m_3\right)\right]}{M} \\
a_{02} &= \frac{m_0 r_0\left[l_2\left(m_2+m_3\right)+r_2 m_3\right]}{M} \\
a_{11} &= I_1 + \frac{m_0 m_1 l_1^2 + m_1\left(m_2+m_3\right)r_1^2 + m_0\left(m_2+m_3\right)\left(l_1+r_1\right)^2}{M} \\
a_{12} &= \frac{\left[l_1 m_0+\left(m_0+m_1\right)r_1\right]\left[l_2\left(m_2+m_3\right)+m_3 r_2\right]}{M} \\
a_{22} &= I_2 + \frac{m_2 m_3 r_2^2 + m_2\left(m_0+m_1\right)l_2^2 + m_3\left(m_0+m_1\right)\left(l_2+r_2\right)^2}{M} \\
a_{33} &= I_3 + \frac{m_3\left(m_0+m_1+m_2\right)l_3^2}{M}
\end{aligned}
\tag{2-7}
$$

Το 4x4 σύστημα που προέκυψε εμπεριέχει την Ιακωβιανή του συστήματος, η διακρίνουσα της οποίας δίνει τα σημεία στα οποία μπορεί να εμφανιστούν Δυναμικές Ιδιομορφίες:

$$
\det\left(\mathbf{J}^*\right) = \frac{ab\,{}^0D_2\,\mathrm{s}_{q_1} + bc\,{}^0D_0\,\mathrm{s}_{q_2} - ac\,{}^0D_1\,\mathrm{s}_{q_1+q_2}}{{}^0D} \tag{2-8}
$$

Τέλος, η δυναμική του συστήματος, έπειτα από εφαρμογή της μεθόδου Lagrange δίνεται από:

$$
\mathbf{H}(\mathbf{q})\ddot{\mathbf{q}} + \mathbf{C}^*(\mathbf{q},\dot{\mathbf{q}},h_{CM})\dot{\mathbf{q}} + \mathbf{g}_h(\mathbf{q},h_{CM}) = \boldsymbol{\tau} \tag{2-9}
$$

όπου:

$$
\begin{aligned}
\mathbf{H}(\mathbf{q}) &= {}^0\mathbf{D}_{qq} - {}^0\mathbf{D}_q^T\,{}^0D^{-1}\,{}^0\mathbf{D}_q \\
{}^0\mathbf{D}_{qq} &= \sum_{j=1}^{N}\sum_{i=1}^{N} {}^0\mathbf{F}_i^T\,{}^0\mathbf{D}_{ij}\,{}^0\mathbf{F}_j \\
\mathbf{C}^*(\mathbf{q},\dot{\mathbf{q}},h_{CM}) &= \mathbf{C} + \mathbf{C}_h \\
\mathbf{C}(\mathbf{q},\dot{\mathbf{q}}) &= \frac{1}{2}\frac{\partial\left(\dot{\mathbf{q}}^T\,{}^0\,{}^0D^{-1}\,{}^0\mathbf{D}_q\right)}{\partial\mathbf{q}} + \frac{\partial\left({}^0\mathbf{D}_{qq}\dot{\mathbf{q}}\right)}{\partial\mathbf{q}} - \frac{1}{2}\frac{\partial\left(\dot{\mathbf{q}}^T\,{}^0\mathbf{D}_{qq}\right)}{\partial\mathbf{q}} - \frac{\partial\left({}^0\mathbf{D}_q^T\,{}^0D^{-1}\,{}^0\mathbf{D}_q\dot{\mathbf{q}}\right)}{\partial\mathbf{q}} \\
\mathbf{C}_h(\mathbf{q},h_{CM}) &= h_{CM}\left[\frac{\partial\left({}^0D^{-1}\,{}^0\mathbf{D}_q^T\right)}{\partial\mathbf{q}} - \frac{\partial\left({}^0D^{-1}\,{}^0\mathbf{D}_q\right)}{\partial\mathbf{q}}\right] \\
\mathbf{g}_h &= \frac{1}{2}h_{CM}^2\,\frac{\partial\left({}^0D^{-1}\right)}{\partial\mathbf{q}} \\
{}^0\mathbf{F}_k &= \left[{}^0\mathbf{R}_1 \quad \dots \quad {}^0\mathbf{R}_k \quad \mathbf{0}_{3(N-k)}\right]
\end{aligned}
\tag{2-10}
$$

3 Προβλεπτικός Έλεγχος (MPC)

Ο όρος «Προβλεπτικός Έλεγχος» (MPC) αναφέρεται σε μία ομάδα αλγορίθμων ελέγχου με διάφορα κοινά χαρακτηριστικά. Όλοι χρησιμοποιούν ένα μοντέλο με σκοπό να προβλέψουν την έξοδο του μελετούμενου συστήματος ενώ παράλληλα ελαχιστοποιούν μία συνάρτηση κόστους. Επιπλέον, χρησιμοποιούν κινούμενο ορίζοντα πρόβλεψης (receding horizon), δηλαδή η τελική χρονική στιγμή της πρόβλεψης συνεχώς αυξάνεται όσο αυξάνεται ο χρόνος ενώ παράλληλα εφαρμόζεται μόνο η αρχική τιμή του σήματος ελέγχου στο σύστημα. Ο έλεγχος που θα μελετηθεί σε αυτή τη διπλωματική εργασία είναι ένας γραμμικός MPC που χρησιμοποιεί state-space μοντέλο.

Έστω ότι η διάταξη που επιθυμείται να ελεγχθεί περιγράφεται από:

$$\begin{aligned}\dot{\mathbf{x}}_\mathbf{m}(t) &= \mathbf{A}_\mathbf{m}\mathbf{x}_\mathbf{m}(t) + \mathbf{B}_\mathbf{m}\mathbf{u}(t)\\ \mathbf{y}(t) &= \mathbf{C}_\mathbf{m}\mathbf{x}_\mathbf{m}(t)\end{aligned} \tag{3-1}$$

όπου $\mathbf{x_m}$ είναι η μεταβλητή κατάστασης, $\mathbf{u}$ είναι η είσοδος και $\mathbf{y}$ η έξοδος ενώ οι πίνακες $\mathbf{A_m}$, $\mathbf{B_m}$, $\mathbf{C_m}$ έχουν σταθερές τιμές.

Το μοντέλο που θα ελεγχθεί προέρχεται από τη διαφοροποίηση της παραπάνω εξίσωσης:

$$\begin{aligned}\dot{\mathbf{x}}(t) &= \begin{bmatrix}\ddot{\mathbf{x}}_\mathbf{m}(t)\\ \dot{\mathbf{y}}(t)\end{bmatrix} = \begin{bmatrix}\mathbf{A_m} & \mathbf{0}_\mathbf{m}^\mathbf{T}\\ \mathbf{C_m} & \mathbf{0_{q\times q}}\end{bmatrix}\begin{bmatrix}\dot{\mathbf{x}}_\mathbf{m}(t)\\ \mathbf{y}(t)\end{bmatrix} + \begin{bmatrix}\mathbf{B_m}\\ \mathbf{0_{q\times m}}\end{bmatrix}\dot{\mathbf{u}}(t) = \mathbf{A}\mathbf{x}(t) + \mathbf{B}\dot{\mathbf{u}}(t)\\ \mathbf{y}(t) &= \begin{bmatrix}\mathbf{0_m} & \mathbf{I_{q\times q}}\end{bmatrix}\begin{bmatrix}\dot{\mathbf{x}}_\mathbf{m}(t)\\ \mathbf{y}(t)\end{bmatrix} = \mathbf{C}\mathbf{x}(t)\end{aligned} \tag{3-2}$$

Για την μελέτη του ελέγχου σε συνεχή χρόνο, η παράγωγος του σήματος ελέγχου πρέπει να προσεγγισθεί χρησιμοποιώντας ορθοκανονικές συναρτήσεις. Επιλέχθηκαν οι Laguerre συναρτήσεις που περιγράφονται από τις εξισώσεις:

$$\mathbf{L}(t) = e^{\mathbf{A_p}t}\mathbf{L}(0)$$

$$\mu\varepsilon\quad \mathbf{A_p} = \begin{bmatrix}-p & 0 & \dots & 0\\ -2p & -p & \dots & 0\\ \vdots & \ddots & \ddots & \vdots\\ -2p & \dots & -2p & -p\end{bmatrix}\quad \kappa\alpha\iota\quad \mathbf{L}(0) = \sqrt{2p}\begin{bmatrix}1\\ 1\\ \vdots\\ 1\end{bmatrix} \tag{3-3}$$

όπου η παράμετρος p ονομάζεται παράγοντας κλίμακας, είναι προδιαγραφή σχεδιασμού (όπως και ο αριθμός των Laguerre συναρτήσεων N) και καθορίζει τον εκθετικό ρυθμό μείωσης των συναρτήσεων.

Χρησιμοποιώντας τις συναρτήσεις αυτές, η παράγωγος του σήματος ελέγχου περιγράφεται από:

$$\dot{u}_i(\tau) = \sum_{j=1}^{\mathrm{N}} c_j l_j(t) = \mathbf{L}_i(\tau)^{\mathrm{T}}\boldsymbol{\eta}_i \qquad i = 1, 2, \dots m \tag{3-4}$$

όπου $\boldsymbol{\eta}_\mathbf{i} = [c_1\ \ c_2\ \ \dots\ c_N]^{\mathrm{T}}$ είναι το διάνυσμα των συντελεστών.

Θεωρώντας ότι η συνάρτηση κόστους δίνεται από την εξίσωση:

$$J = \int_0^{T_p} (\mathbf{x}(t_i + \tau \mid t_i)^T \mathbf{Q}\mathbf{x}(t_i + \tau \mid t_i) + \dot{\mathbf{u}}(\tau)^T \mathbf{R}\dot{\mathbf{u}}(\tau))d\tau \quad 0 \le \tau \le T_p \tag{3-5}$$

αποδεικνύεται ότι ελαχιστοποιείται όταν ισχύει:

$$\begin{gathered} \boldsymbol{\eta} = -\boldsymbol{\Omega}^{-1}\boldsymbol{\Psi}\mathbf{x}(t_i) \\ \mu\varepsilon \quad \boldsymbol{\Omega} = \int_0^{T_p} \boldsymbol{\Phi}(\tau)\mathbf{Q}\boldsymbol{\Phi}(\tau)^{\mathrm{T}} d\tau + \mathbf{R}_{\mathbf{L}} \quad \& \quad \boldsymbol{\Psi} = \int_0^{T_p} \boldsymbol{\Phi}(\tau)\mathbf{Q}e^{\mathbf{A}\tau} d\tau \qquad 0 \le \tau \le T_p \end{gathered} \tag{3-6}$$

ενώ ο πίνακας $\boldsymbol{\Phi}(\tau)$ δίνεται από την επίλυση της εξίσωσης:

$$\mathbf{A}\boldsymbol{\varphi}_i(\tau)^T - \boldsymbol{\Phi}_i(\tau)^T \mathbf{A}_{\mathbf{p}_i}^T = -\mathbf{B}_i\mathbf{L}_i(\tau)^T + e^{\mathbf{A}\tau}\mathbf{B}_i\mathbf{L}_i(0)^T \qquad i = 1, 2, \ldots m \tag{3-7}$$

Δεδομένου ότι διατηρείται μόνο η πρώτη τιμή του σήματος ελέγχου κάθε πρόβλεψης, η παράγωγος του σήματος ελέγχου τελικά δίνεται από τη σχέση:

$$\begin{aligned} \dot{\mathbf{u}}(t) &= \begin{bmatrix} \mathbf{L_1}(0)^T & \mathbf{0_2} & \ldots & \mathbf{0_m} \\ \mathbf{0_1} & \mathbf{L_2}(0)^T & \ldots & \mathbf{0_m} \\ \vdots & \vdots & \ddots & \vdots \\ \mathbf{0_1} & \mathbf{0_2} & \ldots & \mathbf{L_m}(0)^T \end{bmatrix} \begin{bmatrix} \boldsymbol{\eta}_1 \\ \boldsymbol{\eta}_2 \\ \vdots \\ \boldsymbol{\eta}_m \end{bmatrix} = \\ &= -\begin{bmatrix} \mathbf{L_1}(0)^T & \mathbf{0_2} & \ldots & \mathbf{0_m} \\ \mathbf{0_1} & \mathbf{L_2}(0)^T & \ldots & \mathbf{0_m} \\ \vdots & \vdots & \ddots & \vdots \\ \mathbf{0_1} & \mathbf{0_2} & \ldots & \mathbf{L_m}(0)^T \end{bmatrix} \boldsymbol{\Omega}^{-1}\boldsymbol{\Psi} \begin{bmatrix} \dot{\mathbf{x}}_{\mathbf{m}}(t) \\ \mathbf{y}(t) - \mathbf{y}_d(t) \end{bmatrix} \end{aligned} \tag{3-8}$$

ενώ το σήμα ελέγχου δίνεται από την ολοκλήρωση της παραπάνω εξίσωσης:

$$\mathbf{u}(t) = \int_0^t \dot{\mathbf{u}}(\gamma)d\gamma \tag{3-9}$$

Ο MPC έχει το πλεονέκτημα της εύκολης εισαγωγής περιορισμών (εισόδου ή/και εξόδου). Για να εισαχθούν πρέπει να έχουν τη μορφή:

$$\mathbf{A}_{constr}\boldsymbol{\eta} \le \mathbf{b} \tag{3-10}$$

Χρησιμοποιώντας τη μέθοδο βελτιστοποίησης «Hildreth's quadratic programming procedure», βρίσκονται οι τιμές του $\boldsymbol{\eta}$ που ικανοποιούν τους περιορισμούς.

Οι περιορισμοί εισόδου του σήματος ελέγχου προκύπτουν από τη σχέση:

$$\begin{bmatrix} \Delta t\mathbf{L}(0)^T \\ -\Delta t\mathbf{L}(0)^T \end{bmatrix} \boldsymbol{\eta} \le \begin{bmatrix} \mathbf{u}_{\max} - \mathbf{u}(t_i - \Delta t) \\ -(\mathbf{u}_{\min} - \mathbf{u}(t_i - \Delta t)) \end{bmatrix} \tag{3-11}$$

ενώ οι περιορισμοί της εξόδους ή της μεταβλητής κατάστασης από την σχέση:

$$\dot{\mathbf{x}}_{\min} - \mathbf{A}\mathbf{x}_{\min} \le \mathbf{b}\mathbf{L}(0)^T \boldsymbol{\eta}(t_i) \le \dot{\mathbf{x}}_{\max} - \mathbf{A}\mathbf{x}_{\max} \tag{3-12}$$

4 Εφαρμογή Προβλεπτικού Ελέγχου σε Ελεύθερα Αιωρούμενο Διαστημικό Ρομποτικό Σύστημα

Σε αυτό το κεφάλαιο μελετάται ο σχεδιασμός των νόμων ελέγχου για ένα Ελεύθερα Αιωρούμενο ΔΡΣ. Όπως αναφέρθηκε προηγουμένως, η χρήση Ελέγχου Βασιζόμενου στο Μοντέλο είναι απαραίτητη για την γραμμικοποίηση του συστήματος. Για το λόγο αυτό, οι νόμοι ελέγχου που μελετώνται είναι ο Model Based PD Controller, ο Model Based PID Controller και ο Model Based PD Controller with an auxiliary MPC Input. Οι δύο τελευταίοι θα συγκριθούν στο επόμενο κεφάλαιο.

Συγκεκριμένα, για κίνηση στο χώρο των αρθρώσεων, ο Model Based PD Controller περιγράφεται από την εξίσωση:

$$\boldsymbol{\tau} = \mathbf{H}\left[\ddot{\mathbf{q}}_d + \mathbf{K}_D\left(\dot{\mathbf{q}}_d - \dot{\mathbf{q}}\right) + \mathbf{K}_P\left(\mathbf{q}_d - \mathbf{q}\right)\right] + \mathbf{C}^*\dot{\mathbf{q}} + \mathbf{g}_h \tag{4-1}$$

όπου $\mathbf{K_D}$ και $\mathbf{K_P}$ είναι 3x3 διαγώνιοι πίνακες που περιέχον τα κέρδη του PD κομματιού του ελέγχου και καθορίζουν τη δυναμική συμπεριφορά του συστήματος.

Ο Model Based PID Controller περιγράφεται από:

$$\boldsymbol{\tau} = \mathbf{H}\left[\ddot{\mathbf{q}}_d + \mathbf{K}_D\left(\dot{\mathbf{q}}_d - \dot{\mathbf{q}}\right) + \mathbf{K}_P\left(\mathbf{q}_d - \mathbf{q}\right) + \mathbf{K}_I\int_0^t\left(\mathbf{q}_d(x) - \mathbf{q}(x)\right)dx\right] + \mathbf{C}^*\dot{\mathbf{q}} + \mathbf{g}_h \tag{4-2}$$

όπου $\mathbf{K_I}$ είναι επίσης 3x3 διαγώνιος πίνακας.

Ο Model Based PD Controller with an auxiliary MPC Input περιγράφεται από:

$$\boldsymbol{\tau} = \mathbf{H}\left[\ddot{\mathbf{q}}_d + \mathbf{K}_D\left(\dot{\mathbf{q}}_d - \dot{\mathbf{q}}\right) + \mathbf{K}_P\left(\mathbf{q}_d - \mathbf{q}\right) + \mathbf{u}_{MPC}\right] + \mathbf{C}^*\dot{\mathbf{q}} + \mathbf{g}_h \tag{4-3}$$

όπου το σήμα που προέρχεται από τον MPC απαιτεί την εφαρμογή της μεθοδολογίας που παρουσιάστηκε στο Κεφάλαιο 3. Το μοντέλο στο οποίο εφαρμόζεται ο MPC δίνεται από:

$$\begin{gathered}\dot{\mathbf{x}}_\mathbf{m}(t) = \mathbf{A}_\mathbf{m}\mathbf{x}_\mathbf{m}(t) + \mathbf{B}_\mathbf{m}u(t)\\ y(t) = \mathbf{C}_\mathbf{m}\mathbf{x}_\mathbf{m}(t)\end{gathered} \tag{4-4}$$

$$with\ \ \mathbf{x}_\mathbf{m} = \begin{bmatrix} x_{m,1} \\ x_{m,2}\end{bmatrix} = \begin{bmatrix} e_i \\ \dot{e}_i\end{bmatrix},\ \mathbf{A}_\mathbf{m} = \begin{bmatrix} 0 & 1 \\ -K_{P,i} & -K_{D,i}\end{bmatrix},\ \mathbf{B}_\mathbf{m} = \begin{bmatrix} 0 \\ -1\end{bmatrix},\ \mathbf{C}_\mathbf{m} = \begin{bmatrix}1 & 0\end{bmatrix},\ \ i = 1,2,3$$

Για την κίνηση στον Καρτεσιανό χώρο, οι ροπές των επενεργητών δίνονται από τον τύπο:

$$\boldsymbol{\tau} = \mathbf{J}^T\mathbf{f} \tag{4-5}$$

όπου $\mathbf{J}$ η Ιακωβιανή του συστήματος.

Θεωρώντας μηδενική στροφορμή, οι δυναμικές εξισώσεις του ΔΡΣ για να περιγράψουν την κίνηση στον Καρτεσιανό χώρο μετατρέπονται σε:

$$\mathbf{H}_x(\mathbf{q},\theta_0)\ddot{\mathbf{x}} + \mathbf{C}_x^*(\mathbf{q},\dot{\mathbf{q}},\theta_0,\dot{\theta}_0)\dot{\mathbf{x}} = \mathbf{f} = \mathbf{J}^{-T}\boldsymbol{\tau} \tag{4-6}$$

όπου:

$$\begin{aligned}\mathbf{H}_x(\mathbf{q},\theta_0) &= \mathbf{J}^{-T}\mathbf{H}\mathbf{J}^{-1}\\ \mathbf{C}_x^*(\mathbf{q},\dot{\mathbf{q}},\theta_0,\dot{\theta}_0) &= \mathbf{J}^{-T}\left(\mathbf{C}^* - \mathbf{H}\mathbf{J}^{-1}\dot{\mathbf{J}}\right)\mathbf{J}^{-1}\end{aligned} \tag{4-7}$$

Αντίστοιχα με τον έλεγχο στον χώρο των αρθρώσεων, στον Καρτεσιανό χώρο ο Model Based PD Controller περιγράφεται από την εξίσωση:

$$\mathbf{f} = \mathbf{H}_x\left[\ddot{\mathbf{x}}_d + \mathbf{K}_D\left(\dot{\mathbf{x}}_d - \dot{\mathbf{x}}\right) + \mathbf{K}_P\left(\mathbf{x}_d - \mathbf{x}\right)\right] + \mathbf{C}_x^*\dot{\mathbf{x}}$$
$$\boldsymbol{\tau} = \mathbf{J}^T\mathbf{f} \tag{4-8}$$

Ο Model Based PID Controller περιγράφεται από:

$$\mathbf{f} = \mathbf{H}_x\left[\ddot{\mathbf{x}}_d + \mathbf{K}_D\left(\dot{\mathbf{x}}_d - \dot{\mathbf{x}}\right) + \mathbf{K}_P\left(\mathbf{x}_d - \mathbf{x}\right) + \mathbf{K}_I\int_0^t\left(\mathbf{x}_d(\lambda) - \mathbf{x}(\lambda)\right)d\lambda\right] + \mathbf{C}_x^*\dot{\mathbf{x}}$$
$$\boldsymbol{\tau} = \mathbf{J}^T\mathbf{f} \tag{4-9}$$

ενώ ο Model Based PD Controller with an auxiliary MPC Input περιγράφεται από:

$$\mathbf{f} = \mathbf{H}_x\left[\ddot{\mathbf{x}}_d + \mathbf{K}_D\left(\dot{\mathbf{x}}_d - \dot{\mathbf{x}}\right) + \mathbf{K}_P\left(\mathbf{x}_d - \mathbf{x}\right) + \mathbf{u}_{MPC}\right] + \mathbf{C}_x^*\dot{\mathbf{x}}$$
$$\boldsymbol{\tau} = \mathbf{J}^T\mathbf{f} \tag{4-10}$$

Οι προσομοιώσεις της παρούσας εργασίας πραγματοποιήθηκαν στο περιβάλλον του Matlab/Simulink με την χρήση δυναμικού μοντέλου δημιουργούμενου στο MSC Adams. Στο Σχήμα 4-1 φαίνεται το ΔΡΣ έτσι όπως αναπαρίσταται από το Adams.

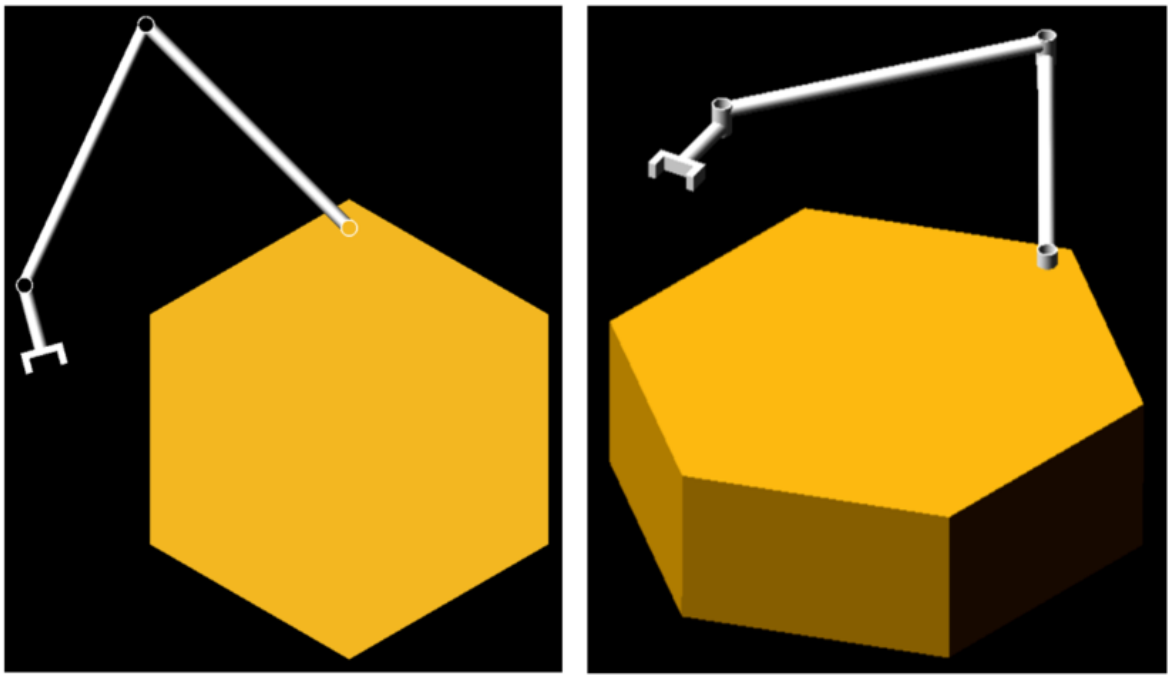

Σχήμα 4-1. Εικόνα του μοντέλου που χρησιμοποιείται για την αναπαράσταση του μελετούμενου ΔΡΣ στο MSC Adams (a) Κάτοψη, (b) Ισομετρική Όψη.

5 Προσομοιώσεις & Περιπτώσεις Μελέτης

Στο κεφάλαιο αυτό συγκρίνονται ο Model Based PID Controller με το Model Based PD Controller with an auxiliary MPC Input με βάση τα σφάλματα, τις ροπές και τον υπολογιστικό χρόνο για 4 σενάρια. Ο Πίνακας 5-1 παρουσιάζει τις παραμέτρους του μελετούμενου ΔΡΣ.

Πίνακας 5-1. Παράμετροι ΔΡΣ.

Body	Mass - m_i (kg)	Moment of Inertia - I_i (kg·m^2)	Before-CM Length - l_i (m)	After-CM Length - r_i (m)
0	600	500	-	1.4
1	40	20	1	1
2	40	20	1	1
3	20	15	0.25	0.25

5.1 Σενάριο 1: Σταθερές Διαταραχές

Για το σενάριο αυτό, πολυώνυμα 5^{ης} τάξης χρησιμοποιήθηκαν για τον σχεδιασμό της τροχιάς στον Καρτεσιανό χώρο. Ο στόχος θεωρήθηκε σταθερός. Οι τιμές των διαταραχών που εφαρμόστηκαν στις αρθρώσεις του βραχίονα είναι:

$$\mathbf{d} = \begin{bmatrix} 12 & 6 & 4 \end{bmatrix}^T (Nm) \tag{5-1}$$

Οι εξισώσεις των συγκρινόμενων νόμων ελέγχου παρουσιάζονται στο προηγούμενο κεφάλαιο. Τα κέρδη που εφαρμόσθηκαν στον Model Based PID Controller είναι:

$$\begin{aligned} K_D &= diag(18.0768, 18.0768, 18.0768) \\ K_P &= diag(136.1545, 136.1545, 136.1545) \\ K_I &= diag(427.2981, 427.2981, 427.2981) \end{aligned} \tag{5-2}$$

ενώ τα κέρδη του Model Based PD Controller with an auxiliary MPC Input καθώς και οι λοιπές παράμετροι αυτού είναι:

$$\begin{aligned} K_{D,MPC} &= diag(10.5448, 10.5448, 10.5448) \\ K_{P,MPC} &= diag(56.7310, 56.7310, 56.7310) \end{aligned} \tag{5-3}$$

$$\begin{aligned} p = 5.5110,\ N = 10,\ T_p = 6s \\ \mathbf{Q} = \mathbf{C}^T\mathbf{C} = \begin{bmatrix} 0 & 0 & 0 \\ 0 & 0 & 0 \\ 0 & 0 & 1 \end{bmatrix},\ \mathbf{R} = 10^{-6} \end{aligned} \tag{5-4}$$

Στο Σχήμα 5-1 παρουσιάζονται τα σφάλματα των δύο ελέγχων για MPC χωρίς περιορισμούς. Είναι προφανές ότι ο έλεγχος με τον MPC παρουσιάζει καλύτερη συμπεριφορά. Συγκεκριμένα, ο MPC επιτυγχάνει:

- 43% μείωση του σφάλματος της x-Συντεταγμένης
- 43% μείωση του σφάλματος της y-Συντεταγμένης
- 43% μείωση του σφάλματος της περιστροφής

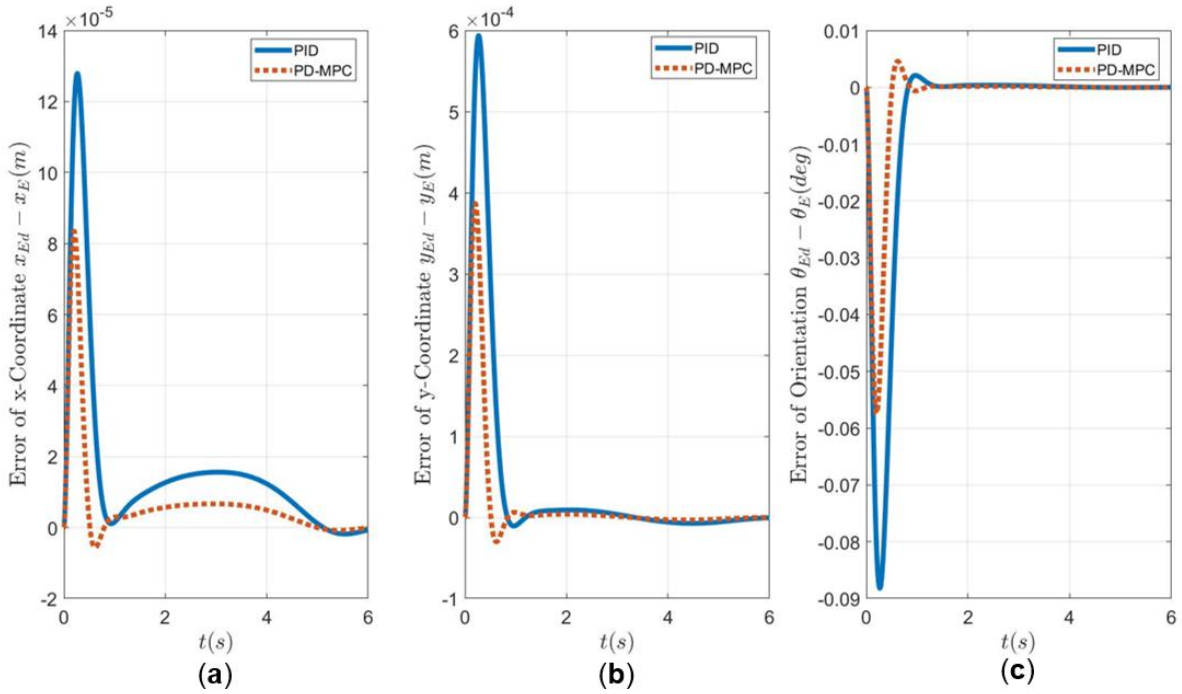

Σχήμα 5-1. Σφάλματα Πραγματικής και Επιθυμητής Τιμής των Μεγεθών του Τελικού Σημείου Δράσης για το 1ο Σενάριο (a) x-Συντεταγμένη, (b) y-Συντεταγμένη, (c) Περιστροφή.

Εφαρμόζοντας περιορισμούς στον MPC η απόδοση του ελέγχου μπορεί να βελτιωθεί ακόμη περισσότερο. Συγκεκριμένα, εισάγονται οι παρακάτω περιορισμοί μέχρι τη χρονική στιγμή $t = 0.01$s:

$$\mathbf{x}_{\max} = \begin{bmatrix} 10^{-6} & 10^{-6} & 10^{-4}\pi/180 \end{bmatrix}^T$$
$$\mathbf{x}_{\min} = -\mathbf{x}_{\max} \tag{5-5}$$

ενώ για ασφάλεια εισάγονται και περιορισμοί στις εισόδους:

$$\mathbf{u}_{\max} = \begin{bmatrix} 0.5 & 0.5 & 0.5 \end{bmatrix}^T$$
$$\mathbf{u}_{\min} = -\mathbf{u}_{\max} \tag{5-6}$$

Με αυτούς τους περιορισμούς, ο MPC πετυχαίνει:

- 90% μείωση του σφάλματος της x-Συντεταγμένης
- 80% μείωση του σφάλματος της y-Συντεταγμένης
- 96% μείωση του σφάλματος της περιστροφής

Τέλος, οι μέγιστες απαιτούμενες ροπές και για τις δύο περιπτώσεις είναι ίσες για όλους τους ελέγχους ενώ παρατηρήθηκε ότι ο χρόνος προσομοίωσης των νόμων ελέγχου είναι σχετικά ίδιος.

5.2 Σενάριο 2: Παραμετρική Αβεβαιότητα

Για το σενάριο αυτό, ο σχεδιασμός τροχιάς είναι ίδιος με αυτόν που παρουσιάστηκε στο Σενάριο 1. Επιπλέον, οι νόμοι ελέγχου έχουν επίσης τις ίδιες παραμέτρους. Ωστόσο, εδώ δεν εφαρμόζονται σταθερές διαταραχές αλλά θεωρείται ότι οι παράμετροι του ΔΡΣ δεν είναι ακριβείς.

Συγκεκριμένα, πραγματοποιείται μία προσομοίωση Monte-Carlo με 200 κύκλους στους οποίους οι παράμετροι του ΔΡΣ λαμβάνουν τυχαίες τιμές σύμφωνα με:

$$\begin{aligned} &0.95l_{i,nominal} \le l_i \le 1.05l_{i,nominal} \quad i=1-3 \\ &0.95r_{i,nominal} \le r_i \le 1.05r_{i,nominal} \quad i=1-3 \\ &0.95m_{i,nominal} \le m_i \le 1.05m_{i,nominal} \quad i=1-3 \\ &0.80m_{0,nominal} \le m_0 \le 1.05m_{0,nominal} \end{aligned} \tag{5-7}$$

Ο Πίνακας 5-2 παρουσιάζει τα μέγιστα σφάλματα και των δύο νόμων ελέγχου καθώς και τις παραμέτρους του ΔΡΣ για τις οποίες αυτά προκύπτουν. Είναι εμφανές ότι και σε αυτή τη περίπτωση ο έλεγχος που περιέχει τον MPC έχει καλύτερη απόδοση.

Πίνακας 5-2. Μέγιστα Σφάλματα της Προσομοίωσης Monte-Carlo και οι παράμετροι τους.

	$x_{E,d}$ - x_d	$y_{E,d}$ - y_d	$\theta_{E,d}$ - θ_d
Max_{PID}	$7.919\cdot10^{-5}$	$7.176\cdot10^{-5}$	$18\cdot10^{-4}$
Max_{PD-MPC}	$3.925\cdot10^{-5}$	$3.645\cdot10^{-5}$	$8.818\cdot10^{-4}$
m_0 (kg)	540.9	595.1	510.7
(m_1, m_2, m_3) (kg)	(39.81, 41.80, 20.98)	(38.65, 41.51, 20.77)	(38.61, 40.82, 20.93)
r_0 (m)	1.384	1.376	1.364
(r_1, r_2, r_3) (m)	(1.019, 1.046, 0.2576)	(0.9631, 1.046, 0.2534)	(1.016, 1.042, 0.2511)
(l_1, l_2, l_3) (m)	(1.042, 0.993, 0.244)	(0.9611, 1.037, 0.2552)	(0.9631, 1.049, 0.2405)

Στο Σχήμα 5-2 φαίνονται τα σφάλματα όταν εφαρμόζονται οι παράμετροι του ΔΡΣ για τις οποίες προκύπτουν τα μέγιστα σφάλματα της x-Συντεταγμένης του τελικού σημείου δράσης. Παρατηρείται ότι τα διαγράμματα δεν συγκλίνουν στο μηδέν. Αυτό το πρόβλημα μπορεί να αντιμετωπιστεί μερικώς εισάγοντας περιορισμούς στον MPC. Συγκεκριμένα, εφαρμόζονται οι παρακάτω περιορισμοί από τη χρονική στιγμή t = 4.5s μέχρι το τέλος της προσομοίωσης:

$$\begin{aligned} \mathbf{x}_{\max} &= \begin{bmatrix} 5\cdot10^{-6} & 5\cdot10^{-6} & 5\cdot10^{-6}\pi/180 \end{bmatrix}^T \\ \mathbf{x}_{\min} &= -\mathbf{x}_{\max} \end{aligned} \tag{5-8}$$

ενώ για ασφάλεια εισάγονται και περιορισμοί στις εισόδους:

$$\begin{aligned} \mathbf{u}_{\max} &= \begin{bmatrix} 2 & 2 & 2 \end{bmatrix}^T \\ \mathbf{u}_{\min} &= -\mathbf{u}_{\max} \end{aligned} \tag{5-9}$$

Το Σχήμα 5-3 παρουσιάζει τα σφάλματα όταν εφαρμόζονται οι παραπάνω περιορισμοί. Είναι εμφανές ότι ο MPC επιτυγχάνει τη σύγκλιση του διαγράμματος της περιστροφής.

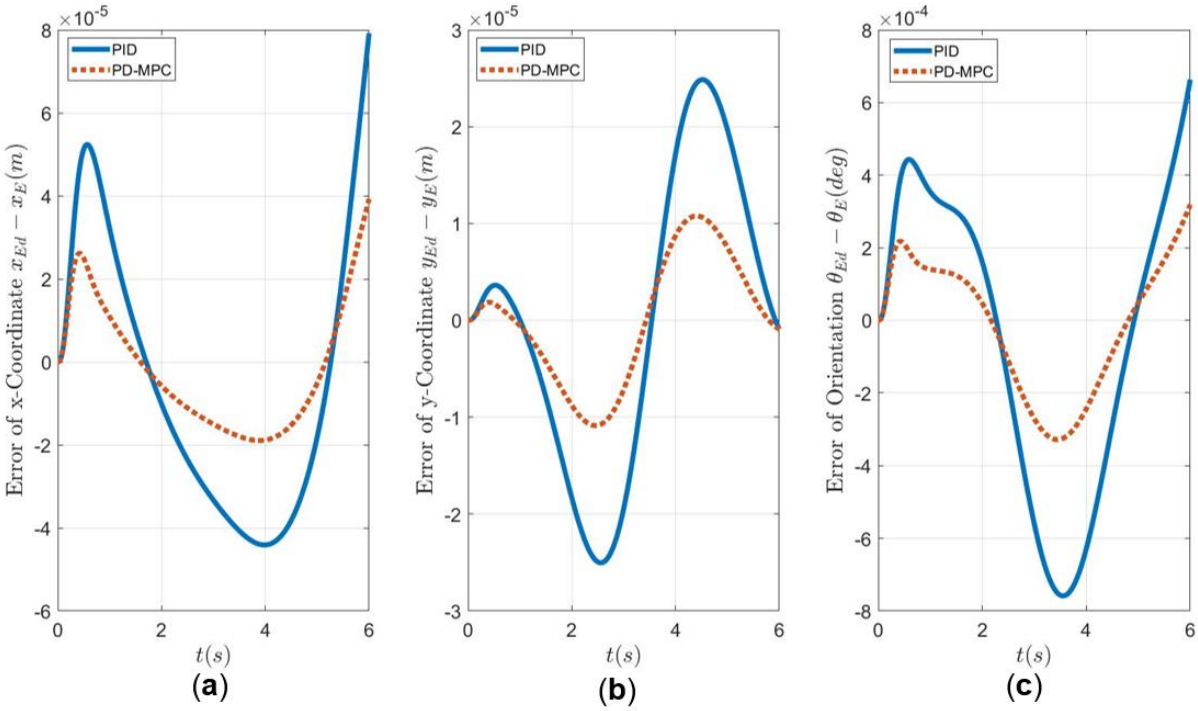

Σχήμα 5-2. Σφάλματα Πραγματικής και Επιθυμητής Τιμής των Μεγεθών του Τελικού Σημείου Δράσης για το 2ο Σενάριο (a) x-Συντεταγμένη, (b) y-Συντεταγμένη, (c) Περιστροφή.

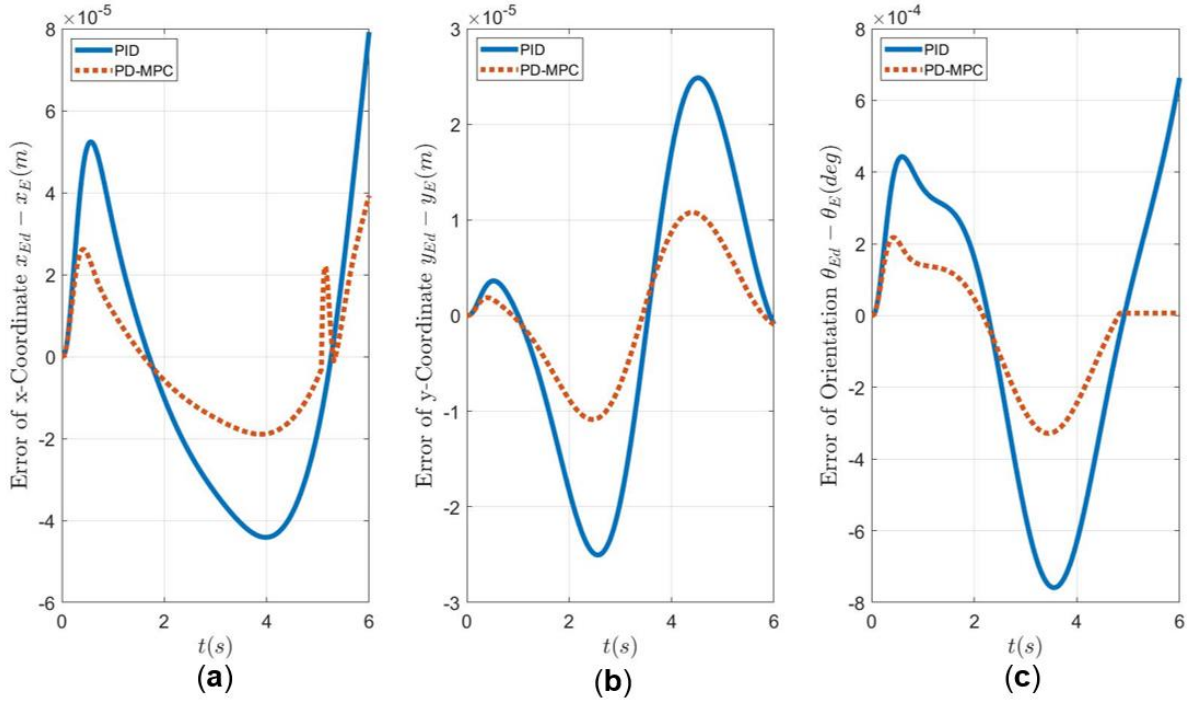

Σχήμα 5-3. Σφάλματα Πραγματικής και Επιθυμητής Τιμής των Μεγεθών του Τελικού Σημείου Δράσης για το 2ο Σενάριο και εφαρμόζοντας MPC με περιορισμούς (a) x-Συντεταγμένη, (b) y-Συντεταγμένη, (c) Περιστροφή.

5.3 Σενάριο 3: Μετακίνηση Στόχου Απροσδιόριστης Μάζας

Στο σενάριο αυτό παρουσιάζεται η μετακίνηση ενός αντικειμένου που έχει πιάσει το ΔΡΣ και του οποίου οι παράμετροι δεν είναι ακριβείς. Ο σχεδιασμός τροχιάς πραγματοποιήθηκε στο χώρο των αρθρώσεων χρησιμοποιώντας πολυώνυμα 5ης τάξης. Ο Πίνακας 5-3 παρουσιάζει τις παραμέτρους του αντικειμένου-στόχου.

Πίνακας 5-3. Παράμετροι Στόχου.

Captured Object	Nominal Value	Estimated Value
Mass m_s (kg)	200	220
Moment of Inertia I_s (kg·m^2)	100	110
Distance r_s (m)	0.8	0.76

Στο Σχήμα 5-4 παρουσιάζονται τα σφάλματα των γωνιών των αρθρώσεων. Είναι προφανές ότι ο έλεγχος με τον επιπλέον βρόχο MPC έχει καλύτερη απόδοση από τον άλλο νόμο ελέγχου. Συγκεκριμένα, ο MPC πετυχαίνει:

- 52% μείωση του σφάλματος της γωνίας της 1ης Άρθρωσης
- 52% μείωση του σφάλματος της γωνίας της 2ης Άρθρωσης
- 56% μείωση του σφάλματος της γωνίας της 3ης Άρθρωσης

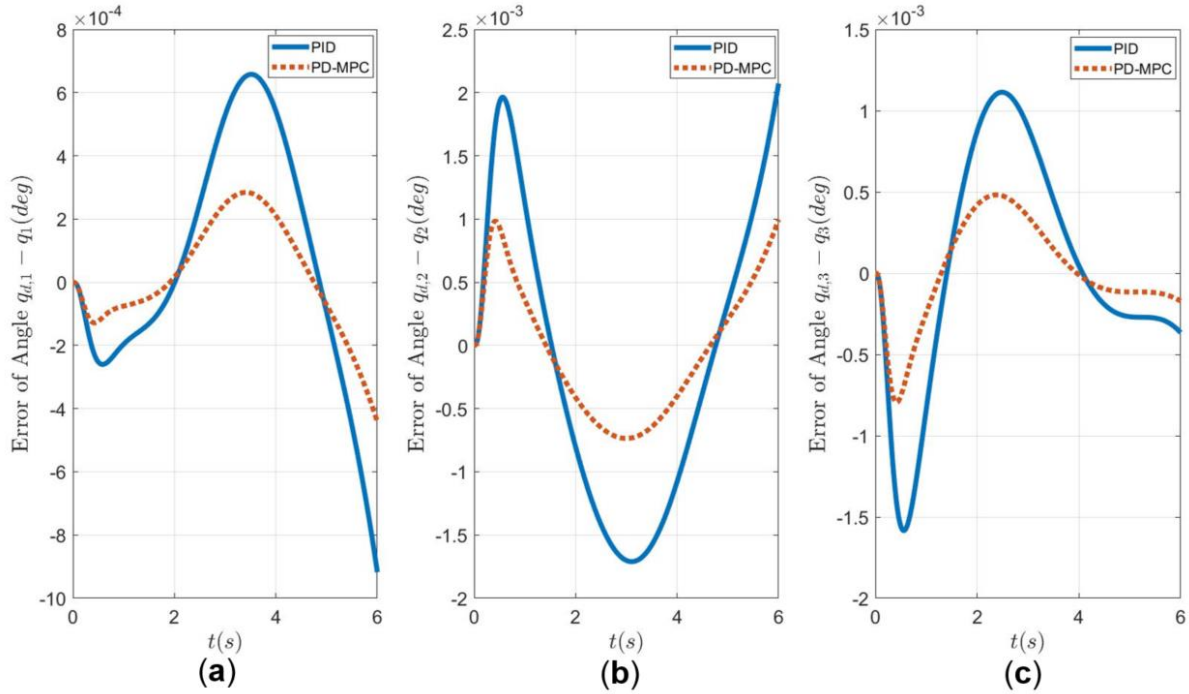

Σχήμα 5-4. Σφάλματα Πραγματικής και Επιθυμητής Τιμής των Γωνιών των Αρθρώσεων για το 3ο Σενάριο (a) 1η Άρθρωση, (b) 2η Άρθρωση, (c) 3η Άρθρωση.

5.4 Σενάριο 4: Θόρυβος

Στο σενάριο αυτό μελετάται η απόδοση των νόμων ελέγχου όταν οι μετρήσεις περιέχουν θόρυβο. Συγκεκριμένα, οι μεταβλητές που περιέχουν θόρυβο είναι οι: $q_1, q_2, q_3, \dot{q}_1, \dot{q}_2, \dot{q}_3, \theta_0, \dot{\theta}_0, x_E, y_E, \theta_E, \dot{x}_E, \dot{y}_E, \dot{\theta}_E$ ενώ ο θόρυβος ακολουθεί κανονική κατανομή με μηδενική μέση τιμή και μεταβλητότητα ίση με $\sigma^2 = 10^{-10}$ ή $\sigma^2 = 10^{-8}$.

Για το σενάριο αυτό, ο στόχος θεωρείται κινούμενος στο επίπεδο με σταθερή σχετική ταχύτητα. Ίδια πολυώνυμα 5ου βαθμού χρησιμοποιούνται για το σχεδιασμό της τροχιάς μόνο που οι τελικές επιθυμητές γραμμικές ταχύτητες του τελικού σημείου δράσης είναι μη μηδενικές και συμπίπτουν με αυτές του στόχου.

Παρατηρείται ότι ο θόρυβος με μεταβλητότητα $\sigma^2 = 10^{-10}$ επηρεάζει ελάχιστα τη λειτουργία και των δύο νόμων ελέγχου. Ωστόσο, ο θόρυβος με μεταβλητότητα $\sigma^2 = 10^{-8}$ προκαλεί αισθητά προβλήματα. Στο Σχήμα φαίνονται οι ροπές των αρθρώσεων. Παρατηρείται ότι μεταβάλλονται πολύ απότομα έτσι ώστε να αντισταθμίσουν τον θόρυβο. Αυτό μπορεί να αποτελέσει πρόβλημα για τους επενεργητές. Τέλος, πάλι παρατηρείται ότι ο νόμος ελέγχου με τον MPC βρόχο έχει καλύτερη απόδοση καθώς οι ροπές του είναι μικρότερες ενώ τα σφάλματα της θέσης και της περιστροφής του τελικού σημείου δράσης είναι τα ίδια.

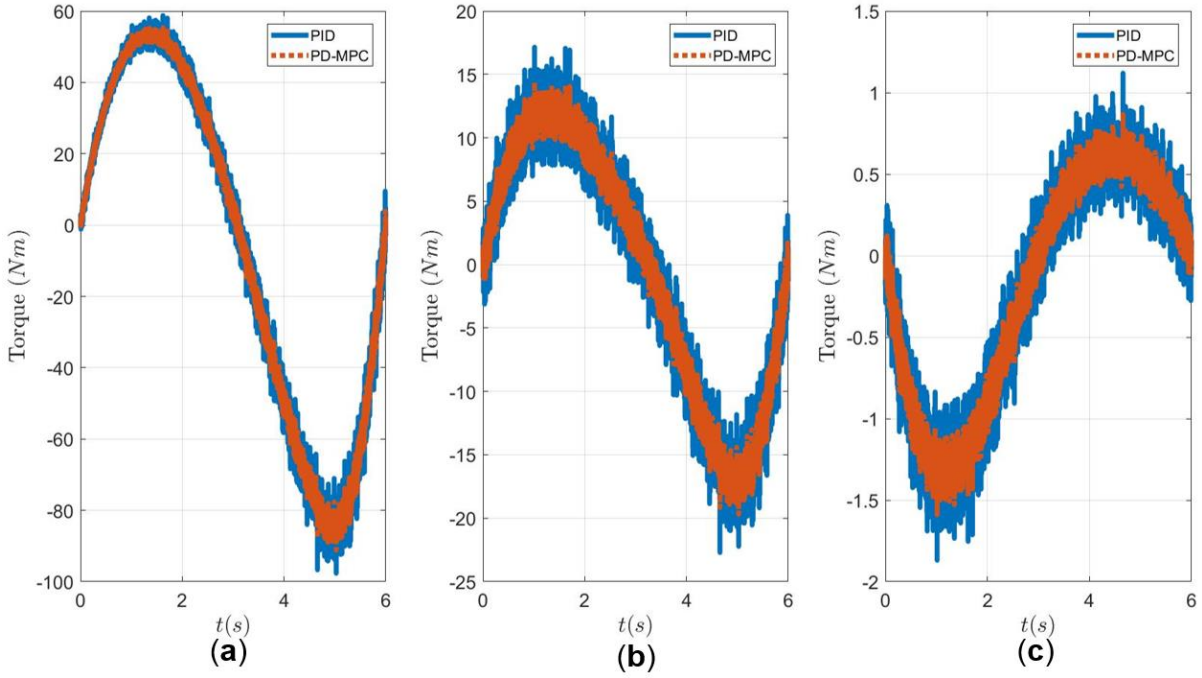

Σχήμα 5-5. Ροπές των Επενεργητών των Αρθρώσεων για το 4ο Σενάριο και για Θόρυβο με Μεταβλητότητα 10^{-8} (a) 1η Άρθρωση, (b) 2η Άρθρωση, (c) 3η Άρθρωση.

6 Συμπεράσματα & Μελλοντική Εργασία

Βασικός σκοπός αυτής της διπλωματικής εργασίας είναι η μελέτη της λειτουργίας του προβλεπτικού ελέγχου όταν εφαρμόζεται σε ένα Ελεύθερα Αιωρούμενο ΔΡΣ. Ο σκοπός αυτός επιτεύχθηκε μέσα από τη σύγκριση του MPC με έναν συνηθισμένο PID έλεγχο. Και στα τέσσερα σενάρια που ερευνήθηκαν, ο MPC παρουσίασε σημαντικά καλύτερη συμπεριφορά από ότι ο απλός PID. Είτε για κίνηση στον χώρο των αρθρώσεων, είτε στον Καρτεσιανό χώρο, ο MPC είχε μικρότερα σφάλματα από τις επιθυμητές τροχιές σε σχέση με τον απλό PID ενώ οι μέγιστες ροπές παρέμεναν ίσες. Εξαίρεση αποτελεί το τέταρτο σενάριο στο οποίο ενώ τα σφάλματα των δύο ελέγχων ήταν ίδια, ο MPC απαιτούσε μικρότερες αλλαγές τροχιών, προσφέροντάς του ένα ακόμα πλεονέκτημα.

Η μελέτη αυτή μπορεί να αποτελέσει εφαλτήριο για περαιτέρω έρευνα. Καθ’ όλη την εργασία, το ΔΡΣ θεωρήθηκε ότι έχει μηδενική στροφορμή, ο βραχίονάς του είναι άκαμπτος και ότι κινείται στο επίπεδο. Ένα ρεαλιστικό σενάριο θα λάμβανε υπόψιν αυτές τις υποθέσεις ενώ θα περιείχε επίσης και κάποιο παρατηρητή ή φίλτρο εκτίμησης της κατάστασης για τον έλεγχο. Επιπρόσθετα, ιδιαίτερο ενδιαφέρον παρουσιάζει και η σύγκριση του MPC με άλλους νόμους ελέγχου όπως ο H-infinity ή ο προσαρμοστικός έλεγχος ή ακόμα και με άλλους τύπους MPC όπως ο min-max MPC.